NATIONAL HURRICANE RESEARCH PROJECT

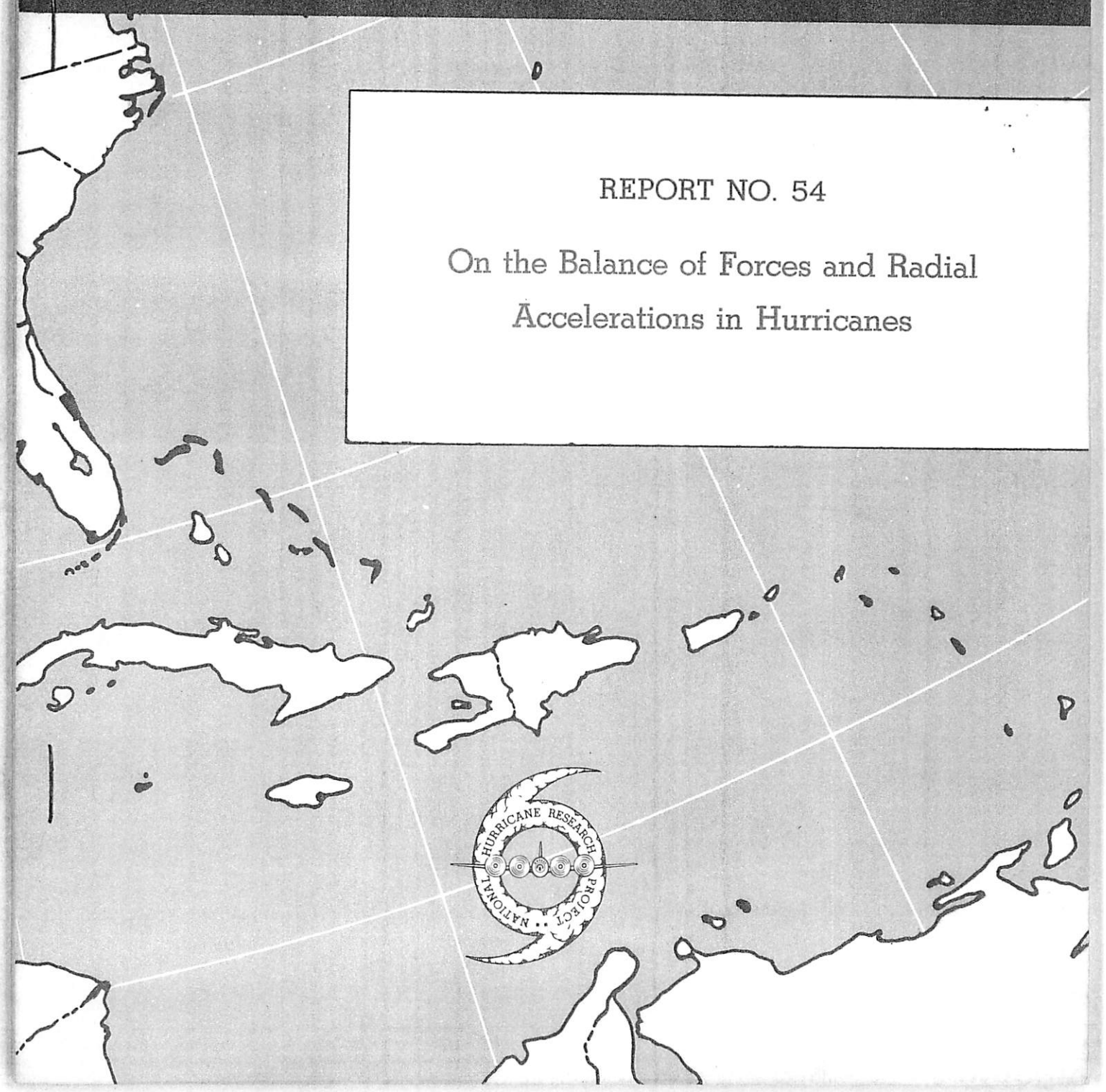

REPORT NO. 54

On the Balance of Forces and Radial Accelerations in Hurricanes

U. S. DEPARTMENT OF COMMERCE
Luther H. Hodges, Secretary
WEATHER BUREAU
F. W. Reichelderfer, Chief

NATIONAL HURRICANE RESEARCH PROJECT

REPORT NO. 54

On the Balance of Forces and Radial Accelerations in Hurricanes

by

William M. Gray

Colorado State University, Fort Collins, Colo.

A report on research conducted under contracts between the U. S. Weather Bureau, Colorado State University, and The University of Chicago.

Washington, D. C.
May 1962

NATIONAL HURRICANE RESEARCH PROJECT REPORTS

Reports by Weather Bureau units, contractors, and cooperators working on the hurricane problem are preprinted in this series to facilitate immediate distribution of the information among the workers and other interested units. As this limited reproduction and distribution in this form do not constitute formal scientific publication, reference to a paper in the series should identify it as a preprinted report.

No. 1. Objectives and basic design of the NHRP. March 1956.
No. 2. Numerical weather prediction of hurricane motion. July 1956.
Supplement: Error analysis of prognostic 500-mb. maps made for numerical weather prediction of hurricane motion. March 1957.
No. 3. Rainfall associated with hurricanes. July 1956.
No. 4. Some problems involved in the study of storm surges. December 1956.
No. 5. Survey of meteorological factors pertinent to reduction of loss of life and property in hurricane situations. March 1957.
No. 6. A mean atmosphere for the West Indies area. May 1957.
No. 7. An index of tide gages and tide gage records for the Atlantic and Gulf coasts of the United States. May 1957.
No. 8. Part I. Hurricanes and the sea surface temperature field. Part II. The exchange of energy between the sea and the atmosphere in relation to hurricane behavior. June 1957.
No. 9. Seasonal variations in the frequency of North Atlantic tropical cyclones related to the general circulation. July 1957.
No. 10. Estimating central pressure of tropical cyclones from aircraft data. August 1957.
No. 11. Instrumentation of National Hurricane Research Project aircraft. August 1957.
No. 12. Studies of hurricane spiral bands as observed on radar. September 1957.
No. 13. Mean soundings for the hurricane eye. September 1957.
No. 14. On the maximum intensity of hurricanes. December 1957.
No. 15. The three-dimensional wind structure around a tropical cyclone. January 1958.
No. 16. Modification of hurricanes through cloud seeding. May 1958.
No. 17. Analysis of tropical storm Frieda 1957. A preliminary report. June 1958.
No. 18. The use of mean layer winds as a hurricane steering mechanism. June 1958.
No. 19. Further examination of the balance of angular momentum in the mature hurricane. July 1958.
No. 20. On the energetics of the mature hurricane and other rotating wind systems. July 1958.
No. 21. Formation of tropical storms related to anomalies of the long-period mean circulation. September 1958.
No. 22. On production of kinetic energy from condensation heating. October 1958.
No. 23. Hurricane Audrey storm tide. October 1958.
No. 24. Details of circulation in the high energy core of hurricane Carrie. November 1958.
No. 25. Distribution of surface friction in hurricanes. November 1958.
No. 26. A note on the origin of hurricane radar spiral bands and the echoes which form them. February 1959.
No. 27. Proceedings of the Board of Review and Conference on Research Progress. March 1959.
No. 28. A model hurricane plan for a coastal community. March 1959.
No. 29. Exchange of heat, moisture, and momentum between hurricane Ella (1958) and its environment. April 1959.
No. 30. Mean soundings for the Gulf of Mexico area. April 1959.
No. 31. On the dynamics and energy transformations in steady-state hurricanes. August 1959.
No. 32. An interim hurricane storm surge forecasting guide. August 1959.
No. 33. Meteorological considerations pertinent to standard project hurricane, Atlantic and Gulf coasts of the United States. November 1959.
No. 34. Filling and intensity changes in hurricanes over land. November 1959.
No. 35. Wind and pressure fields in the stratosphere over the West Indies region in August 1958. December 1959.
No. 36. Climatological aspects of intensity of typhoons. February 1960.
No. 37. Unrest in the upper stratosphere over the Caribbean Sea during January 1960. April 1960.
No. 38. On quantitative precipitation forecasting. August 1960.
No. 39. Surface winds near the center of hurricanes (and other cyclones). September 1960.
No. 40. On initiation of tropical depressions and convection in a conditionally unstable atmosphere. October 1960.
No. 41. On the heat balance of the troposphere and water body of the Caribbean Sea. December 1960.
No. 42. Climatology of 24-hour North Atlantic tropical cyclone movements. January 1961.
No. 43. Prediction of movements and surface pressures of typhoon centers in the Far East by statistical methods. May 1961.
No. 44. Marked changes in the characteristics of the eye of intense typhoons between the deepening and filling states. May 1961.
No. 45. The occurrence of anomalous winds and their significance. June 1961.
No. 46. Some aspects of hurricane Daisy, 1958. July 1961.
No. 47. Concerning the mechanics and thermodynamics of the inflow layer of the mature hurricane. September 1961.
No. 48. On the structure of hurricane Daisy (1958). October 1961.
No. 49. Some properties of hurricane wind fields as deduced from trajectories. November 1961.
No. 50. Proceedings of the Second Technical Conference on Hurricanes, June 27-30, 1961, Miami Beach, Fla. March 1962.
No. 51. Concerning the general vertically averaged hydrodynamic equations with respect to basic storm equations. April 1962.
No. 52. Inventory, use, and availability of NHRP meteorological data gathered by aircraft. April 1962.
No. 53. On the momentum and energy balance of hurricane Helene (1958). April 1962.

CONTENTS

ON THE BALANCE OF FORCES AND RADIAL ACCELERATIONS IN HURRICANES

William M. Gray
Colorado State University, Fort Collins, Colo.

1. INTRODUCTION

Hurricanes have often been described as vortices in which the cyclostrophic wind equation should be valid in the core of maximum winds and the gradient wind equation in the periphery. But the degree to which these equations really describe the balance of forces has not been determined. This has been due to lack of reliable wind and pressure-height information. With the installation of the National Hurricane Research Project of the United States Weather Bureau in 1956, and with technical development of the gyro-navigation system and other instruments, these observational inadequacies have been reduced and to some extent overcome. The Doppler navigation system has given for the first time accurate wind data over ocean areas. Within the limits of accuracy of observations, the question concerning the form of the laws of motion applicable in hurricanes can now be answered in certain respects for several storms which were thoroughly covered by research missions of the National Hurricane Research Project.

This paper presents a first attempt to take up some special aspects of the balance of forces computed from the flight data. Computations are made for Atlantic hurricanes Carrie (1957), Cleo (1958), Daisy (1958), and Helene (1958).

Instrumentation of Aircraft. - During the hurricane seasons of 1957-1958, the National Hurricane Research Project operated three aircraft in conjunction with the U. S. Air Force. There were two B-50's and one B-47. The instrumentation installed and maintained in these planes has been described by Hilleary and Christensen [4]. It will therefore suffice to note that the instrumentation of interest for this study consisted of a Doppler (gyro) Navigation wind measurement, radio and pressure altimeter for determination of the altimeter correction ("D"), and a vortex thermometer for temperature measurements. Punch card systems were installed in the back of the aircraft. Instantaneous values of the above parameters were punched at specified time intervals - one card every two to ten seconds - with the more rapid punching in the hurricane cores. The punch card decks were taken to National Hurricane Research Project after each mission and evaluated by machine processing. Note was taken of the hurricane displacement over the duration of the mission and all quantities were plotted in a latitude-longitude coordinate system fixed with respect to the storm center.

In this study, use is made of the horizontal winds and the observed "D" values. Temperatures are used only for checking on the computed vertical thicknesses, obtained from the "D" values between isobaric surfaces.

Research Missions in Hurricane Daisy (1958). - Hurricane Daisy began to form on August 24, just to the northeast of the Bahama Islands (fig. 1). By 1200 GMT on August 25, the maximum winds in the core were 70 kt. It was at this time that National Hurricane Research Project aircraft first entered Daisy. One Air Force B-50 made radial penetrations into the eye at 830 mb.; additional legs were executed at 1600 and 2800 ft. The second B-50 operated in the middle troposphere at 570 mb. The B-47 aircraft carried out a mission in and around the storm at 237 mb.

Two missions were flown into Daisy on the 26th, but without radial penetration. On August 27 and 28, radial penetrations were made at 630 and 620 mb. respectively. Daisy reached its peak intensity on the 27th, with maximum winds above 115 kt. A plot of central pressure with time is given in figure 2.

Mission into Hurricane Cleo (1958). - Cleo formed in an easterly wave west of the Canary Islands on August 9. It moved steadily westward for six days to approximately 15°N., 48°W., and then turned northward moving steadily in this direction until it took on extratropical characteristics southeast of Newfoundland on the 19th. It reached maximum intensity on the 14th, just before turning northward. The maximum winds were approximately 120 kt. and minimum pressure 945 mb. A three-plane NHRP mission was flown into the storm on August 18 when Cleo was moving in an approximately steady state toward the north-northeast at 14 kt. Maximum winds were approximately 95 kt. and minimum pressure 970 mb. The storm eye was nearly 25 miles in diameter and the eye wall clouds quite extensive. One mission was accomplished at 820 mb., another at 580 mb., and a third at 255 mb. See the storm track in figure 3.

Missions into Hurricane Carrie (1957). - Carrie formed from an easterly wave near 20° N., 35°W., on September 5. It moved steadily west and northwest. By September 15 it was located at 30°N., 58°W., moving to the northwest at 12 kt. in approximate steady state. Its central pressure was 965 mb. and maximum winds 85 kt. A mid-tropospheric probe (605 mb.) was made at this time. Another mid-tropospheric flight into Carrie (690 mb.) was made on September 17 when the storm had changed direction and was moving toward the east-northeast at 13 kt. Minimum pressure and maximum winds were nearly the same as on the 15th. See the storm track in figure 4.

Missions in Hurricane Helene (1958). - This storm started to develop on September 22 at 22°N., 65°W., or 200 n. mi. north-northeast of San Juan, P.R. It moved almost directly northwestward for the next four days, while slowly intensifying (see storm track fig. 5). A flight at 635 mb. was made on September 24 when the central pressure was approximately 995 mb. and maximum winds were 60 kt. Another flight was made on September 25 at 810 mb. when the storm's central pressure was approximately 980 mb. and maximum winds approximately 90 kt. Other flights into Helene were made by NHRP aircraft on September 26. Only the results of the two flights on the 24th and 25th are presented in this paper.

Each day's data was collected in six to ten hours between the approximate hours of 1400 and 2400 GMT. For computational purposes, an essentially steady state must be assumed for this period of flight, even though some changes could be noted when aircraft repeatedly passed the same point with respect to the storm center.

Table 1 contains the storms, levels, dates, maximum winds, etc., for which computations were performed. The ten levels with the asterisk are those where at least six radial legs were flown (except Cleo 820 mb. which had five radial legs). It is at these levels that field analysis of computed values could be made. A typical sample of a flight path along one of these levels is shown in figure 7.

Table 1. - Levels to which radial acceleration computations were made.

Storm	Date	Pressure Level (mb.)	Approx. Max. Wind at Flight Level (kt.)	Approx. Central Pressure (mb.)	Central Pressure Change	Storm Direction	Storm Speed (kt.)
Daisy	8-25-58	950	65	990	deepening	320	7
*Daisy	8-25-58	830	60	990	deepening	320	7
*Daisy	8-25-58	570	60	990	deepening	320	7
Daisy	8-25-58	237	45	990	deepening	320	7
*Daisy	8-27-58	630	120	940	deepening then steady	030	8
*Daisy	8-28-58	620	105	945	filling rapidly	010	18
*Carrie	9-15-57	605	85	965	steady	310	12
*Carrie	9-17-57	690	95	970	steady	080	13
*Cleo	8-18-58	820	90	970	steady	015	14
*Cleo	8-18-58	580	85	970	steady	015	15
Cleo	8-18-58	255	50	970	steady	015	14
*Helene	9-24-58	635	60	995	deepening	320	10
*Helene	9-25-58	810	80	980	deepening	310	6
Helene	9-26-58	265	75	950	deepening	300	11

* Used in 10-level composite.

** Composite 1600 ft. and 2800 ft.

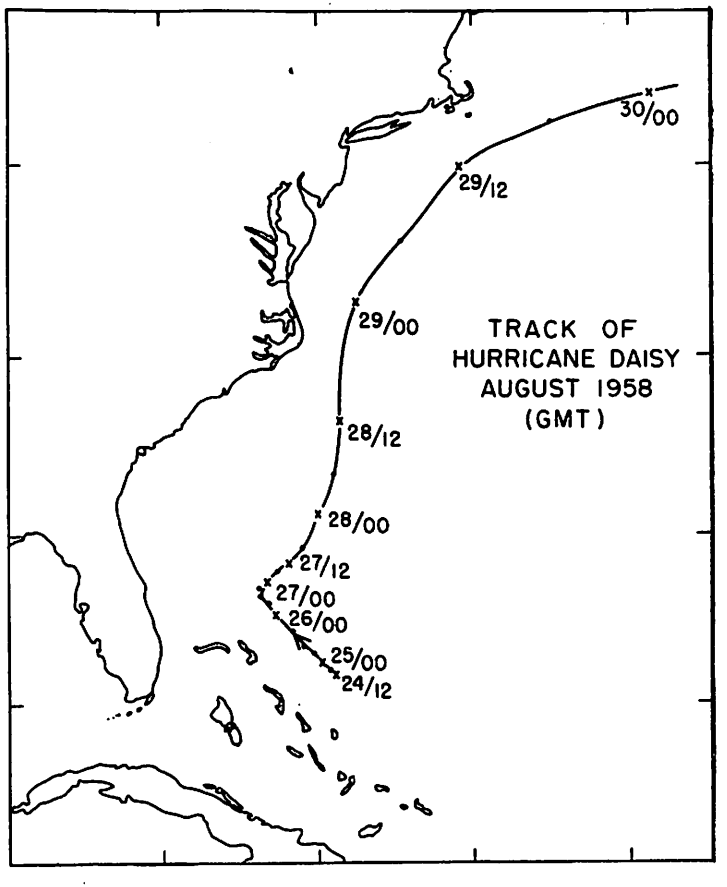

Figure 1.

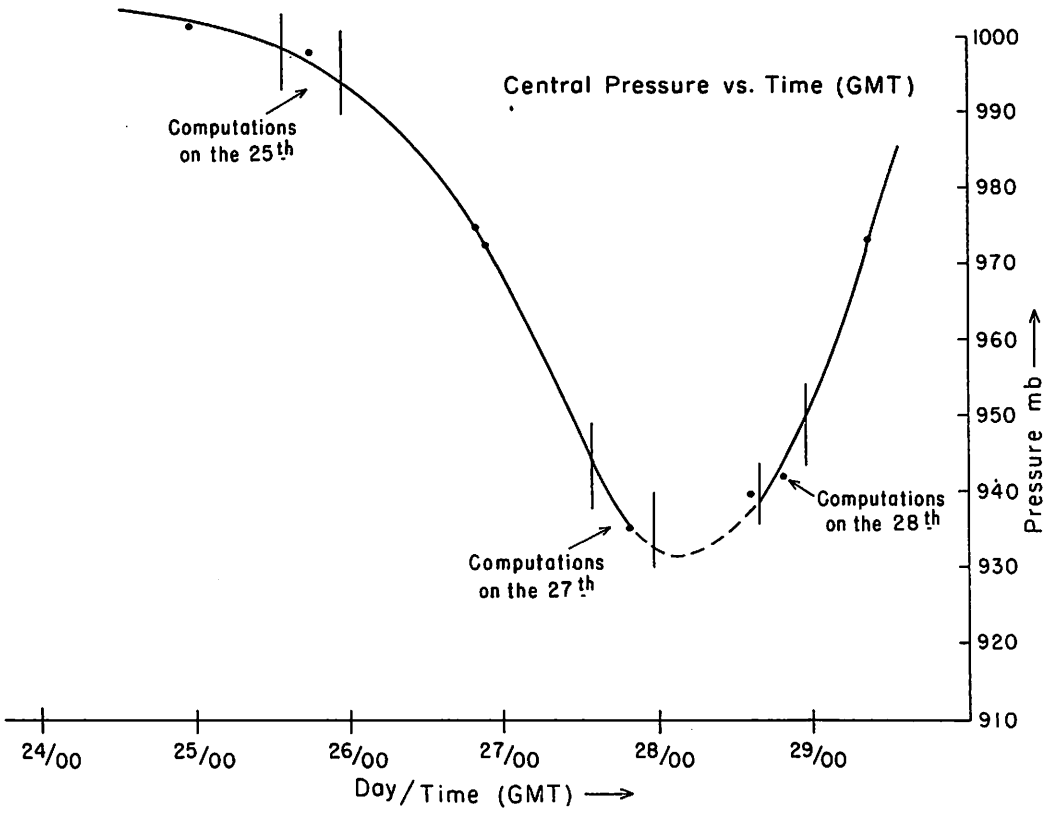

Figure 2. - Central pressure vs. date/time for hurricane Daisy.

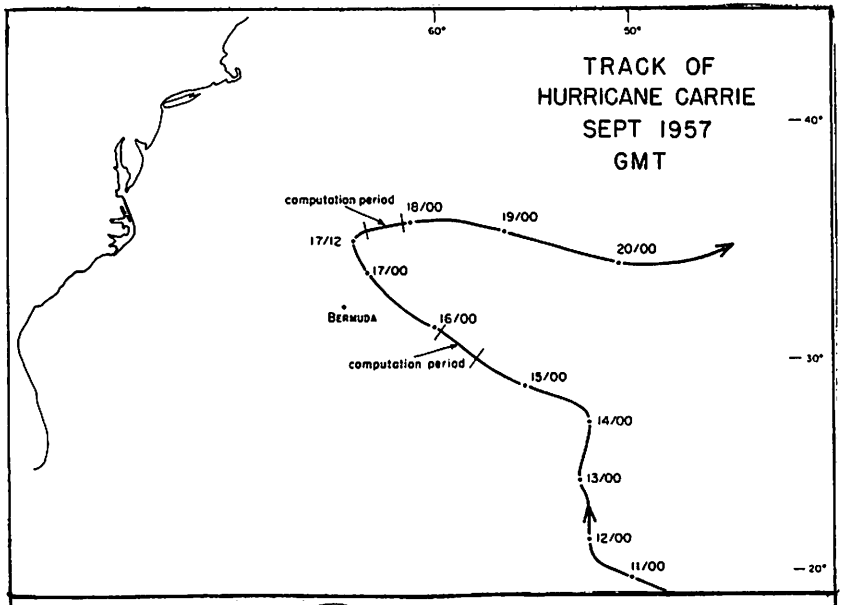

Figure 3.

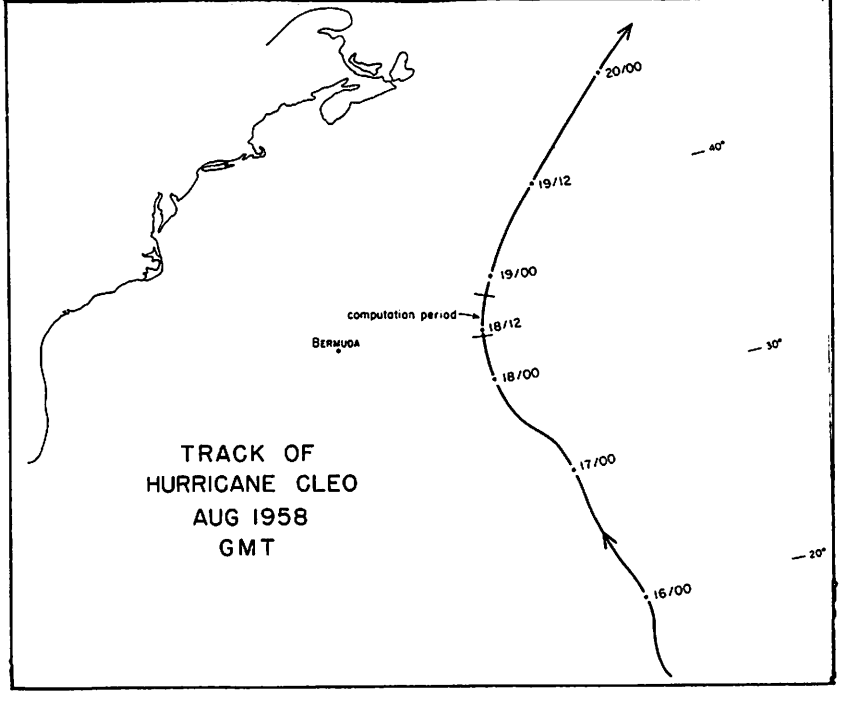

Figure 4.

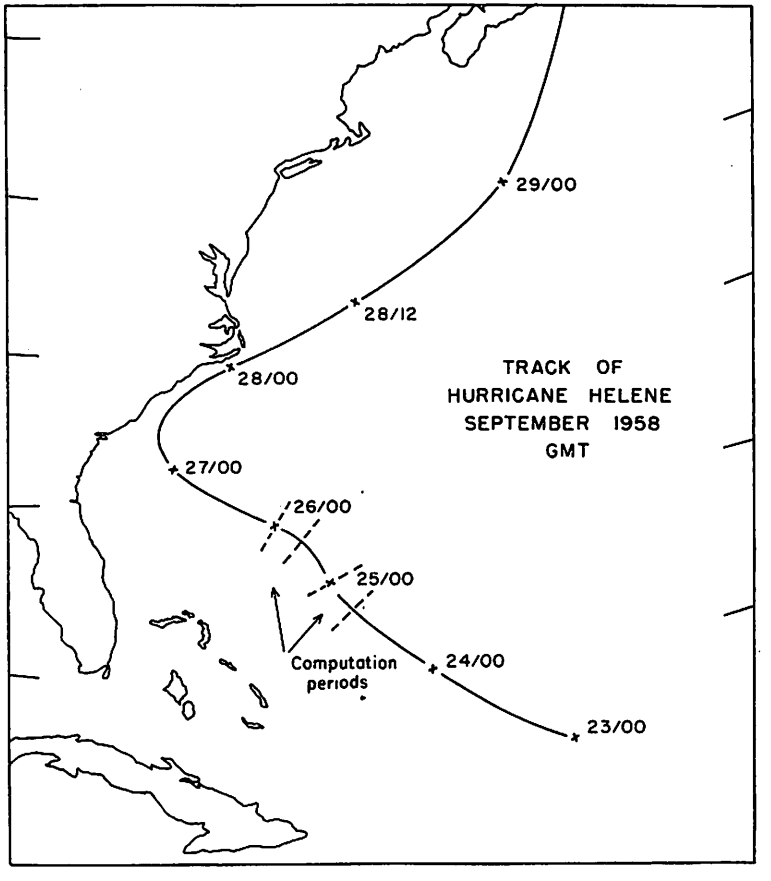

Figure 5.

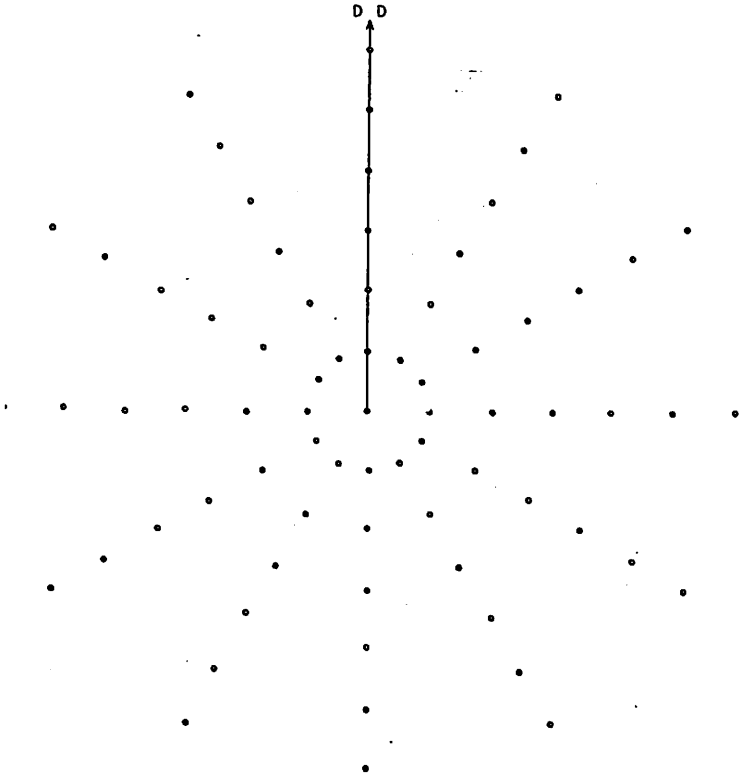

Figure 6. - Grid used in computations.

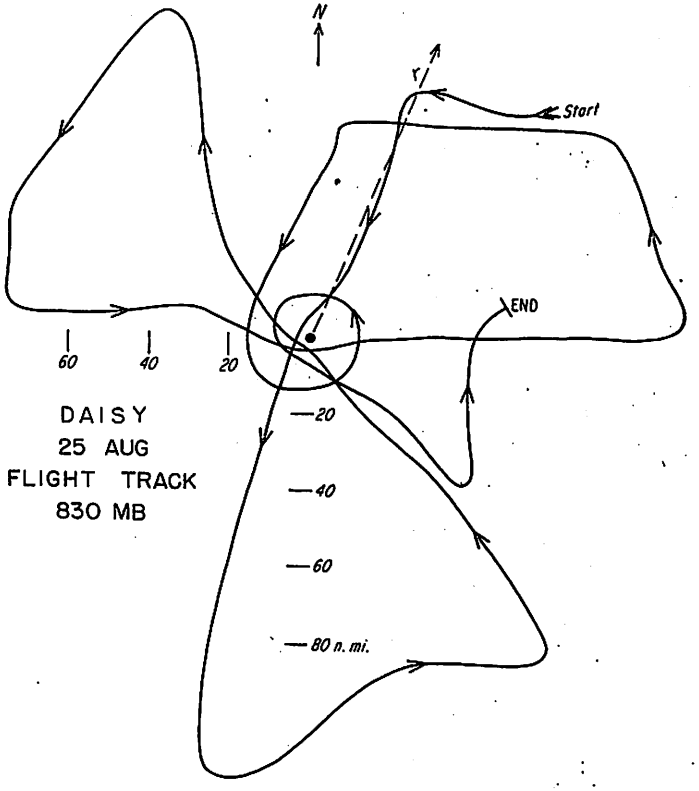

Figure 7. - Example of a flight path.

2. EQUATIONS OF MOTION AND COMPUTATIONAL PROCEDURE

Aircraft observations of necessity are taken in a mixed space-time coordinate system. But, as already stated, usually the complexity of the reference frame can be reduced by the assumption, usually valid in the first approximation, that the storm remains in essentially steady state for the duration of a flight mission. Granted this premise, all observations can be assigned a location in a coordinate system fixed with respect to the moving center. Given a plot of the data in this form, an investigation of the forces and accelerations present may be provided from a variety of viewpoints. Three of the most common approaches are the following:

(1) Computation of the actual forces with respect to the instantaneous center position along the radial and tangential axis of a polar coordinate system.

(2) A similar computation in a moving reference frame where at first the translatory storm velocity is subtracted from all winds, so that the wind field studied is that relative to the moving center.

(3) Computations in a natural coordinate system in which the forces acting on individual air particles are determined.

The last system, a Lagrangian one, is in some respects the most attractive. But computations depend on knowledge of the radius of trajectory curvature, a quantity which is not measured but must be obtained by indirect means based on the field distribution of data. In such a procedure the shortcomings of the steady state assumption and of the frequent wide gaps between flight legs are essential.

Now in hurricanes, much interest reasonably centers on the radial accelerations since they are related to the mass flow through the system and have the energy releases which produce and maintain these cyclones. Given the objective of investigating these accelerations, the first two coordinate systems are not subject to the difficulties encountered in the natural frame, so all requisite data are furnished by single radial flight legs of perhaps 15 minutes duration and the whole job can be done by machine process if desired. In contrast, calculations along the tangential direction not only give less promise of insight into the hurricane but they are also difficult to accomplish since airplanes cannot fly circles around hurricanes and since gradients of wind and pressure usually are very weak along this axis compared to the radial axis.

Since the course to be pursued will be to determine whatever is possible about radial accelerations, most calculations will be made with respect to the disturbance's center position since it is felt that the greatest importance resides in the radial coordinates. Later, however, the transformation of moving coordinates will be made as there is the advantage that local time changes are eliminated, and advective changes are then referred to the storm's center rather than to a point fixed on earth. Finally, radii of trajectory curvature will be determined from the polar coordinate grid at certain special points. This calculation will be made and the results compared with approximations of the radius of trajectory curvature from kinematic methods.

The polar coordinate system will be applied to constant pressure surfaces which then are treated as quasi-horizontal surfaces, where it may be noted that even in the areas with strongest pressure gradient the slope of a constant pressure surface will not exceed the order of 1:100 (pressure gradient of 2 mb./mile). The radius r will be considered positive outward and the polar angle θ positive counterclockwise. Given the horizontal velocity components v_r and v_θ along r and θ, the altimeter correction D, the acceleration of gravity g, and the time t, the cylindrical equations of motion are

$$\dot{v}_r = \frac{v_\theta^2}{r} + f v_\theta - g \, \partial D/\partial r + F_r \tag{1}$$

$$\dot{v}_\theta = - \frac{v_\theta v_r}{r} - f v_r - g \frac{\partial D}{r \partial \theta} + F_\theta \tag{2}$$

Here the dot denotes substantial time differentiation and F_r and F_θ are the components of the frictional force along r and θ, respectively. $\dot{v}_r$ is positive when directed outward along r. Only the first of these two equations will be treated in view of the preceding statement of objective.

Given $\dot{v}_r = 0$, $F_r = 0$, a type of gradient wind balance along r may be defined to be given by

$$\frac{\frac{v_\theta^2}{r} + f v_\theta}{g \frac{\partial D}{\partial r}} = 1 \tag{3}$$

The extent to which this equation is applicable will be determined.

Defining

$$\dot{v}_r)_{gr} = \dot{v}_r - F_r \tag{4}$$

equation (1) may be written

$$\dot{v}_r)_{gr} = \frac{v_\theta^2}{r} + f v_\theta - g \frac{\partial D}{\partial r} \tag{5}$$

The first calculation will be concerned with the question to what extent $\dot{v}_r)_{gr}$ may be neglected compared to the centrifugal, Coriolis, and pressure gradient terms; thus to what extent the pressure gradient balances the centrifugal and Coriolis terms. Later, the imbalances between these forces (if present) will be apportioned to the amounts of advective and/or frictional acceleration occurring.

These calculations were performed for flight legs which were radial or which departed little from the radial direction. This restriction would not be required for storms with tangential symmetry. Such symmetry, however, was not observed.

Computational Procedure - The computational procedure begins with the plotting of v_θ and of "D" values vs. radius on graph paper and the drawing of smooth curves of best fit through the data points (figs. 8 and 9). Scattering of individual values was not great and representative curves were obtained in all cases for v_θ; however, there remained some leeway in drawing the "D" profiles, especially close to the center.

Next, the curves of v_θ and "D" were divided into finite radial intervals starting at 5 n.mi. from the center, going outward. Integrating from r_1 to r_2 where $r_2 > r_1$, $g\int_{r_1}^{r_2} d\ D/dr\ dr = g(D_2 - D_1)$ where the total derivative has been substituted for the partial derivative. This is permissible since only a one-dimensional equation with r as independent variable is being solved.

Integration of the centrifugal acceleration is given by $\int_{r_1}^{r_2} v_\theta^2 / r\ dr = \overline{v_\theta^2} \ln r_2/r_1$, where $\overline{v_\theta^2}$ is the mean value of v_θ^2 between $\ln r_1$ and $\ln r_2$. This quantity is obtained by plotting v_θ^2 vs. ln r and taking mean values between chosen intervals of ln r. Figure 10 illustrates the method for graphical determination of $\overline{v_\theta^2}$ between the 10 and 15 n.mi. radii.

The Coriolis acceleration is obtained by solving $\int_{r_1}^{r_2} fv_\theta dr = f\overline{v}_\theta (r_2 - r_1)$, where $\overline{v_\theta}$ is the mean of v_θ between r_2 and r_1 and f is considered constant. Graphical determination of $\overline{v_\theta}$ is illustrated in figure 8.

The value of f at the location of the storm center was used for each computation period. The greatest latitudinal extent of the computations was only 2.50°. This is equivalent to a maximum variation of f at 25° of only 9 percent. Since the magnitude of the Coriolis acceleration was usually much less than that of the centrifugal term - especially at high wind speeds near the center where $f\overline{v}_\theta$ was less than 5 percent of $\overline{v_\theta^2}/r$ - the error in assuming f constant over the whole storm area is negligible. Therefore it was permissible to use a single value for each flight.

We may define

$$g\,(D_2 - D_1)_{gr} = \overline{v_\theta^2}\,\ln\frac{r_2}{r_1} + f\,\overline{v_\theta}\,(r_2 - r_1) \qquad (6)$$

where the subscript "gr" denotes the D-difference which the airplane should have observed with the wind field present (i.e. - in the case of $\dot{v}_r)_{gr} = 0$). This result may be compared with the observed or actual D-value gradient denoted by the subscript "act". We shall define

$$g\,(D_2 - D_1)' = g\,(D_2 - D_1)_{gr} - g\,(D_2 - D_1)_{act} \qquad (7)$$

where the prime denotes the "unbalanced" portion of the D-difference. Then

$$\int_{r_1}^{r_2} \dot{v}_r)_{gr}\,dr = +\,g\,(D_2 - D_1)',$$

or

$$\overline{\dot{v}_r)_{gr}} = g\,\frac{(D_2 - D_1)'}{r_2 - r_1} \qquad (8)$$

The computations corresponding to the radial traverse along the eastern leg of Daisy on August 25 at 830 mb. are shown in Table 2. Increments of $r_2 - r_1$ were taken as 5 or 10 n.mi. from 5 to 20 n. mi. radius, and as 10 n. mi. farther out. The largest radius to which computations could be carried was 60 to 80 n.mi. in most cases. These distances are quite sufficient for a description of the acceleration field in the outer storm areas. Inside of the 10 n.mi. radius computation could not usually be made due to uncertainties of center location. Results in the interval from 10 to 15 miles are, at times, questionable for the same reason.

Along the flight leg illustrated in Table 2, the gradient along r of D_{gr} exceeded that of D_{act} along r, so that $\overline{\dot{v}_r)_{gr}}$ was positive and directed outward. Profiles of both D_{gr} and D_{act} are shown in figure 9 for the whole traverse from west to east side of Daisy on August 25. Note that while the slope of the D_{gr} profile was greater than that of D_{act} in the east, the reverse was true in the west. The accumulated differences are substantial - about one-third of the total D-drop. Up to this point, the procedure was nearly rigorous. Finally a more qualitative step was taken.

Computed values of $\overline{\dot{v}_r)_{gr}}$ for each radial interval did not always yield smooth radial curves. This was caused partly by the integration intervals - i.e., only 5 to 10 n. mi. - but primarily it was due to the limit of accuracy to which the gradient of "D" could be measured. Whereas the winds are integrated over the radial interval of r_1 to r_2, the $D_2 - D_1$ values are obtained

Table 2. - Computations of $\dot{v}_r)_{gr}$ along eastern radial leg of Daisy August 25, 830 mb.

Radius (n.mi.)	$\ln \frac{r_2}{r_1}$	$\overline{v_\theta^2}$ (in 10^2 m.^{2}/sec.^{2})	$\frac{1}{g}\overline{v_\theta^2} \ln \frac{r_2}{r_1}$ (in ft.)	$\overline{v_\theta}$ (m./sec.)	$\frac{f}{g}$ dr (in ft.)	$\frac{\overline{f}}{\overline{v_\theta}} \frac{f}{g}$ dr (in ft.)	Total (in ft.) $\frac{1}{g}\overline{v_\theta^2} \ln \frac{r_2}{r_1} + \overline{v_\theta} \frac{f}{g}$ dr	Computed "D" profile (in ft.)*	Observed "D" profile (in ft.)*	Computed minus observed "D" profile (in ft.)	Gradient of "D" profile difference (in ft.)	Conversion factor for (kt./hr.)	$\dot{v}_r)_{gr}$ (in kt./hr.)*	$\dot{v}_r)_{gr}$ with dr increased (in kt./hr.)
5								-170	-170	0				
	.693	4.9	111	22	.2	4	115				+25	2.36	+59	+39
10								- 55	- 80	+ 25				
	.405	8.1	107	28.5	.2	6	113				+ 8	2.36	+19	+44
15								+ 58	+ 25	+ 33				
	.288	8.1	77	29	.2	6	83				+23	2.36	+55	+31
20								+141	+ 85	+ 56				
	.405	6.6	88	26	.4	10	98				+26	1.18	+31	+32
30								+239	+155	+ 84				
	.288	4.5	42	21.5	.4	8	50				+ 5	1.18	+ 8	+13
40								+289	+200	+ 89				
	.223	3.3	24	17.5	.4	7	31				+ 1	1.18	+ 1	+ 4
50								+320	+230	-190				
	.182	3.5	21	18.5	.4	7	28				+ 3	1.18	+ 4	+ 7
60								+348	+255	+ 93				
	.154	3.9	20	20.5	.4	8	28				+13	1.18	+15	+ 7
70								+376	270	+106				
	.134	3.4	15	17.5	.4	7	22				+ 2	1.18	+ 2	+ 9
80								+398	290	-108				

*D-values are given in feet as in the original data. Accelerations are expressed in kt./hr. They have not been converted to c.g.s. units because it was felt that 1 kt./hr. imparts a feeling for the physical magnitudes involved more readily to most readers that 1.4 x 10^{-2} cm.sec.$^{-2}$, its c.g.s. equivalent.

by reading off values at individual radii r_2 and r_1. The original readings (by eye) of radio and pressure altimeters from films of the photo-panel[1] cannot be considered to be more accurate than $\pm$ 10 feet, so that the observed "D" differences over small radial intervals cannot be regarded as exact, even when read from curves of best fit. In order to overcome this difficulty it was often necessary to increase the radial interval of integration to double or triple that chosen originally, especially at the inner radii, where tripling increased the radial interval from 5 to 15 n. mi. This step, although possibly eliminating microscale features, does not obscure hurricane-scale features.

Values of $\overline{\dot{v}_r)}_{gr}$ were plotted on maps at the mid-point of each radial interval $r_2 - r_1$, and isolines were drawn for selected values. A grid was then placed over the analyzed $\overline{\dot{v}_r)}_{gr}$ field in order to obtain averages around the storm at different radii. This averaging yields mean radial profiles of $\overline{\dot{v}_r)}_{gr}$. It should be noted that interpolation by qualitative chart analysis was left to the very end and that all results not depending on this step are free from the subjectivity of line drawing.

Henceforth in this paper the symbol $\overline{\dot{v}_r)}_{gr}$, i.e., the mean value of $\dot{v}_r)_{gr}$ between the radial intervals $r_2 - r_1$, will be denoted just by the symbol $\dot{v}_r)_{gr}$ where the bar has been deleted. Only when averaging is performed around the storm at selected radii will the bar be included to denote circular averaging.

Nearly all computations performed and conclusions drawn in this paper are based on data obtained from the ten levels listed in table 3. These levels were the ten best covered by NHRP aircraft during the 1956 through 1959 seasons--where reliable wind and D-values were obtained.

[1]The altimeters were not included in the automatic data punching system.

Table 3. - Data on which computations based.

Storm and date	Level (mb.)	Max. Wind		Difference right-left quad. (kt.)	Speed of storm x 2 (kt.)	Column 4 / Column 5 (kt.)
		Right quad. (kt.)	Left quad. (kt.)			
Daisy Aug 25	830	65	35	30	14	≈ 2
Daisy Aug 25	570	60	45	15	14	≈ 1
Daisy Aug 27	630	120	85	35	16	≈ 2
Daisy Aug 28	620	105	55	50	36	≈ 1.5
Cleo Aug 18	820	90	50	40	28	≈ 1.5
Cleo Aug. 18	570	85	45	40	28	≈ 1.5
Carrie Aug 15	605	85	50	35	24	≈ 1.5
Carrie Aug.17	690	95	65	30	26	≈ 1.25
Helene Sept 24	635	60	55	5	20	≈ .25
Helene Sept 25	810	80	55	25	12	≈ 2

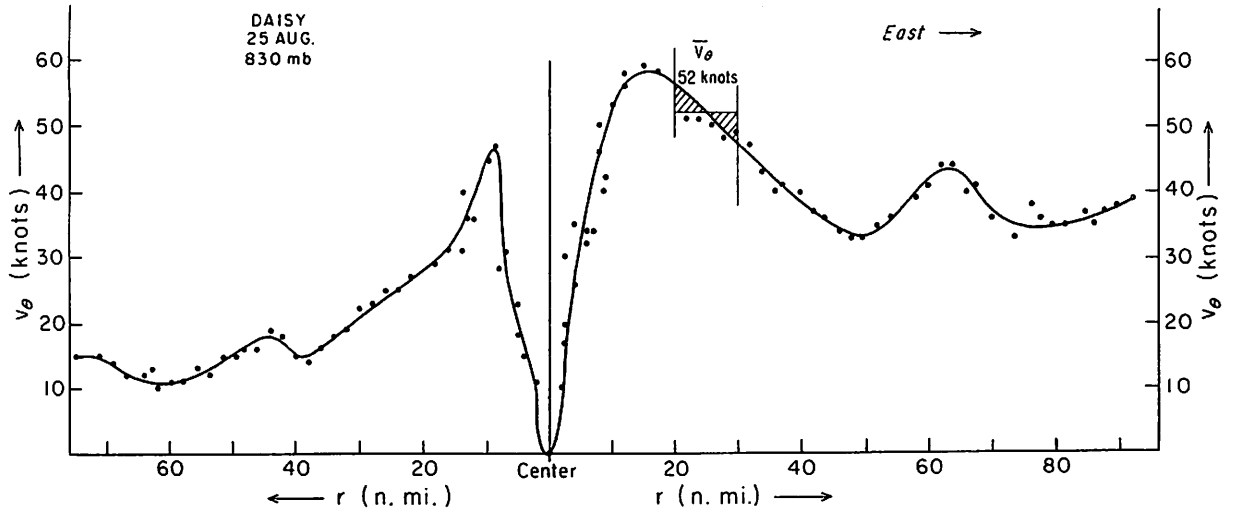

Figure 8. - Profile of the tangential wind (v_θ) on a west-east traverse through the center of Daisy. August 25, 830 mb.

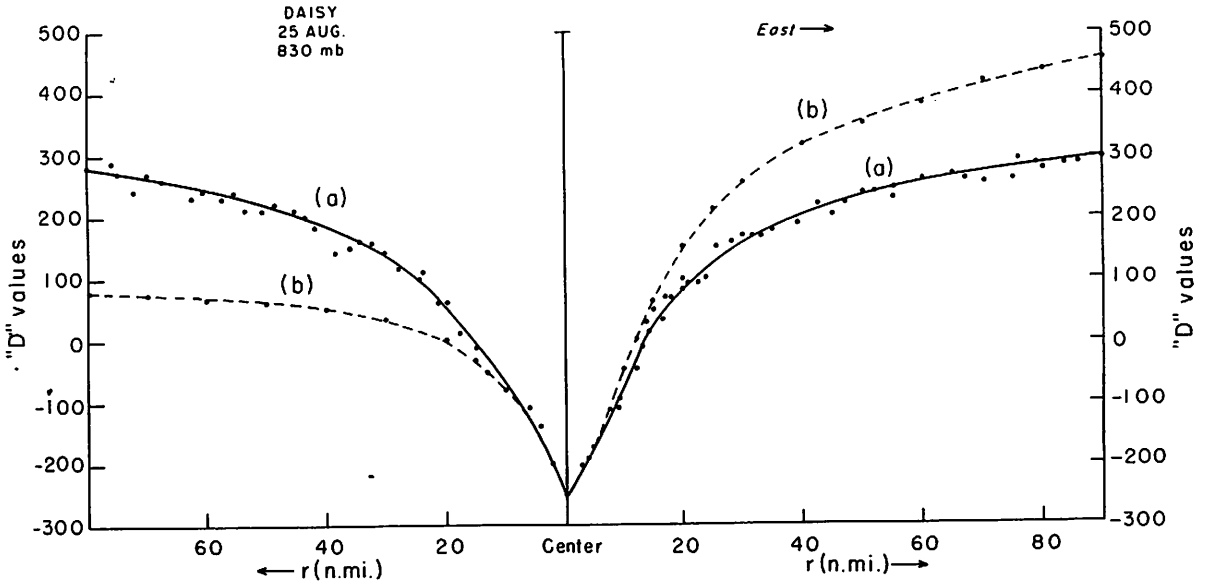

Figure 9. - West-east "D" value profile through the center of Daisy that goes with the v_θ profile in figure 8 . Curve (a), Actual "D" profile. Curve (b), Computed "D" profile (i.e. D_{gr}).

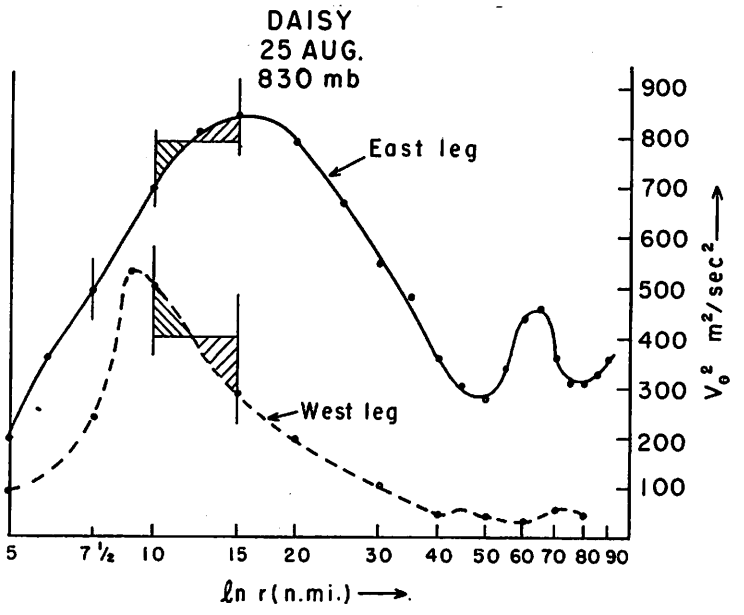

Figure 10. - Comparison of v_θ^2 (m.^{2}/sec.^{2}) profiles along the east and west legs of the traverse through Daisy on the 25th at 830 mb. Values of v_θ^2 are plotted against ln r.

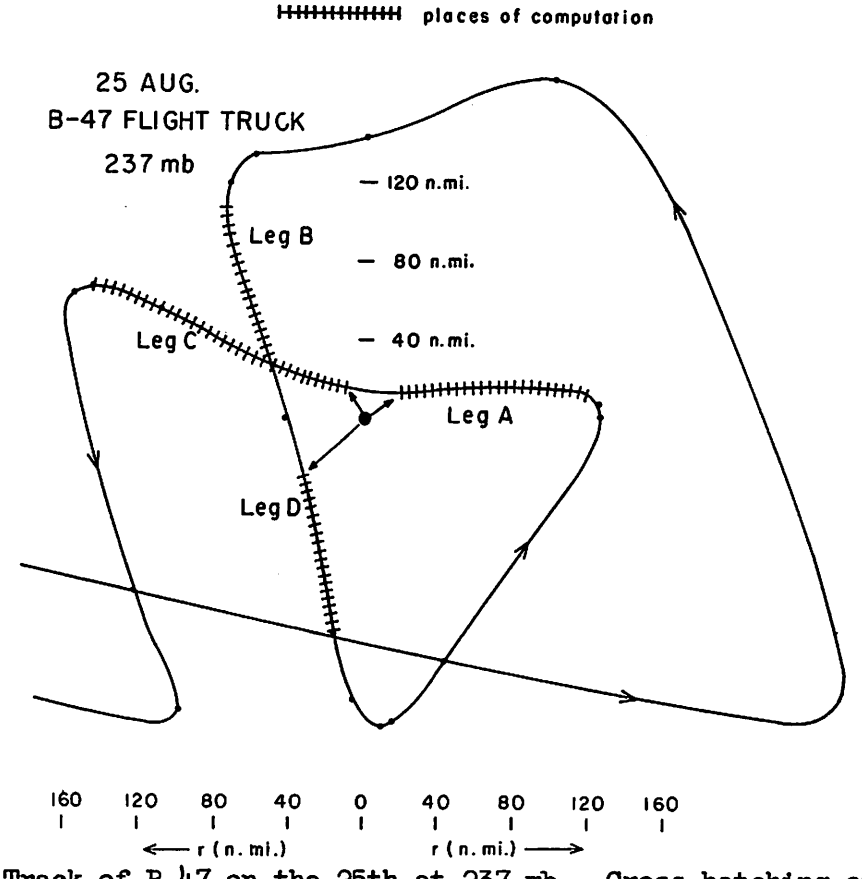

Figure 11. - Track of B-47 on the 25th at 237 mb. Cross-hatching on the track lines indicate places where the $\dot{v}_r)_{gr}$ computation was performed.

3. RESULTS

Radial accelerations - relative to a fixed storm center $(\dot{v}_r)_{gr}$.

Figures 12, 16, 20,24,28,32,36,40,44,48 portray the calculated values of $\dot{v}_r)_{gr}$ along the radial legs at the levels with the asterisk in table 1. All ten levels have large $\dot{v}_r)_{gr}$ values, which shows that the radial gradient wind equation as here defined relative to the fixed storm center (equation 3) does not express the balance of forces along the radial direction. In nearly all cases, the areas of strongest winds were places of large positive $\dot{v}_r)_{gr}$ and the areas of weakest winds places of large negative $\dot{v}_r)_{gr}$. Areas of positive $\dot{v}_r)_{gr}$ were always found in the right quadrants[2] where the winds were the strongest, and negative $\dot{v}_r)_{gr}$ values were found in the left quadrants where the winds were the weakest. With symmetrical pressure distribution around the storm, these would be the proper places for the respective $\dot{v}_r)_{gr}$ accelerations with an asymmetric wind field related, at least in part, to the storm's movement. However, this asymmetry in the wind field can seldom be accounted for by subtracting out the speed of the storm (table 3).

The order of magnitude of $\dot{v}_r)_{gr}$ was 10^1 to 10^2 kt./hr. over most portions of the hurricane with range from zero to approximately 300 kt./hr. The average absolute maximum for all storm levels was between 100 and 200 kt./ hr. These magnitudes are a large fraction of the radial pressure gradient or radial Coriolis and centrifugal accelerations.

Figures 15, 19, 23, 27, 31, 35, 39, 43, 47, 51 contain area distributions of the ratio $\overline{\dot{v}_r)_{gr}}/(f\,\bar{v}_\theta + \bar{v}_\theta^{\,2}/r)$ for the ten levels with the asterisk in table 1. It was unexpected that $\dot{v}_r)_{gr}$ would be so large a fraction of the centrifugal plus Coriolis accelerations. In many places, especially in the western quadrants (Daisy, August 25, 830 mb.; both lower Cleo flights; and Carrie, September 17), this ratio exceeded unity. There the radial pressure gradient force greatly exceeded the radial centrifugal and Coriolis acceleration.

---

[2]The right front quadrant is the area in the 0° to 90° sector - when the direction of movement of the storm is taken as the zero degree line on a 360° compass, counting clockwise. Other sectors have corresponding relations.

Figures 52-55 portray mean radial profiles of $\overline{\dot{v}_r})_{gr}/(f\,\overline{v}_\theta + \overline{v}_\theta^2/r)$ for all ten levels. There $\overline{\dot{v}_r})_{gr}/(f\,\overline{v}_\theta + \overline{v}_\theta^2/r)$ was averaged around the storm at 30° intervals without respect to sign. There are rather large variations between the individual curves, but the storm levels varied in height, and the four storms differed in intensity, maturity, deepening tendency, etc. The large magnitudes of the ratios are, however, evident at all levels except in Daisy, August 27, 630 mb.

Figure 56 contains a radial composite of $\overline{\dot{v}_r})_{gr}/\left(f\,\overline{v}_\theta + \overline{v}_\theta^2/r\right)$ for all ten flights. There $\dot{v}_r)_{gr}$ averages between 50 and 60 percent of the radial centrifugal and Coriolis accelerations. A similar composite of the integrated radial profile of $\overline{\dot{v}_r})_{gr}/\left(\overline{g\partial D/\partial r}\right)$ shows that $\dot{v}_r)_{gr}$ averages 40 to 50 percent of the radial pressure gradient force. The difference between these two composites is due to the fact that the radial pressure force averaged 10 to 15 percent more than the radial Coriolis and centrifugal accelerations (to be discussed later). Figure 61 is a 10-level composite of the absolute values of $\overline{\dot{v}_r})_{gr}$, $\overline{g\partial D/\partial r}$, and $(f\,\overline{v}_\theta + \overline{v_\theta^2}/r)$ plotted against radius. An area composite $\dot{v}_r)_{gr}$, both with and without respect to sign is shown in figures 57 and 58. The area composite with respect to sign clearly shows the asymmetry of $\dot{v}_r)_{gr}$ between right and left quadrants of the storm. All area compositing was done with respect to the direction of motion of the storms.

Radial accelerations - relative to the moving storm center $(\dot{v}_{rr})_{gr}$.

The above results have shown the radial accelerations relative to the instantaneous fixed point of the storm's center. Accelerations relative to the moving storm center will now be considered.

By assuming that the storm moves at constant speed and direction, one can obtain these radial accelerations within the limits of accuracy of the data by subtracting the tangential component of the storm motion (c_θ) from total tangential wind component in equation 5.[3] Other terms which arise from this change of reference to the moving storm center are less than 5 kt./hr. and can be disregarded. This is over an order of magnitude lower than most of the computed $\dot{v}_{rr})_{gr}$ values. The acceleration of the storm displacement also enters into

[3]Rigorous verification of this has been accomplished from the absolute equations of motion in both vector and Cartesian form.

the calculations, but at the times of the calculations the storms were moving at nearly constant direction. Changes in the rate of displacement were also small - less than 1 or 2 kt./hr. Thus the acceleration of the hurricane's movement was neglected.

With these omissions, the equation for the radial acceleration relative to the moving storm center - here denoted by $\dot{v}_{rr})_{gr}$ - is

$$\dot{v}_{rr})_{gr} = -g \frac{\partial D}{\partial r} + f (v_\theta - c_\theta) + \frac{(v_\theta - c_\theta)^2}{r} ,$$

or

$$\dot{v}_{rr})_{gr} = \left(-g \frac{\partial D}{\partial r} + f v_\theta + \frac{v_\theta^2}{r}\right) - \left(f c_\theta + \frac{2 v_\theta c_\theta}{r} - \frac{c_\theta^2}{r}\right) \tag{9}$$

where c_θ is the tangential component of the storm's motion. It is defined positive in the direction of the storm motion. c_θ is thus positive in the right quadrant and negative in the left quadrant. Substituting from equation 5 we obtain

$$\dot{v}_{rr})_{gr} + \left(f c_\theta + \frac{2 v_\theta c_\theta}{r} - \frac{c_\theta^2}{r}\right) = \dot{v}_{r})_{gr} ,$$

or

$$\dot{v}_{rr})_{gr} = \dot{v}_{r})_{gr} - M \tag{10}$$

where

$$M = \left(f c_\theta + \frac{2 v_\theta c_\theta}{r} - \frac{c_\theta^2}{r}\right) \tag{11}$$

The term $f c_\theta$ was always less than 5 kt./hr., hence had little effect on the calculations. The absolute value of $2 v_\theta c_\theta / r$ was usually 4 to 6 times greater than c_θ^2 / r. It is then the $2 v_\theta c_\theta / r$ term that largely determines the value of M. Thus approximately

$$\dot{v}_{rr})_{gr} = \dot{v}_{r})_{gr} - \frac{2 v_\theta c_\theta}{r}$$

In general $\dot{v}_{rr})_{gr} < \dot{v}_{r})_{gr}$. In the right quadrants, where $\dot{v}_{r})_{gr}$ is positive, v_θ and c_θ are also positive so that the corrective term subtracts from $\dot{v}_{r})_{gr}$. In the left quadrants, with $\dot{v}_{r})_{gr}$ negative, v_θ positive, and c_θ negative, $\dot{v}_{r})_{gr}$ is also reduced. Since v_θ is greater in the right than in the left

quadrants, the effect of the correction is strongest in the right quadrants. In the front and rear of the hurricane the correction, of course, is not present as c_θ vanishes.

Values of M were computed and inserted in equation 10. The resulting $\dot{v}_{rr})_{gr}$ patterns differed from those of $\dot{v}_{r})_{gr}$ as follows.

(1) The values of $\dot{v}_{rr})_{gr}$ were generally smaller than those of $\dot{v}_{r})_{gr}$, being approximately 60 to 80 percent of the $\dot{v}_{r})_{gr}$ values.

(2) The positions of many of the $\dot{v}_{rr})_{gr}$ centers were shifted from those of the $\dot{v}_{r})_{gr}$ centers.

(3) Sometimes M exceeded $\dot{v}_{r})_{gr}$ in the right quadrants so that $\dot{v}_{rr})_{gr}$ became negative. In consequence, the area with negative $\dot{v}_{rr})_{gr}$ is very large compared with that of positive $\dot{v}_{rr})_{gr}$ on most of the levels analyzed.

Ten-level area composites of $\dot{v}_{rr})_{gr}$ both <u>with</u> and <u>without</u> respect to sign are shown in figures 59 and 60. Again compositing has been done with respect to the direction of motion of each storm. The composite without respect to sign resembles the $\dot{v}_{r})_{gr}$ pattern in the essential features: Maximum accelerations to the right and left of the direction of motion, respectively (fig. 60). This is an important result in that one might have expected the hurricanes to approach circular symmetry once the effect of center propagation was removed.

Figure 62 shows a radial composite plot of $\dot{v}_{rr})_{gr}$ and $\dot{v}_{r})_{gr}$ <u>without</u> respect to sign. Although some subjectivity is inherent in the averaging it is felt that when averaging is extended over ten storm levels, the important broad-scale features will stand out. It follows that neither the asymmetry nor the radial acceleration field itself is removed by defining the computation with respect to the <u>moving center</u>. Since most flight levels were in the middle troposphere, where the net mass inflow or outflow are small, one might have thought that $\dot{v}_{rr})_{gr}$ should vanish here, especially when integrated around the storm. Such, however, is not the case.

We shall now return to the $\dot{v}_{r})_{gr}$ fields and study their characteristics in relation to other storm features.

<u>Relation of the fields of $\dot{v}_{r})_{gr}$ to v_r and the maximum wind.</u>

Analysis of the fields of the actual radial component of motion at all middle and lower tropospheric levels showed that <u>in general</u> there was a line dividing inward directed and outward directed flow around the hurricane; further that this line usually closely bisected the areas of largest inward directed $\dot{v}_{r})_{gr}$ in the left quadrants and of largest outward directed $\dot{v}_{r})_{gr}$ in

the right quadrants (figs. 12, 14; 16, 18; 20, 22; 24, 26; 28, 30; 32, 34; 36, 38; 40, 42; 44, 46; 48, 50).

A coordinate system fixed to the moving storm center (i.e., one giving relative winds) would of course greatly reduce these winds and would not always show a similar radial pattern because the storm motion would have been subtracted from all the winds.

In the right and left front quadrants of the storm, v_r itself was predominantly directed outward. Inward directed motion occurred mainly in the rear quadrants. Thus in the right front quadrant v_r and $\dot{v}_r)_{gr}$ both pointed outward; in the left rear quadrant they both pointed inward. In the right rear quadrant, where the winds had inward radial components, this component decreased and reversed to the downstream side in agreement with the $\dot{v}_r)_{gr}$ field. The reverse was true for the left quadrant. This observation agrees with findings of a study by Ausman [1] who, working with surface ship data of many hurricanes, has shown that v_r is directed inward in the rear quadrants and outward in the front quadrants at radii from 2° to 6° latitude from the center. From the present findings this appears to be valid over the whole hurricane area, not only at these outer radii, but also near the center.

It is an interesting fact that v_r is zero approximately at the location of the maximum winds; there its sign changes from negative to positive looking downstream. $\dot{v}_r)_{gr}$ is also positive and has maximum values very near this change from negative to positive v_r.

Qualitatively, this coincidence provides insight on the production of the maximum winds. In the region of weak winds in the left quadrants, air is accelerated inward and acquires a large crossing angle toward lower pressure. After some time the wind speed increases sufficiently so that gradient balance in the radial direction is established ($\dot{v}_r)_{gr} = 0$). At this point, however, the mass is still crossing toward lower pressure and gaining kinetic energy. It then overshoots the radius of gradient equilibrium and continues toward the center with $\dot{v}_r)_{gr}$ directed outward. The speed increases until the air moves parallel with the contours of the isobaric surfaces. There the place of strongest winds and also the maximum $\dot{v}_r)_{gr}$ is reached. As the air then turns outward toward higher contours, both wind speed and $\dot{v}_r)_{gr}$ again decrease.

Comparison of the asymmetries of $g\,\partial D/\partial r$ and $(f\,\overline{v_\theta} + \overline{v_\theta^2}/r)$ around the storms.

The question may be asked whether the $\dot{v}_r)_{gr}$ field arises from asymmetries of the pressure gradient force, or of the $(f\,\overline{v_\theta} + \overline{v_\theta^2}/r)$ distribution around the center. In order to answer this question, the fields of D_{act} and D_{gr} were drawn on maps. At selected radii, the averages of D_{act} and of D_{gr} were determined. From a grid (fig. 6) spaced evenly at 30° intervals, the mean deviation from the average around the center was computed at each of the chosen radii.

Figures 63-72 portray the results. Curves (a) show the deviation of D_{gr} (i.e., the wind field), and curves (b) the deviation of D_{act} (i.e., the pressure field). Though the curves on the different days vary considerably, certain features nevertheless stand out. At all levels, except Helene September 24, 635 mb., the mean deviation of D_{act} never exceeded that of D_{gr}. Hence, asymmetry of the wind field in nine of the ten cases was then greater than that of the pressure field. This feature was especially prominent on three of the Daisy flights and in Cleo at 820 mb. This result does not obviously follow from the common knowledge that winds are stronger to the right than to the left of the direction of motion. One might have thought that the D_{gr} field would vary concomitantly with D_{act}. A radial composite for all ten levels is seen in figure 73. The deviation of the pressure field varies little with radius, while the D_{gr} deviations increase greatly toward the storm center. In the core of maximum winds the deviation of D_{gr} exceeds that of D_{act} by a factor of three. Symmetry in the pressure field is produced as the heat released in ascending towers is swept around the center by the strong winds; and the $\dot{v}_r)_{gr}$ field is related more closely to variations of the tangential wind around the storm than to variations of the pressure gradient.

Further analysis of $\dot{v}_r)_{gr}$ field in stationary coordinates.

As the actual radial wind component is rarely observed to exceed 25 kt., and as individual air parcels often blow through areas of $\dot{v}_r)_{gr}$ of 50 to 100 kt./hr. for 30 to 60 minutes, it follows qualitatively that $\dot{v}_r \neq \dot{v}_r)_{gr}$, at least over large portions of a hurricane. This interesting observation will now be analyzed by an attempt to compute $\dot{v}_r$ directly. In Eulerian coordinates

$$\dot{v}_r = \frac{\partial v_r}{\partial t} + v_\theta \frac{\partial v_r}{r\partial\theta} + v_r \frac{\partial v_r}{\partial r} + w \frac{\partial v_r}{\partial z} \qquad (12)$$

Only the term $(v_r)\ \partial v_r/\partial r$ can be evaluated directly from the flight data; the range of magnitude was 1 to 10 kt./ hr. after integration over 10 n.mi. radial legs. Most values were less than 5 kt./hr. however. The vertical advection term cannot be computed at all, but from general knowledge of vertical motion and vertical wind shear fields the order of magnitude should not exceed that of radial advection, again after integration over 10 n.mi. radial distances. The $(w)\ \partial v_r/\partial z$ term was thus neglected. For computing the tangential advection reliable v_θ fields are available through analysis; the weak link is $\partial v_r/r\partial\theta$ which was obtained by tabulating the analysis of v_r prescribed in this paper on the grid of figure 6. In spite of the weakness of the computation, systematic features of the tangential advection were obtained and reliable features should be revealed by the ten cases. The calculated magnitude of this term had the order of 10 kt./hr. with range from 0 to 50 kt./hr.

The quantity $\partial v_r/\partial t$ was determined by moving the v_r field across the fixed grid of figure 6 with the direction and speed of the storm motion. For the fast moving storms changes were computed from one-half hour before to one-half hour after the time when the v_r field center position was connected with the fixed grid center. For more slowly moving systems the time interval chosen for $\partial/\partial t$ was from one hour before to one hour after the time when the center position corresponded with the fixed grid center.

Initial expectation was that $\dot{v}_r)_{gr} = \partial v_r/\partial t + (v_\theta)\ \partial v_r/r\partial\theta + (v_r)\ \partial v_r/\partial r$ within computational limits. This proved not to be correct by wide margins. The Daisy flight of August 27 at 630 mb. provides a typical illustration. Figure 74 contains the field of $\dot{v}_r$, to be compared with figure 20. Only 40-60 percent of the $\dot{v}_r)_{gr}$ field are accounted for by $\dot{v}_r$. Broadly speaking, the orientation of the patterns and the center locations are in fair agreement. Figure 75 contains the difference field. From the earlier definition

$$F_r = \dot{v}_r - \dot{v}_r)_{gr} \qquad (13)$$

it must now be postulated that figure 75 represents the F_r field after subtraction of figure 20 from figure 74 in the sense of equation 13. Admittedly this postulated force field is exceedingly strong (10^{-1} to 3×10^0 dynes/unit mass). But in a strongly turbulent system such as the hurricane, the existence of such strong frictional forces should not be rejected a priori. Further comments on the magnitude of F_r will be offered shortly.

Figure 76 contains radial profiles of $\dot{v}_r)_{gr}$, F_r, and $\dot{v}_r$ averaged around the storm at 10 n.mi. intervals for Daisy, August 27, 630 mb. We see that F_r and $\dot{v}_r$ are nearly equal and average over half the $\dot{v}_r)_{gr}$ values. That $|F_r + \dot{v}_r| > |\dot{v}_r)_{gr}|$ at all radii is due to the lack of exact superpositioning of $\dot{v}_r)_{gr}$ and $\dot{v}_r$ centers.

Similar properties were obtained for the other hurricanes so that it was considered permissible to form the average of all ten cases, figures 61, 77, 78. Here also, F_r and $\dot{v}_r$ are nearly equal. F_r approaches 85 percent of $\dot{v}_r)_{gr}$ at radii from 30 to 60 n.mi., and 70 percent over the whole radial distance. Since $\dot{v}_r)_{gr}$ itself was a large fraction of $g\,\partial D/\partial r$, it follows that frictional and pressure gradient forces have roughly the same magnitude, at least over substantial portions of a hurricane.

In one respect, Daisy, August 27, 630 mb. was not typical, namely that it was the only level studied with net positive $\dot{v}_r)_{gr}$ values after integration around the center. The balancing frictional force had to be directed inward. Daisy on the 27th had reached maximum intensity, its winds were slightly stronger than the pressure gradient and $\dot{v}_r)_{gr}$ was directed outward. The storm was just beginning to fill at this time. In eight of the other nine cases, the pressure gradient force exceeded the centrifugal plus Coriolis acceleration - in the integral around the hurricanes. The net $\dot{v}_r)_{gr}$ field consequently was directed inward and F_r outward.

Figures 79 and 80 portray 10-level area composites with respect to storm direction of F_r with and without respect to sign. Figure 79 illustrates the predominance of outward directed F_r especially well. Figures 81 and 82 portray 10-level area composites of $\dot{v}_r$ both with and without respect to sign. It is clearly evident that the values of $\dot{v}_r$ are not of great enough magnitude to account for the $\dot{v}_r)_{gr}$ accelerations even when individual storm level superpositioning of these two fields is eliminated by the 10-level average.

The above calculations have determined the F_r accelerations relative to an instantaneous fixed point of the storm center. The frictional acceleration with respect to the moving storm center (denoted F_{rr}) is identical with that with respect to the instantaneous fixed center when the storm propagation is assumed constant.[4]

[4] See Appendix for clarification of this point.

Preliminary comments on the magnitude of F_r.

From the discussions of Osborne Reynolds [13] it appears possible to represent F_r by the Reynolds form of eddy stresses. In cylindrical coordinates, F_r then has four components,

$$\frac{\partial}{r\partial\theta}\,\widetilde{v'_\theta v'_r}\,,\quad \frac{\partial}{r\partial r}\,\widetilde{r\,v'^2_r}\,,\quad \frac{\partial}{\partial z}\,\widetilde{v'_r\,w'}\,,\quad \frac{\widetilde{v'^2_\theta}}{r}$$

where the wavy bar denotes area average and the prime represents deviations from this mean. In this form the term $\partial/\partial z\ \widetilde{v'_r w'}$ would be the vertical gradient of the horizontally integrated product of the radial and vertical wind eddies.

Evaluations of v'_r and v'_θ values and their tangential and horizontal gradients were made on a number of mid-tropospheric levels here studied from continuous pitot tube recordings mounted on the aircraft. These pitots measure small changes in atmospheric pressure as the aircraft travels along the radial and tangential legs. These minute pressure changes are converted into their equivalent eddy wind variations. From such information, the Reynolds stresses can be computed.

From the preliminary computations $\frac{\partial\widetilde{v'_\theta v'_r}}{r\partial\theta}$, $\frac{\widetilde{\partial r v'^2_r}}{r\partial r}$, and $\frac{\widetilde{v'^2_\theta}}{r}$ turn out to be quite small and cannot account for F_r. An order of magnitude estimate of the $\partial/\partial z\ \widetilde{v'_r w'}$ term, using determined values of v'_r from the pitot tubes and assuming Malkus' [10] and Riehl's[5] calculations of vertical velocities in hurricane cumulonimbus clouds indicates that this term may have the required magnitude. Vertical gradients of $\widetilde{v'_r w'}$ were determined with a two-layer model, i.e., estimates were made for the mid-tropospheric levels and zero values were assumed for the surface and the tropopause. This is a crude approximation, but it encourages one to seek further experimental data. With improved sampling and measuring techniques a reliable estimate of the importance of the $\partial/\partial z\ \widetilde{v'_r w'}$ term can be achieved. New instrumentation and special flight planning with NHRP aircraft is being contemplated for the 1961 and 1962 seasons with this purpose in mind.

[5] Calculations performed in University of Chicago meteorology laboratory class given by Prof. H. Riehl (1960).

Radius of trajectory curvature.

The gradient wind equation in natural coordinates on a constant pressure surface is

$$0 = -g\,\partial D/\partial n + fV + \frac{V^2}{R} \tag{14}$$

where V is the wind speed
n is distance measured perpendicular to V, and
R is the radius of trajectory curvature.

As mentioned in the introduction, this equation is difficult to solve since R is not observed directly; moreover, $\partial D/\partial n$ also is not always obtainable. However, at places where $v_r = 0$, n is along r, $\partial D/\partial n = \partial D/\partial r$, and $V = v_\theta$. At these locations $v_\theta^2/R + fv_\theta = g\,\partial D/\partial r$, and

$$R = \frac{v_\theta^2}{g\frac{\partial D}{\partial r} - fv_\theta} \tag{15}$$

The radius of trajectory curvature, as given by equation (15) can now be computed directly along the lines of $v_r = 0$ and may be compared with radii determined from kinematic methods. It is apparent that in view of the possible importance of frictional forces, deduced earlier, this comparison should not succeed. R was evaluated with equation (15) and kinematically with Blaton's formula for many places of the ten storm levels where $v_r = 0$ occurred along or close to a flight leg. As expected, R as given by equation (15) was consistently too small to the left and too large to the right of the direction of motion. If equation (15) is amended to include radial friction we have

$$\frac{v_\theta^2}{R} + fv_\theta = g\frac{\partial D}{\partial r} - F_r \tag{16}$$

Addition of equation (16) with the earlier obtained equation, i. e. --

$$\dot{v}_r - \frac{v_\theta^2}{r} - fv_\theta = -g\frac{\partial D}{\partial r} + F_r,$$

yields

$$\frac{v_\theta^2}{R} - \frac{v_\theta^2}{r} + \dot{v}_r = 0\ ,$$

or

$$R = \frac{v_\theta^2}{\frac{v_\theta^2}{r} - \dot{v}_r} \tag{17}$$

This formulation should yield correct values. Computed radii of trajectory curvature with equation (15) often are as low as 7-8 miles to the left and as large as 35 miles to the right of the direction of motion at radii of 20 miles from the center. Comparable values obtained with equation (17) are 12 and 27 miles respectively. These values obtained with equation (17) agree much

with the kinematically determined radii from Blaton's formula. Especially in the left quadrants of the storm is this discrepancy between equations (15) and (17) large.

Another approach, showing the non-validity of the gradient wind assumption in natural coordinates, is to assume $\partial D/\partial n = \partial D/\partial r$ in the areas where $\dot{v}_r)_{gr}$ is negative and compute the values of R necessary for balance from equation $V/R^2 + fV = g\,\partial D/\partial r$, or

$$R = \frac{V^2}{g\frac{\partial D}{\partial r} - fV} \qquad (18)$$

In practically all places where this calculation was performed values of R necessary for gradient wind balance in natural coordinates were smaller than the values of R determined kinematically by Blaton's formula or with equation (17).

This method has the advantage that it can be applied at places where $v_r \neq 0$. The assumption $\partial D/\partial n = \partial D/\partial r$ where $\partial D/\partial n$ always $\geq \partial D/\partial r$ is entirely permissible at places where $\dot{v}_r)_{gr}$ is negative. This assumption decreases rather than increases the difference between the R obtained from equations (15) and (17). Thus substitution of $\partial D/\partial r$ for $\partial D/\partial n$ in equation (14) increases R and causes computed values of R under the gradient wind assumption in natural coordinates to compare more favorably with kinematic and equation (17) determinations. Even with this substitution the computed differences in R in the frictional and non-frictional cases are appreciable.

It follows that the gradient or cyclostrophic assumption, usually made in hurricanes, can be in error by as much as 50 to 100 percent. One cannot hope to obtain the proper constraints in hurricane growth and maintenance with the cyclostrophic approach.

Condensation heating related to radial friction and deepening tendency.

If one averages the D_{act} values around the storm at constant radius at the grid points shown in figure 6 and plots these D_{act} values with respect to radius at 10 n.mi. intervals he obtains a radial profile of the actual "D" values as discussed at the beginning of the report. A similar profile of the D_{gr} values can also be made. If the two profiles are plotted together beginning at a uniform value at an outer reference radius, say 80 or 100 n.mi., the accumulative inward imbalance between the D_{act} and D_{gr} fields is portrayed (fig. 83). The 80 to 100 n.mi. reference radius is a reasonable starting point, since the major condensation warming occurred inside of this limit in all cases.

This integrated height difference between the D_{act} and D_{gr} profiles can be converted into a virtual temperature excess or deficit with the hydrostatic equation from the tropopause region downward, holding a high pressure surface, say 100 mb., constant. A positive integrated value of $(D_{gr} - D_{act})$ means

that the atmosphere is warmer than would be computed with the assumption $\dot{v}_r)_{gr} = 0$. A negative value of $(D_{gr} - D_{act})$ has the opposite meaning.

Heating of the air beyond that demanded for radial balance of forces will be denoted as "excess heating." Part of this heating, if present, is used to maintain the storm against frictional dissipation; another part is available to intensify the storm. There is thus a unique balance between frictional dissipation, intensification, and excess or deficit heating when values integrated around a hurricane are considered. Thus

[EXCESS HEATING] - [FRICTIONAL DISSIPATION] = [STORM INTENSIFICATION]

If the integrated value of $(D_{gr} - D_{act})$ from the outer to the inner storm radius is negative, then not enough condensation heat is relased to maintain the pressure gradient at the value needed to go with the wind pattern even in the frictionless case, and the storm must decay.

Of the ten levels analyzed, eight had large positive integrated values of $(D_{gr} - D_{act})$; i.e., strong excess heating. These hurricanes were deepening or moving in steady state. The other two cases (Daisy August 27, 630 mb.; August 28, 620 mb.) had slightly negative and slightly positive $(D_{gr} - D_{act})$ values, respectively, when averaged around the storm. The condensation heating, although large, that was occurring in Daisy on the 27th and 28th had no large residual to balance the dissipation of kinetic energy by friction. It was on the 27th that Daisy reached maximum intensity and began to fill. On the 28th Daisy was filling rapidly. Retarding frictional effects thus overweighed the generating effects of condensation heating on these two days.

Figures 84 and 85 show the predominance of negative $\dot{v}_r)_{gr}$ and $\dot{v}_{rr})_{gr}$ over positive values of these quantities. Negative values of $\dot{v}_r)_{gr}$ and $\dot{v}_{rr})_{gr}$ correspond to "excess heating" and are proportional to positive integrated values of $(D_{gr} - D_{act})$ from outside to inside of the storm, as shown by equations(8) and (9) when integration is performed in a negative sense along r.

These composite radial profiles, which include Daisy levels on August 27 and 28, bring out clearly the considerable excess of the observed D-value drop from outside to inside of the hurricanes above that required to balance centrifugal plus Coriolis accelerations when composites of the ten levels are made. In these diagrams $|\dot{v}_r)_{gr}|$ and $|\dot{v}_{rr})_{gr}|$ have been averaged around the storm without respect to sign (top curve) and divided into positive and negative parts. The major contribution to $|\dot{v}_r)_{gr}|$ and $|\dot{v}_{rr})_{gr}|$ is clearly seen to be made up of negative values of these quantities; i.e., positive $(D_{gr} - D_{act})$ or excess of pressure gradient over centrifugal and Coriolis acceleration. At some levels, notably the two Carrie flights (figs. 36 and 40) negative $\dot{v}_r)_{gr}$ or $\dot{v}_{rr})_{gr}$ values prevailed over nearly all of the flight level.

These large residual negative $\dot{v}_r)_{gr}$ accelerations are needed to maintain the storm against frictional dissipation and to deepen it. It is no coincidence that the two levels which showed little negative residual of $\dot{v}_r)_{gr}$ were the two where filling was beginning or taking place. Also it is no coincidence that steady state storms must have negative integrated values of $\dot{v}_r)_{gr}$ to balance frictional dissipation.

Condensation heating related to the wind and pressure field on August 25.

Daisy on August 25 was in the deepening stage (fig. 1, 2). Radial legs were flown along four distinct levels on this day (950, 830, 570, 237 mb.). An excellent and unique opportunity thus exists to obtain vertical gradients of the computed $\dot{v}_r)_{gr}$ fields and perhaps obtain some insight into the deepening process that was occurring on this day. At first, vertical thickness values were determined from the actual slopes of the isobaric surfaces and then converted to mean virtual temperature with the hydrostatic equation. Taking the mean virtual temperature in each layer at r = 100 n. mi. as reference temperature, the inward warming was computed over intervals of 20 n.mi. and plotted accumulatively from 100 n.mi. to the center (fig. 87). It is seen that nearly all warming took place inside the 40 n.mi. radius. The computed virtual mean temperature in the eye between 570 and 237 mb. was 4.5°C. warmer than the temperature in the same layer at the 100 n.mi. radius.

This computed cross-section agrees quite well with that obtained from the aircraft temperatures (fig. 88). Figures 87 and 88 corroborate a previous evaluation by Malkus [9], who, using the same data, had found that a good approximation to the D-field in the low troposphere could be obtained by assuming an undisturbed top in the high troposphere and integrating downward hydrostatically with the observed (virtual) temperatures.

We shall now approach the interesting question as to what fraction of this total temperature field is due to "excess" heating as defined above. For this purpose the D_{gr}-D_{act} profiles were plotted together on one diagram. If we set $(D_{gr}-D_{act})=0$ at the storm periphery and then plot $D_{gr}-D_{act}$ as a function of radius at each level, the unbalanced portion of the drop in height of the pressure surfaces will become readily apparent.

At the lower three pressure levels, the radial slope of the actual D-profile - after integrating around the hurricane at each level - exceeded that of the D_{gr} profile. At 237 mb., $(f\overline{v_\theta} + \overline{v_\theta}^2/r)$ exceeded g $\partial D/\partial r$. But $(D_{gr} - D_{act})$ integrated over the entire storm volume was negative. The four radial legs used for computation at 237 mb. are shown in figure 11. It was not possible to obtain values of $\dot{v}_r)_{gr}$ within the 20 n. mi. radius, and radial symmetry over a limited distance had to be assumed for computations along legs D and B. Nevertheless, the cross-hatched part of the curve in figure 86 is believed to be reasonably accurate.

Vertical changes in the profile of $(D_{gr} - D_{act})$ and hence also $\dot{v}_r)_{gr}$ when integrated around the storm, were quite small from 950 to 570 mb. The greatest vertical change in the profiles occurred between 570 and 237 mb.(fig.86).

The portion of the inward temperature increase arising from the $(D_{gr} - D_{act})$ profiles is shown in figures 89 and 90 in profile form. As noted earlier, computations as illustrated in figures 86 to 90 have a less secure basis than those performed along individual radial legs because they are dependent on field analysis by qualitative methods and subsequent integration around the center. If, however, it will be granted that no serious analysis error has been made, a quite interesting result has been obtained. Figures 89 and 90 may be interpreted as showing the heating function which gives rise to storm development and to circulation maintenance against internal and surface friction.

The "free" surface pressure fall at the ground, estimated from figures 89 and 90, is about 4 to 5 mb. - with the assumption of an undisturbed top at 50,000 feet. Some of this pressure fall must, by previous reasoning, be used up in internal and surface frictional dissipation. The amount of heating that is left over after this dissipation is used to intensify the storm. In the case of Daisy on the 25th, internal and surface frictional dissipation was smaller than the excess heating. It also follows that since development of the wind field lagged the pressure field, the drop in central pressure was the primary feature and occurred before intensification of the hurricane winds.

It would appear that from the local thermodynamic viewpoint, the action of the cumulus clouds in the initial disturbance must have been such as to produce a net area warming of the troposphere above 500 mb., with magnitudes of 1°C. above that ordinarily obtained from convection in disturbances.

If Daisy, as observed on August 25, is considered typical of developing hurricanes, then initial warming in the middle and especially in the upper troposphere may be postulated as a definite initial condition of hurricane development. In this connection, it is of interest to record that a reconnaissance plane of the U. S. Navy which scouted the cyclogenetic area about 12 hours before the research missions reached Daisy (2200-2400 GMT, August 24), observed a nearly solid precipitation area on radar with extent of about 10^4 n. mi.^{2} and convective echo tops above 40,000 feet in the precise area where Daisy was forming.

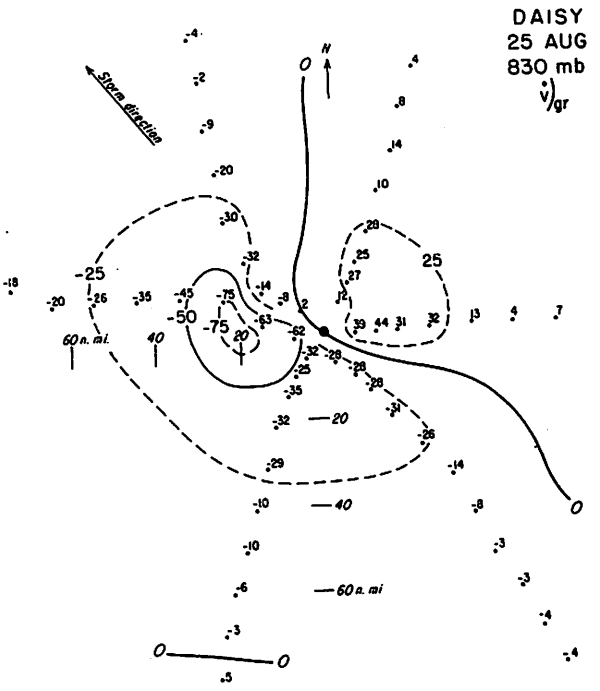

Figure 12.- $\dot{v}_{r})_{gr}$ in kt./hr.

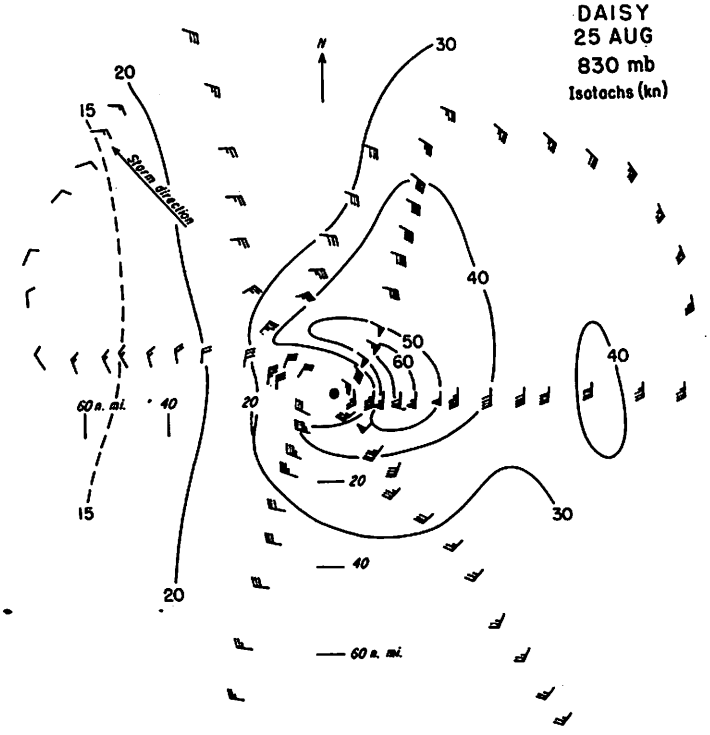

Figure 13.

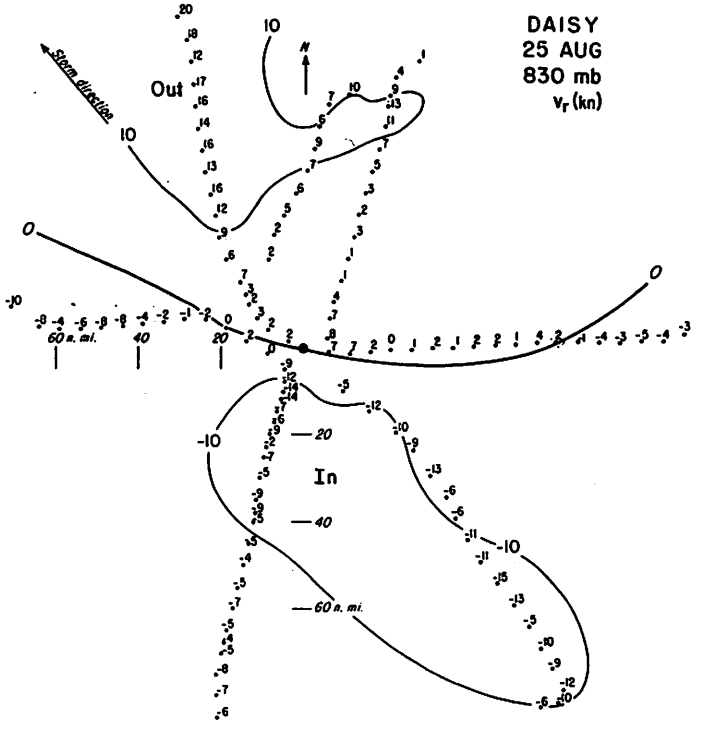

Figure 14. - Radial wind component.

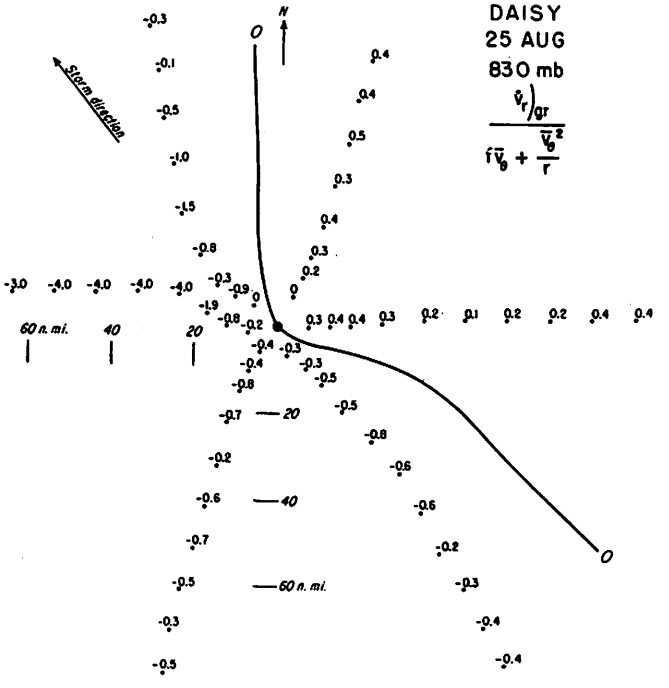

Figure 15.

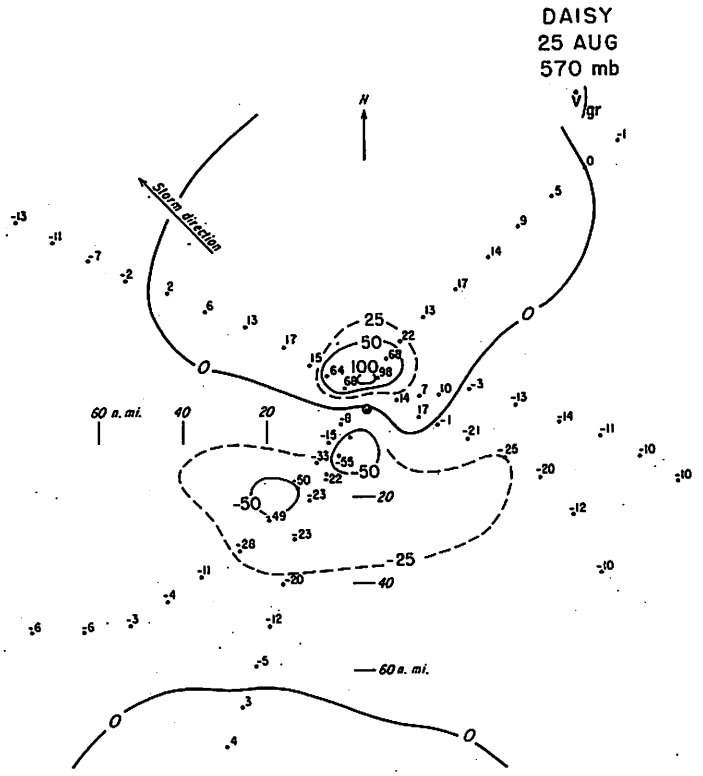

Figure 16. - $\dot{v}_r)_{gr}$ in kt./hr.

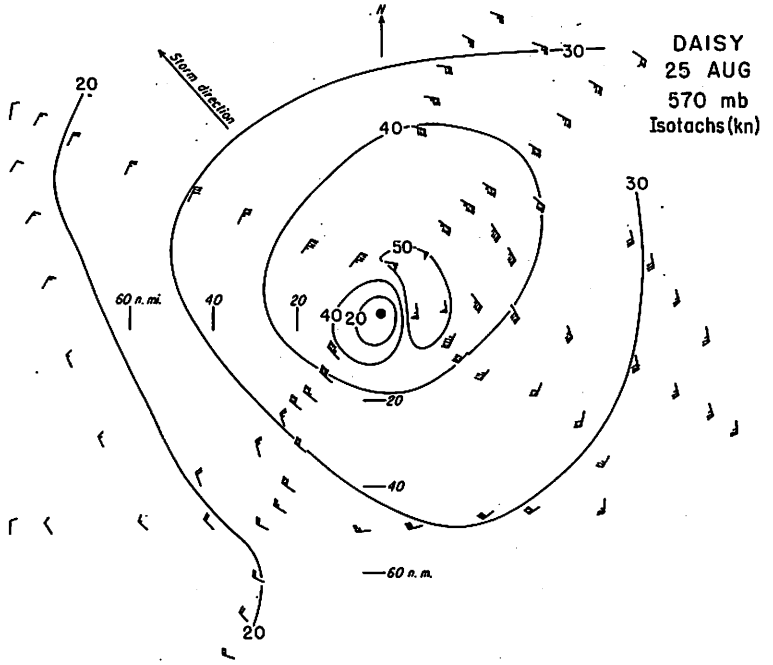

Figure 17.

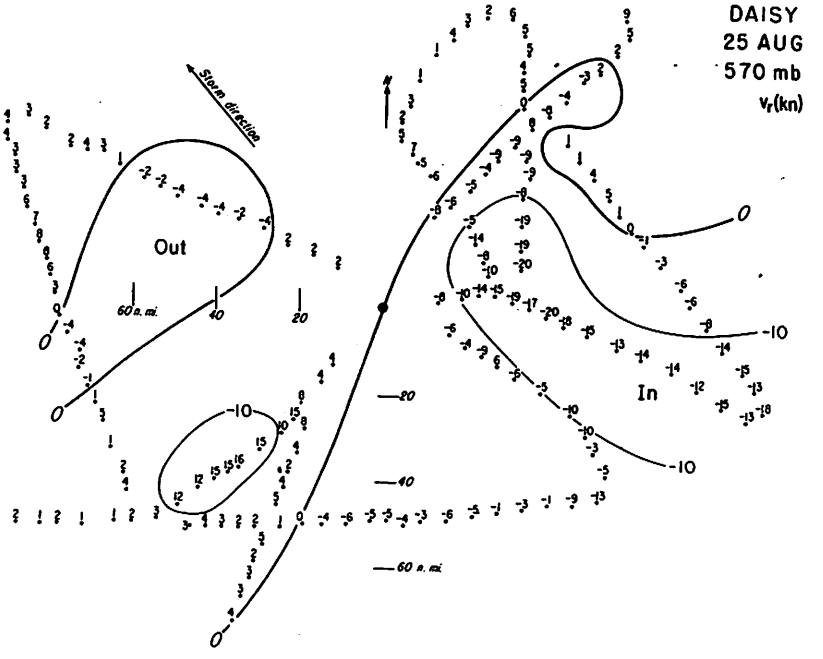

Figure 18. - Radial wind component.

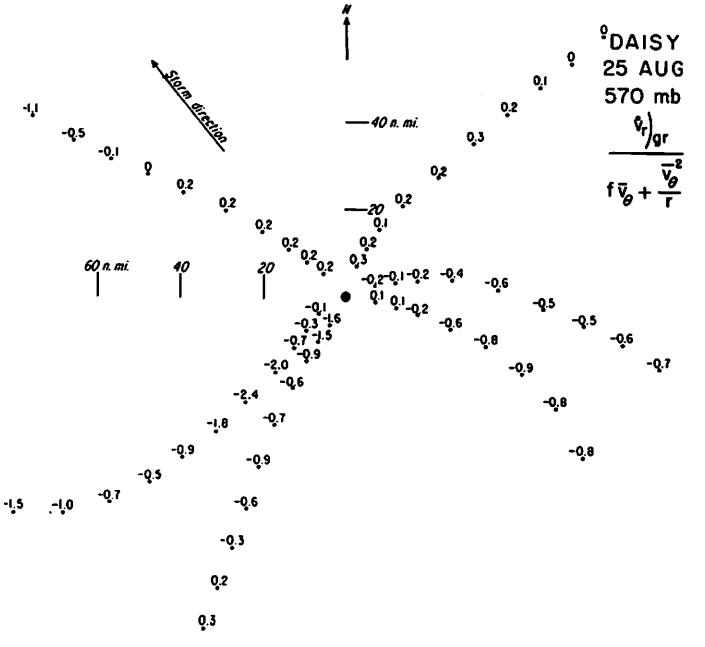

Figure 19.

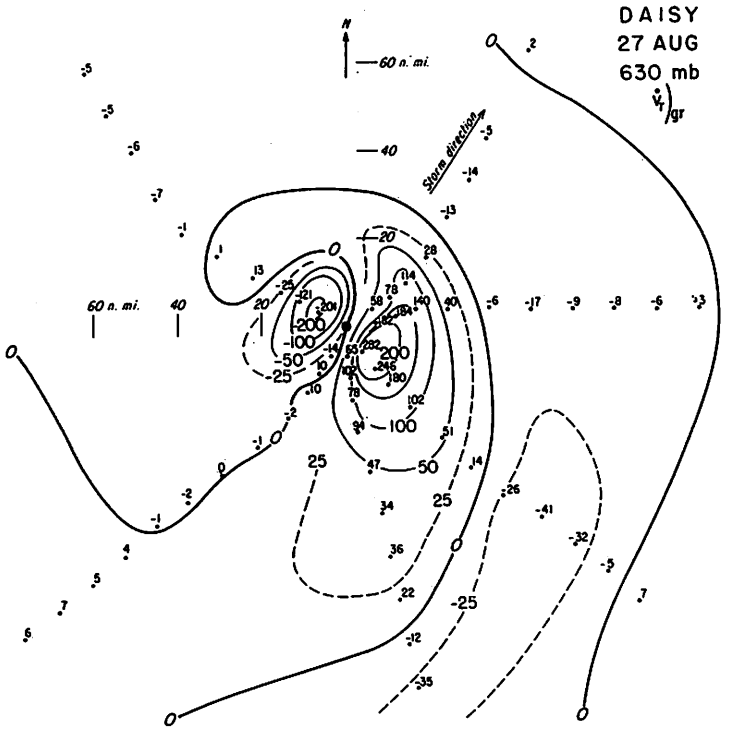

Figure 20. - $\dot{v}_r)_{gr}$ in kt./hr.

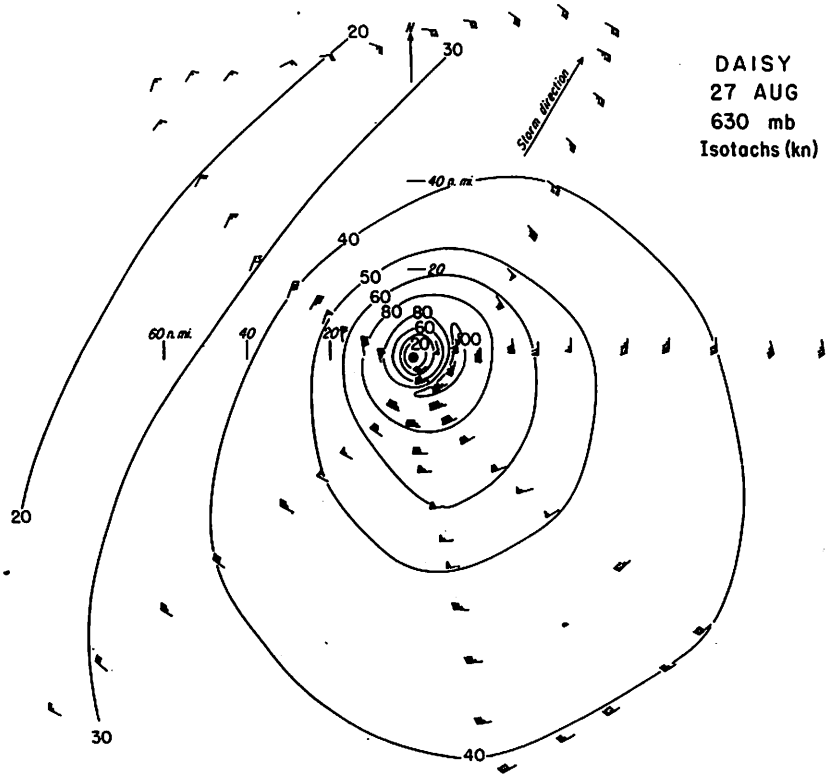

Figure 21.

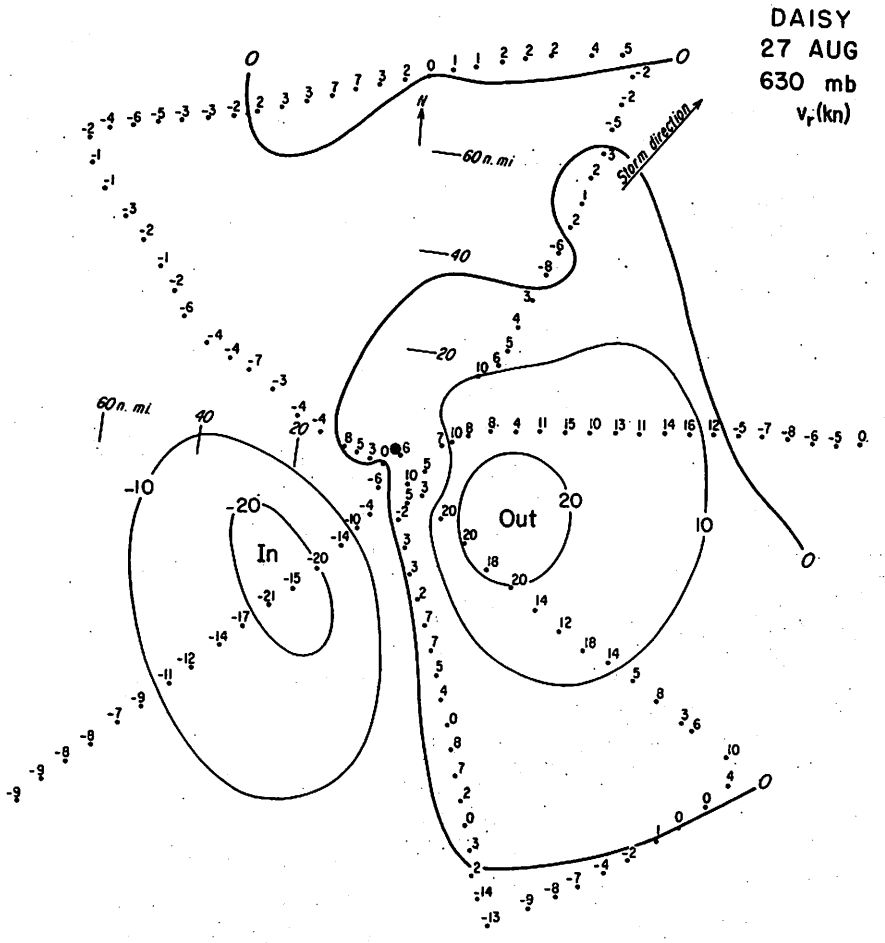

Figure 22. - Radial wind component.

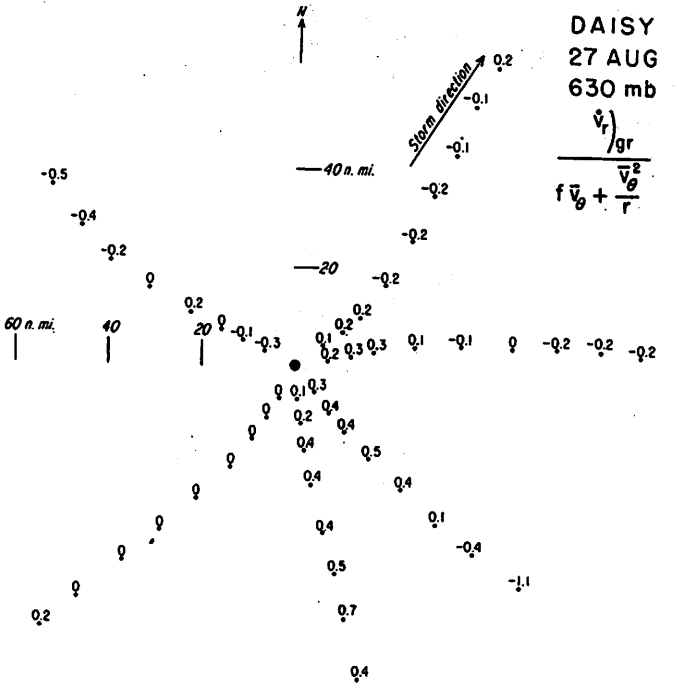

Figure 23.

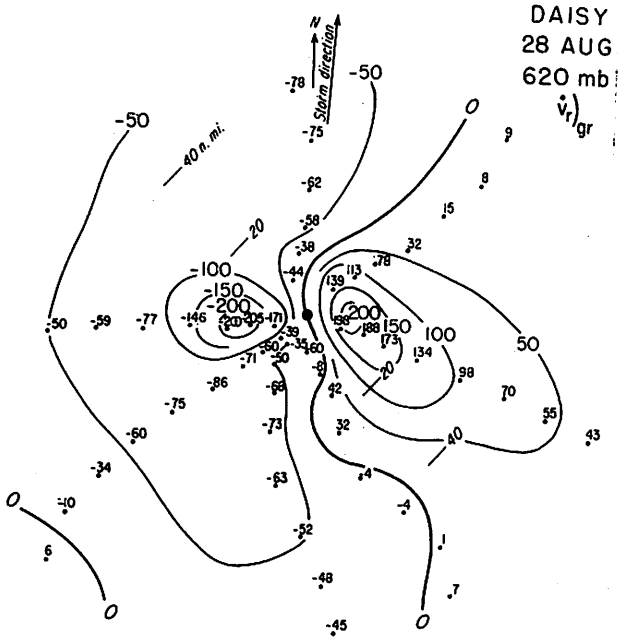

Figure 24. - $\dot{v}_r)_{gr}$ in kt./hr.

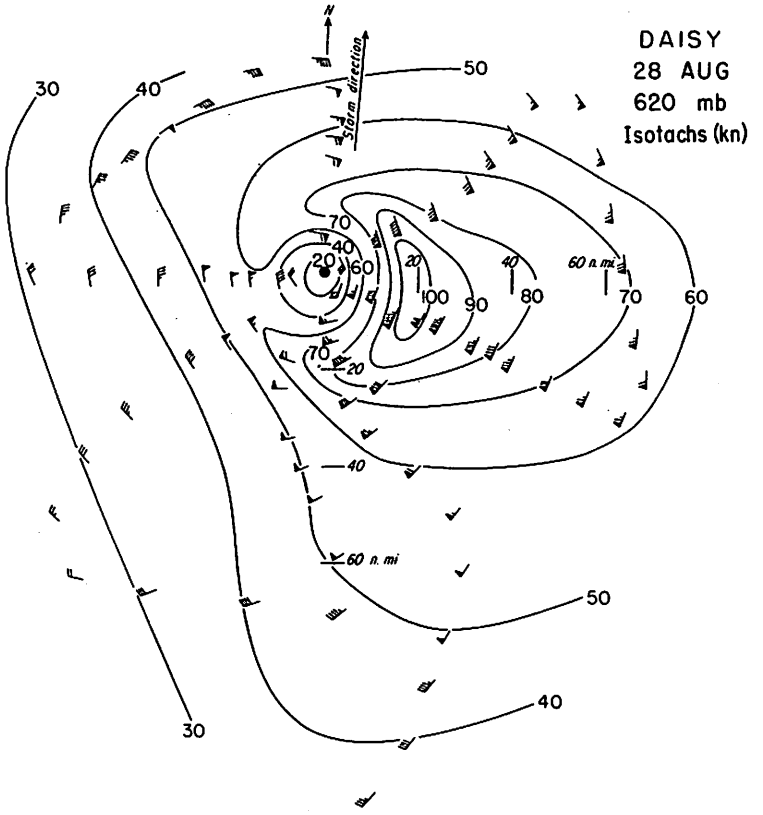

Figure 25.

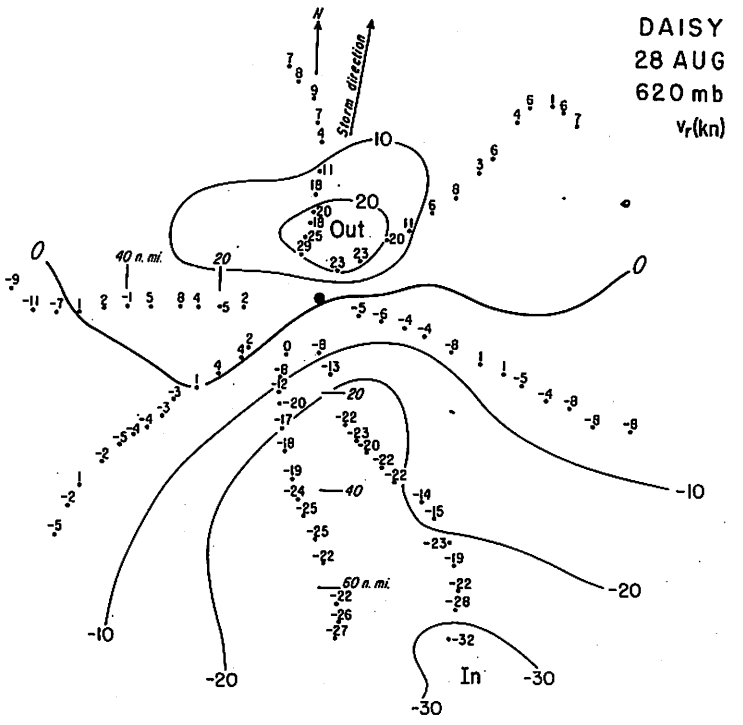

Figure 26. - Radial wind component.

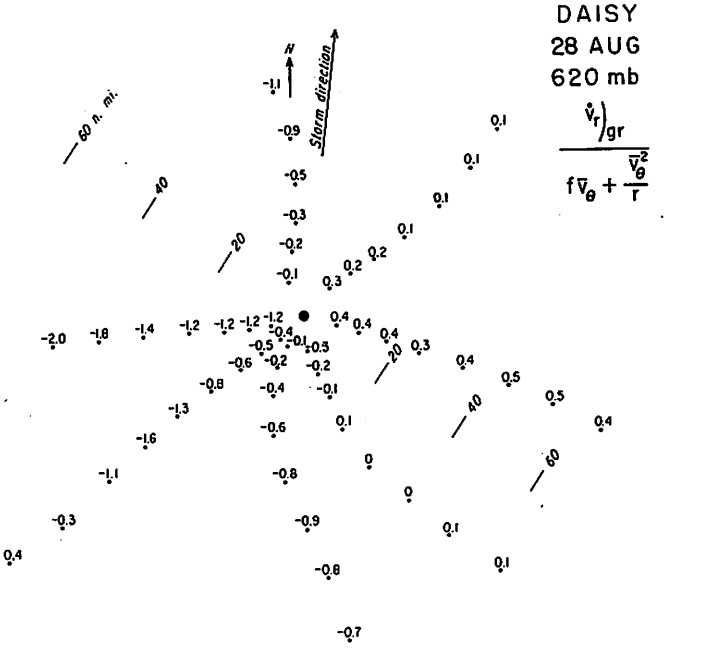

Figure 27.

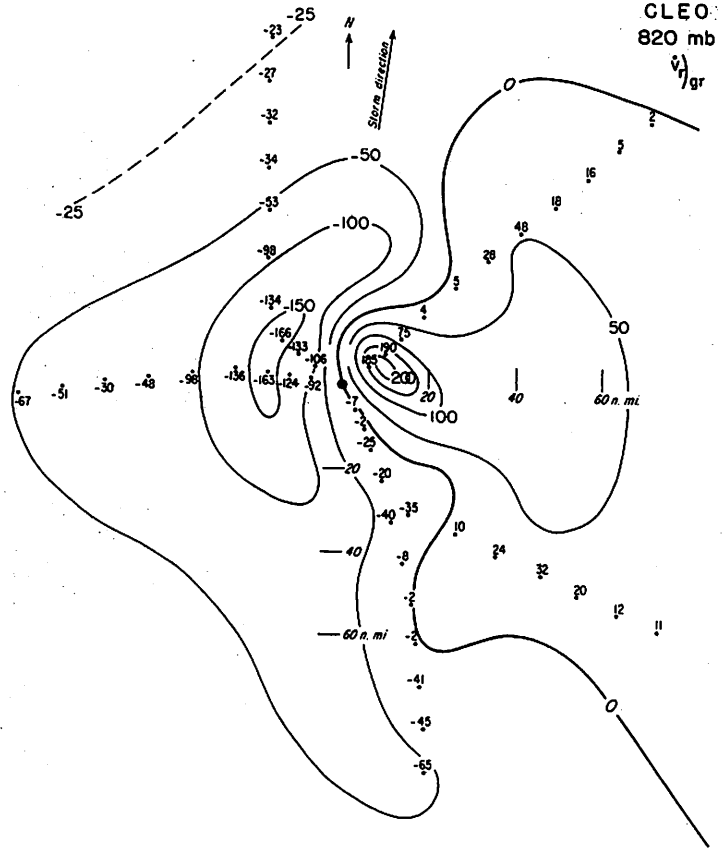

Figure 28. - $\dot{v}_r)_{gr}$ in kt./hr.

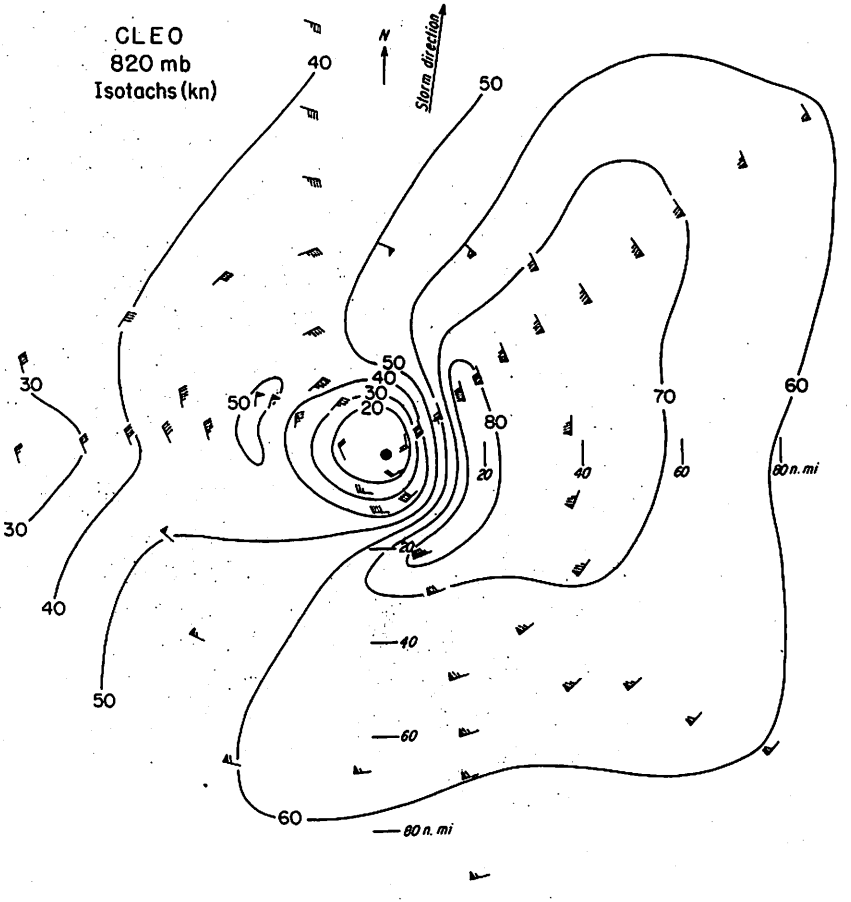

Figure 29.

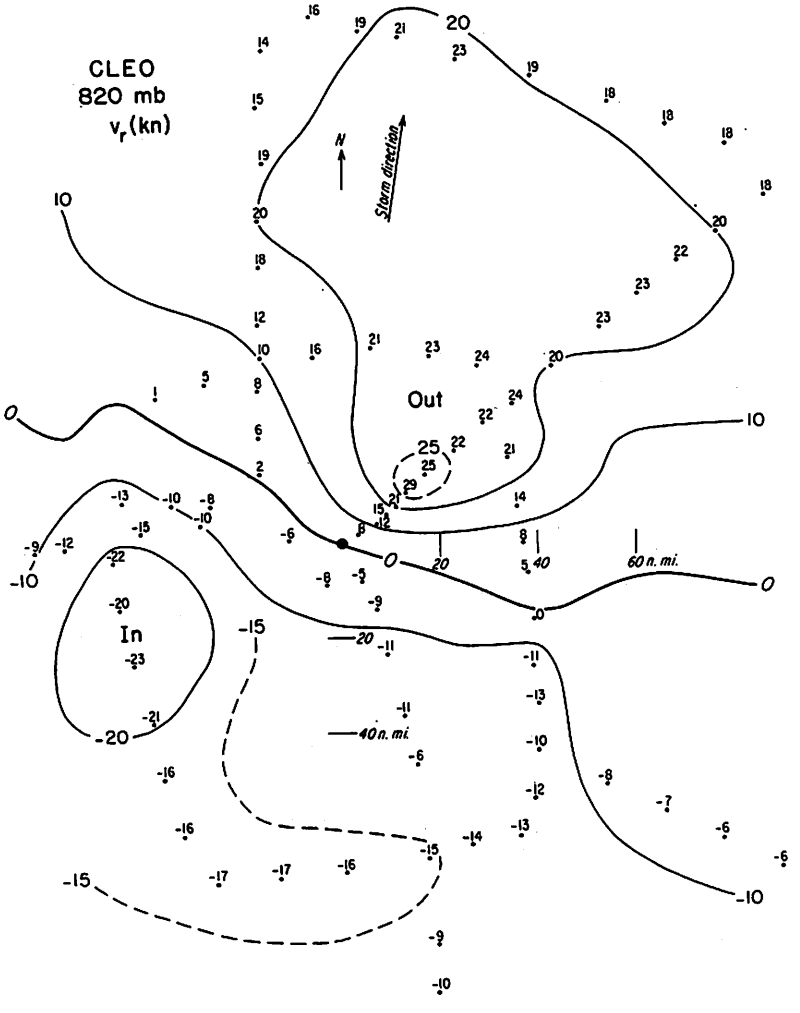

Figure 30. - Radial wind component.

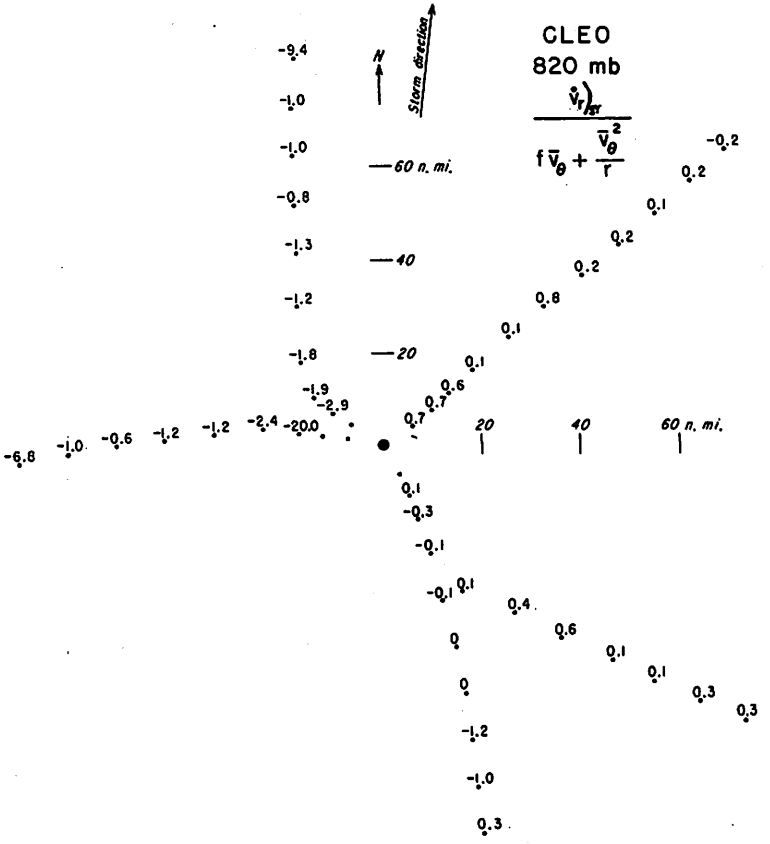

Figure 31.

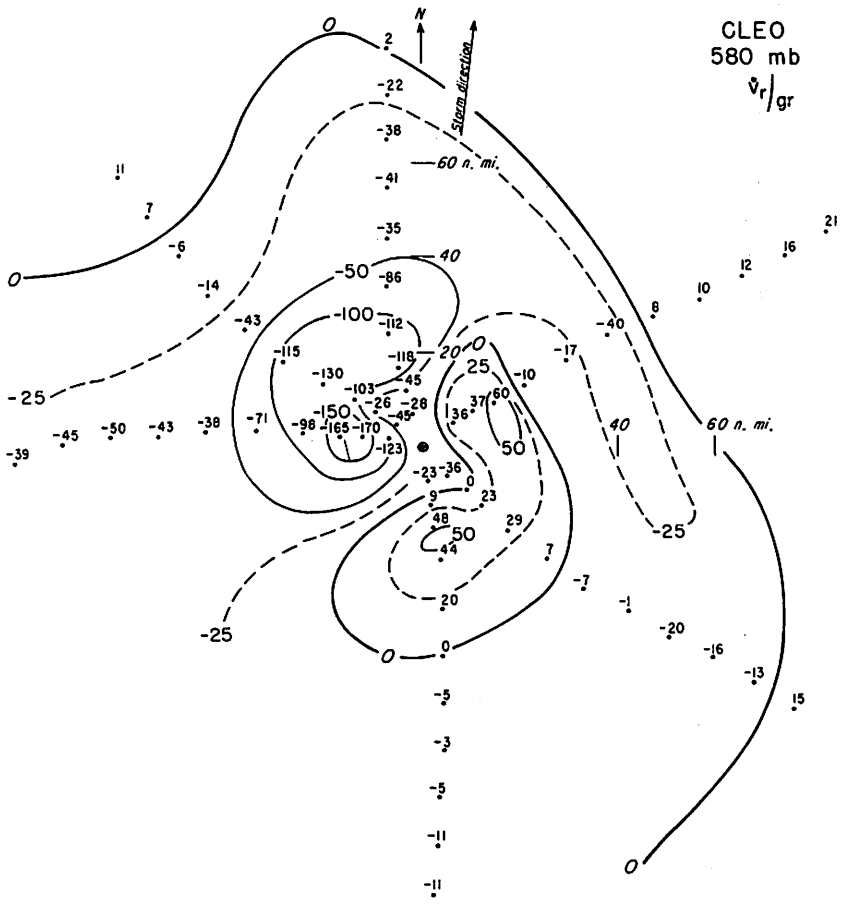

Figure 32. - $\dot{v}_r)_{gr}$ in kt./hr.

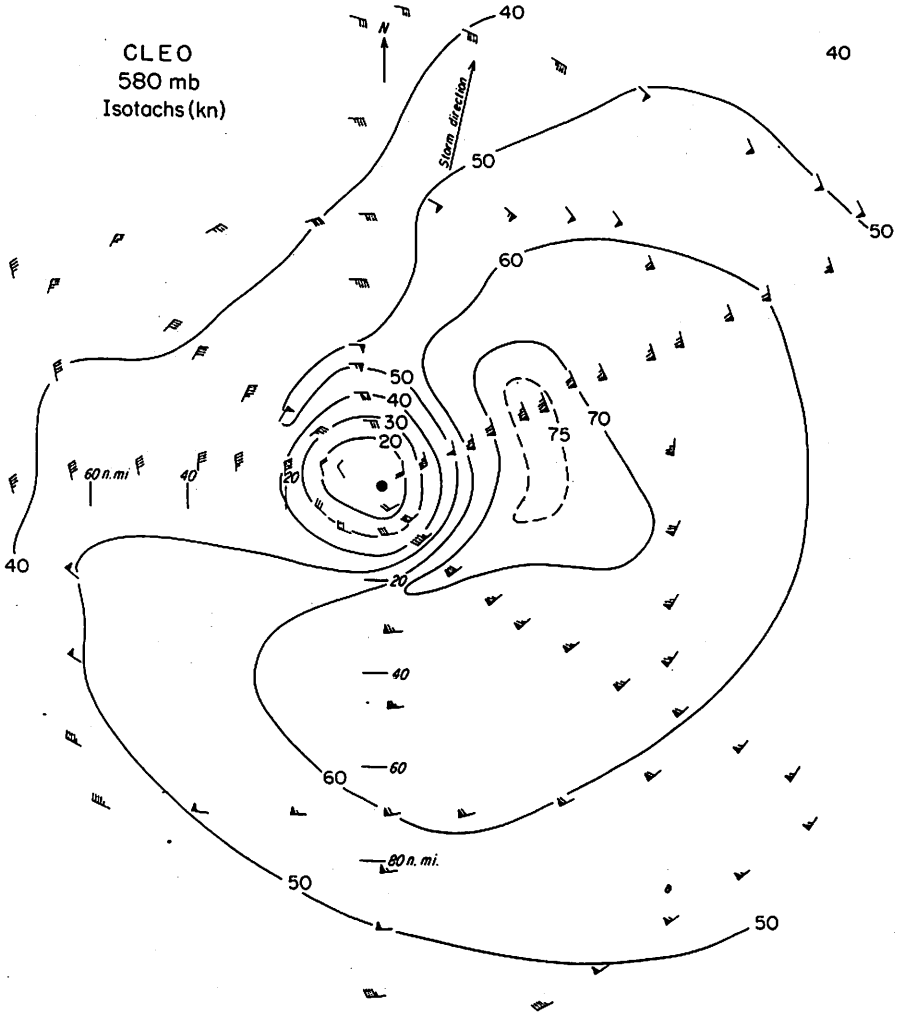

Figure 33.

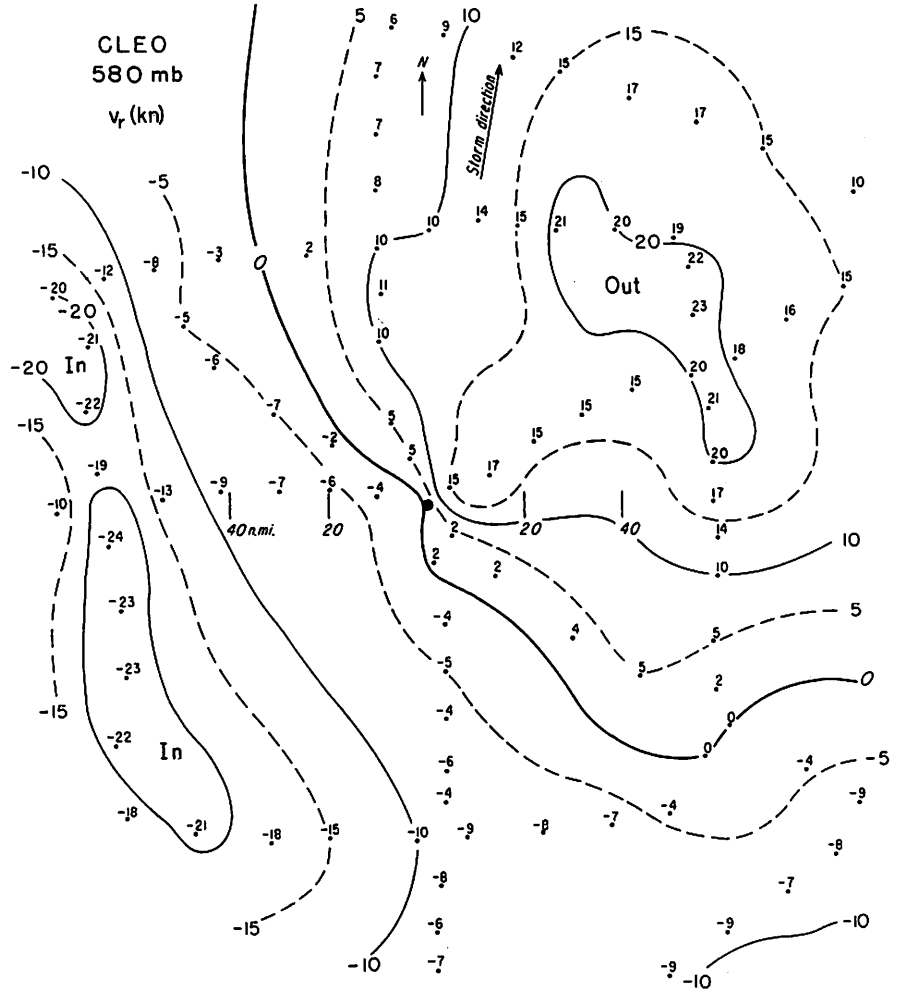

Figure 34. - Radial wind component.

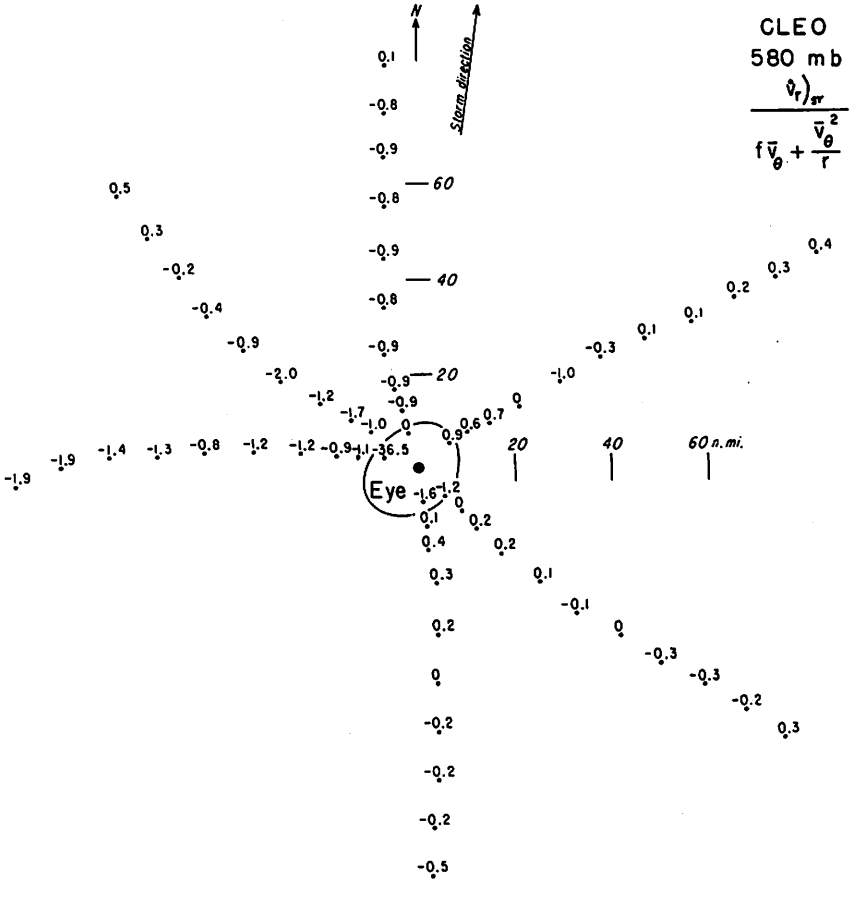

Figure 35.

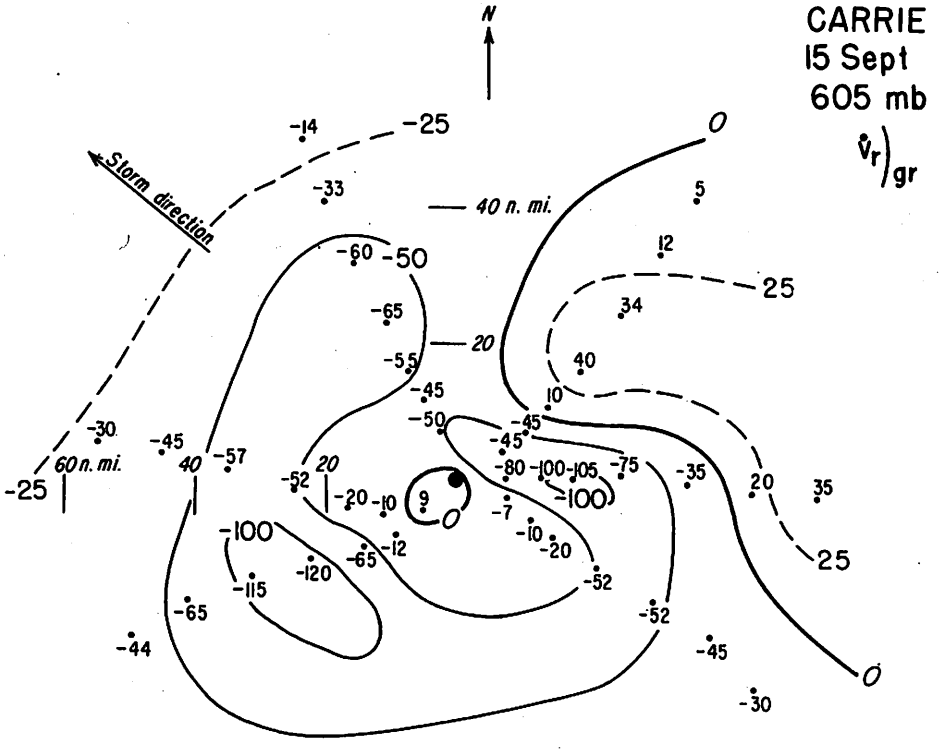

Figure 36. - $\dot{v}_r)_{gr}$ in kt./hr.

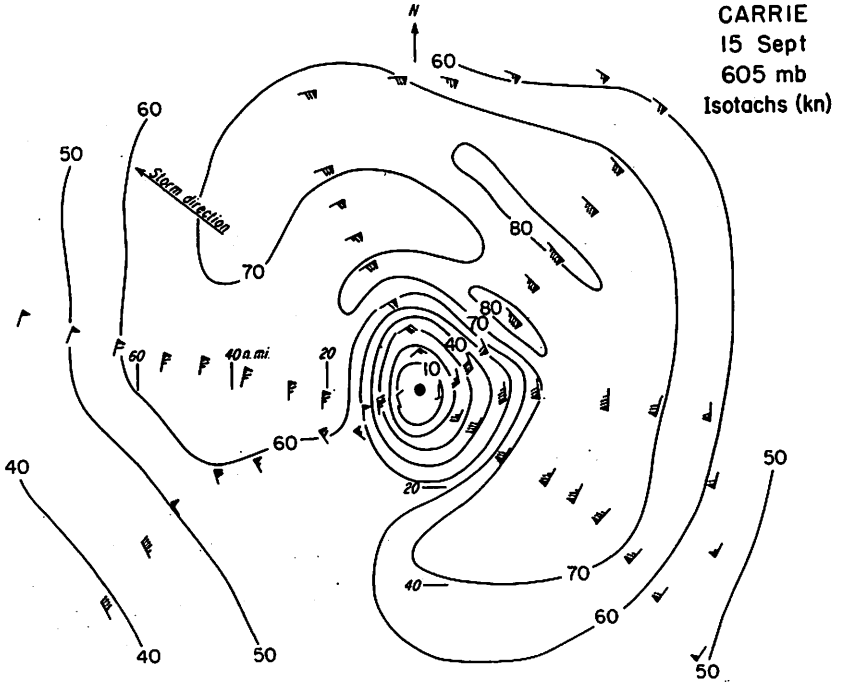

Figure 37.

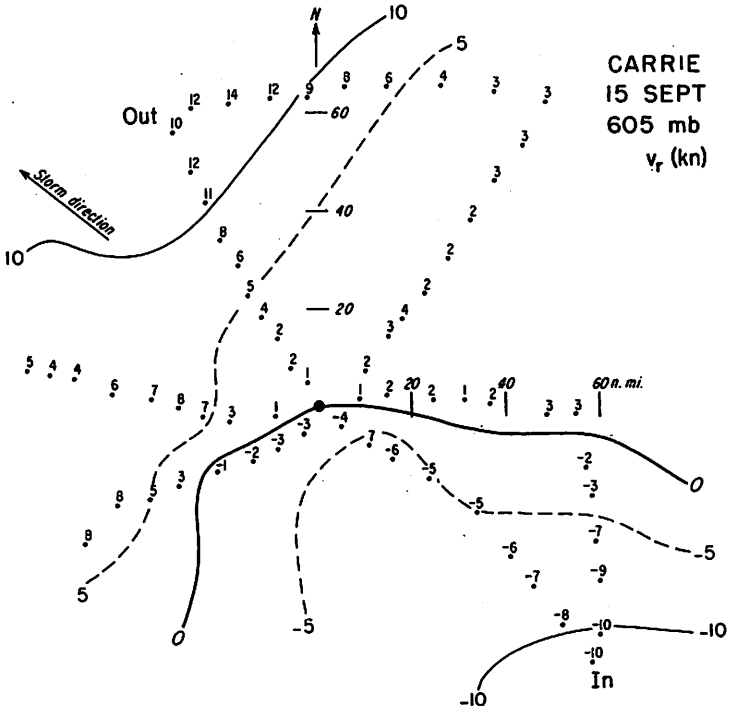

Figure 38. - Radial wind component.

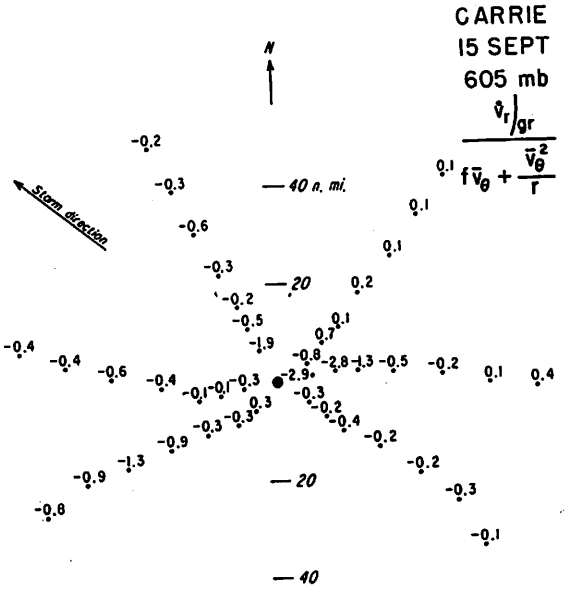

Figure 39.

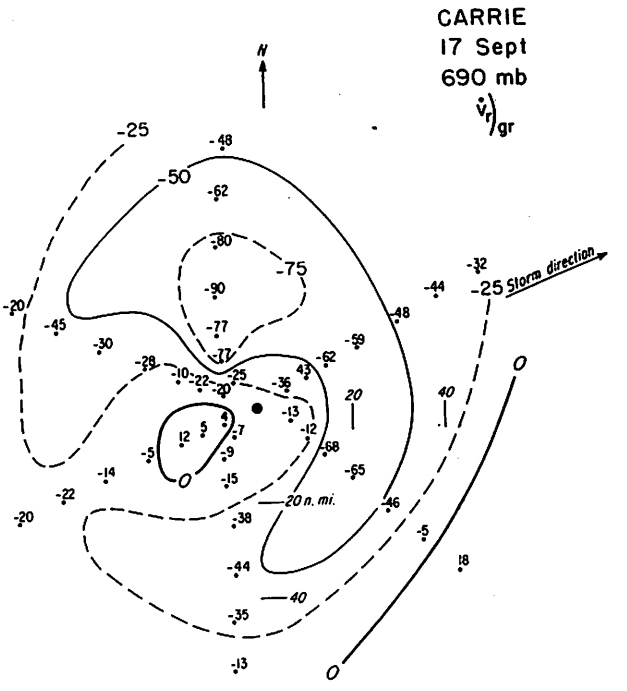

Figure 40. - $\dot{v}_r)_{gr}$ in kt./hr.

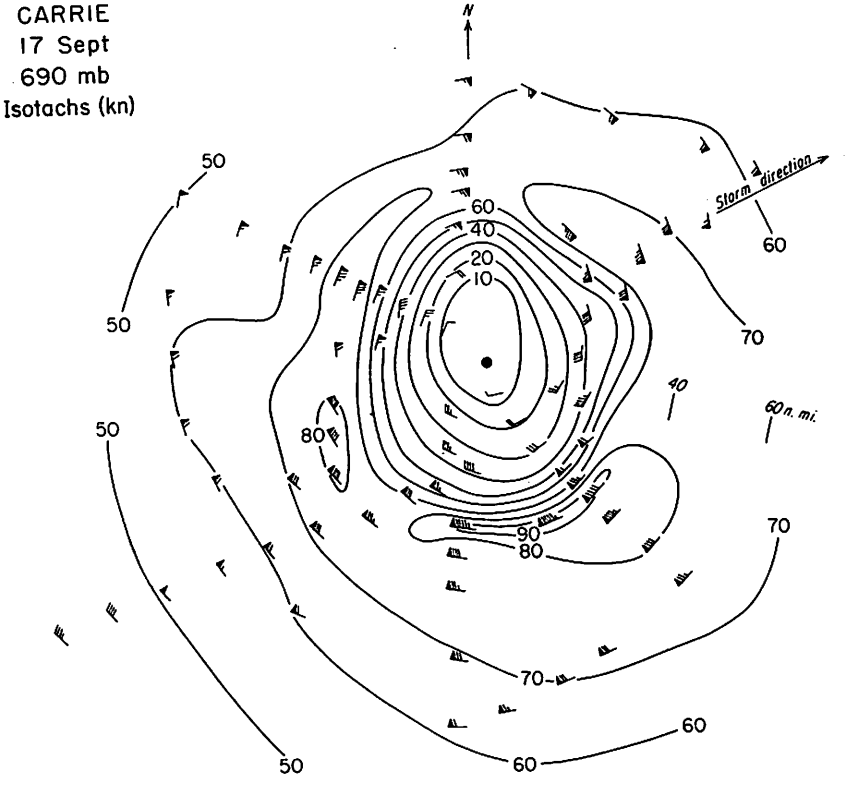

Figure 41.

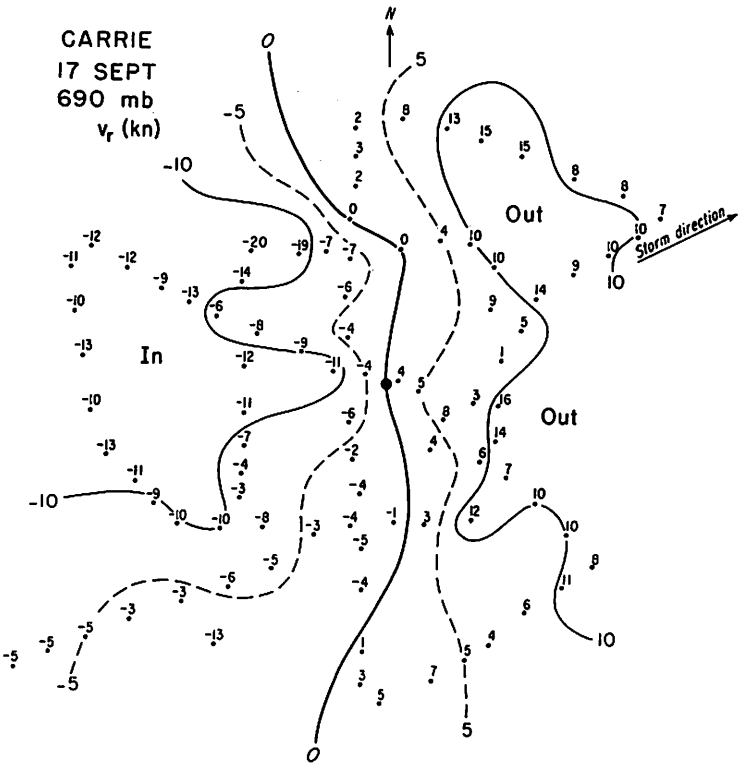

Figure 42. - Radial wind component.

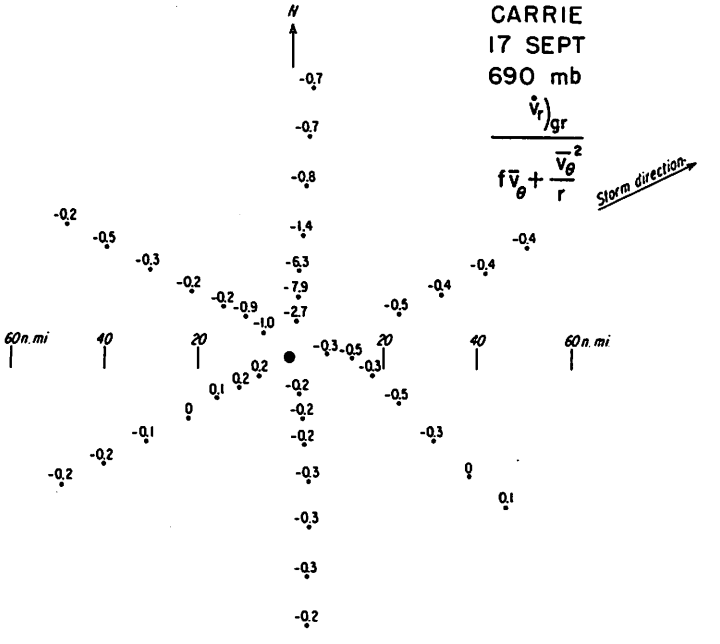

Figure 43.

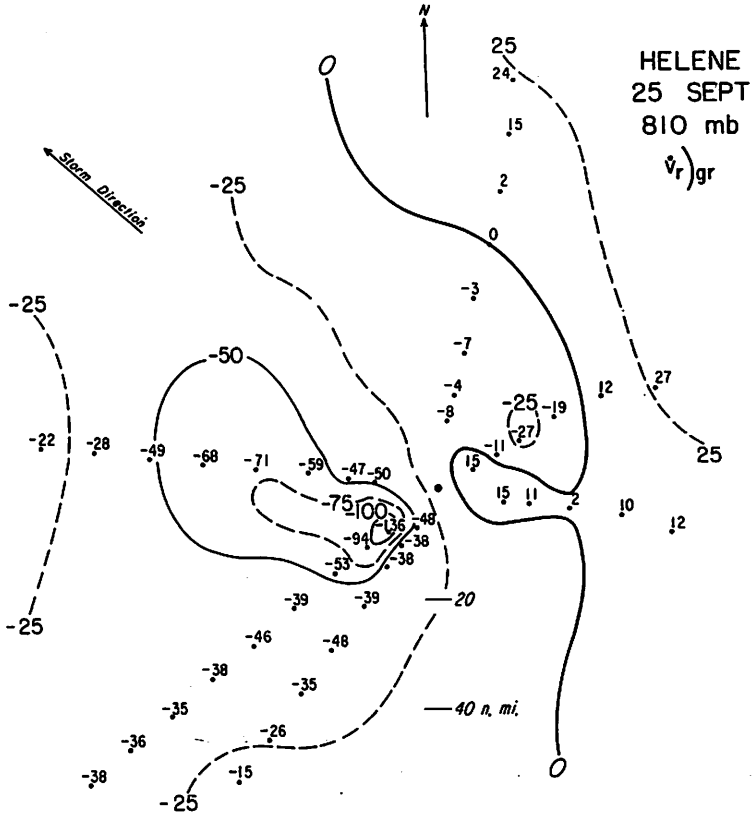

Figure 44. - $\dot{v}_r)_{gr}$ in kt./hr.

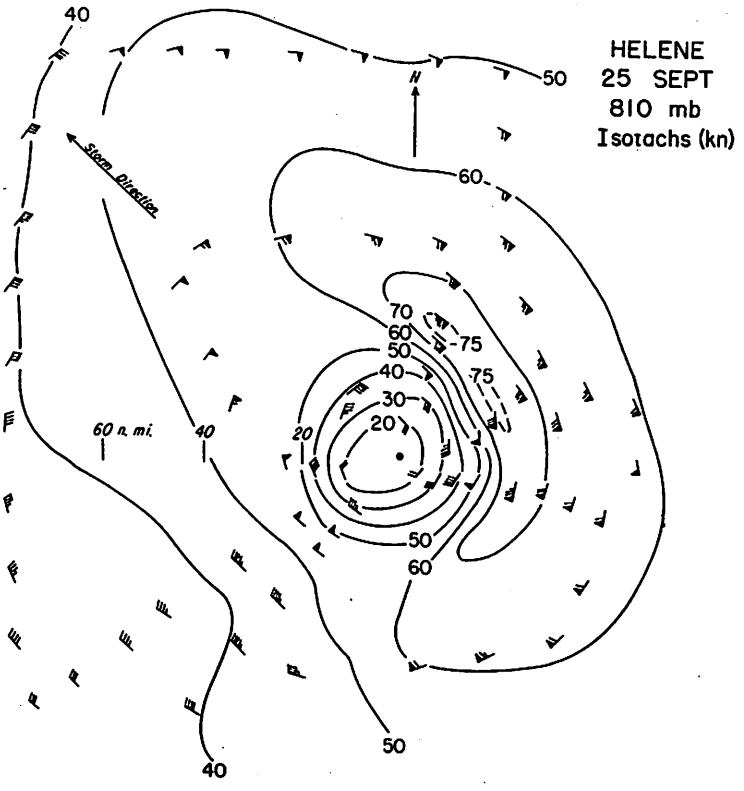

Figure 45.

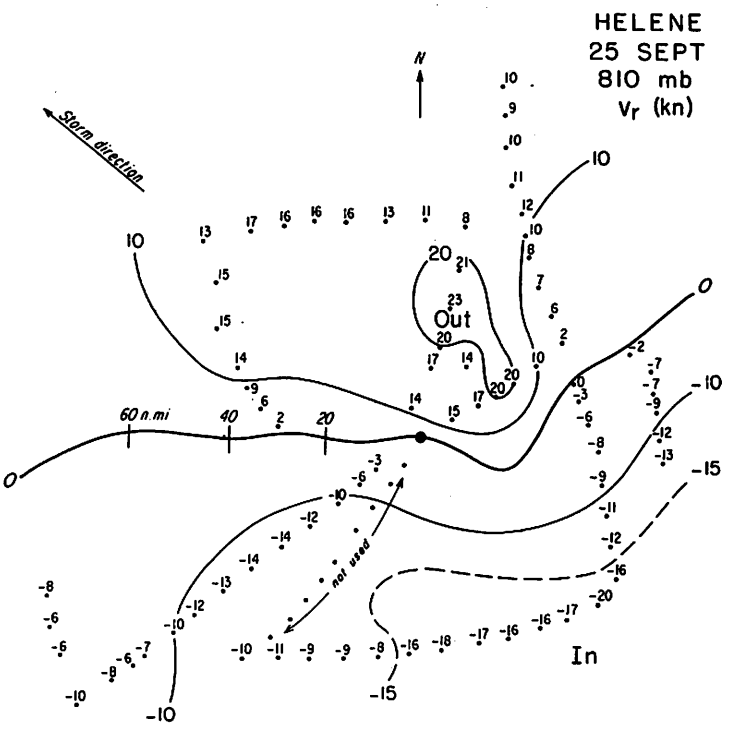

Figure 46. - Radial wind component.

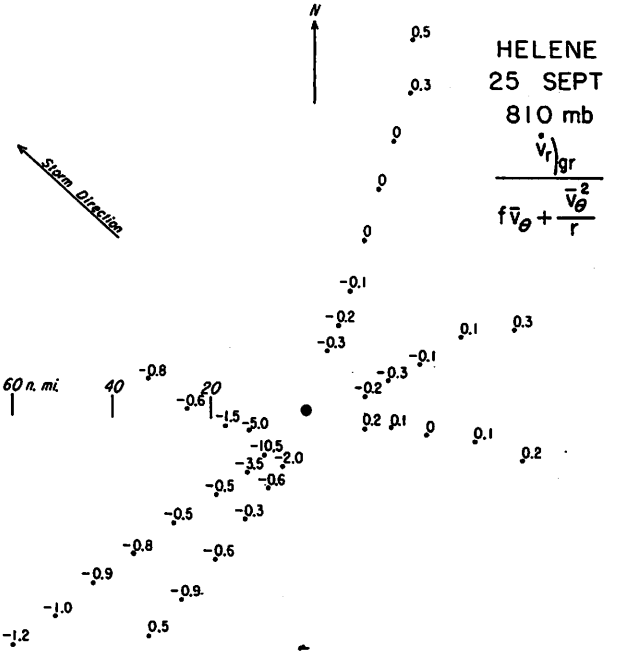

Figure 47.

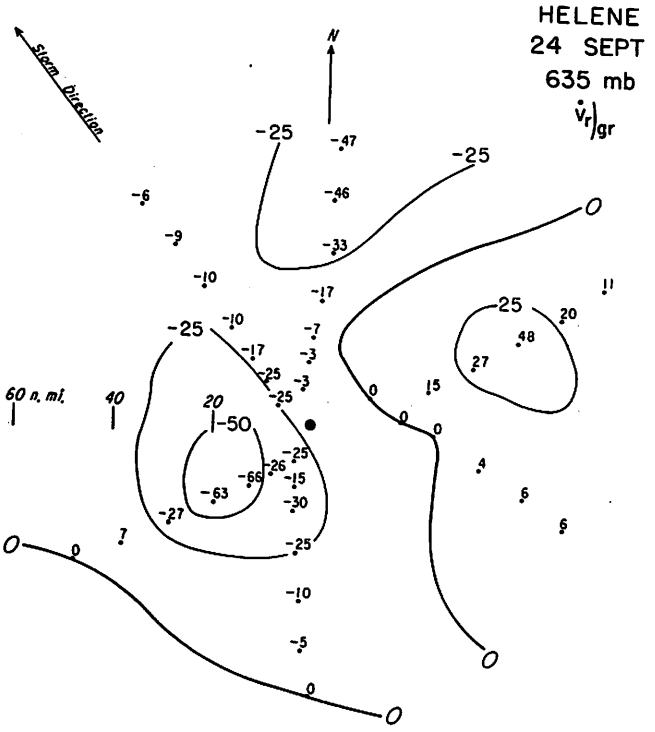

Figure 48. - $\dot{v}_r)_{gr}$ in kt./hr.

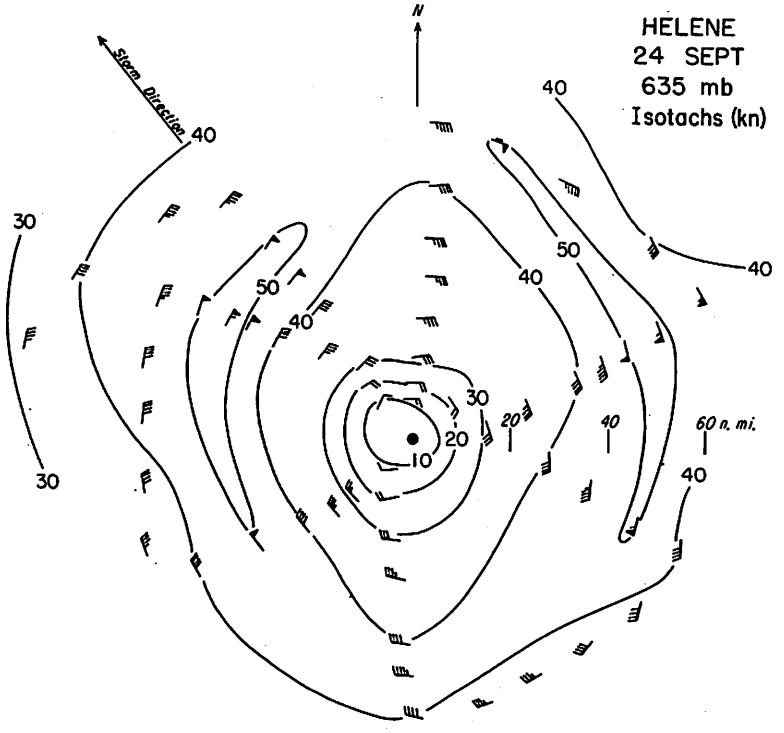

Figure 49.

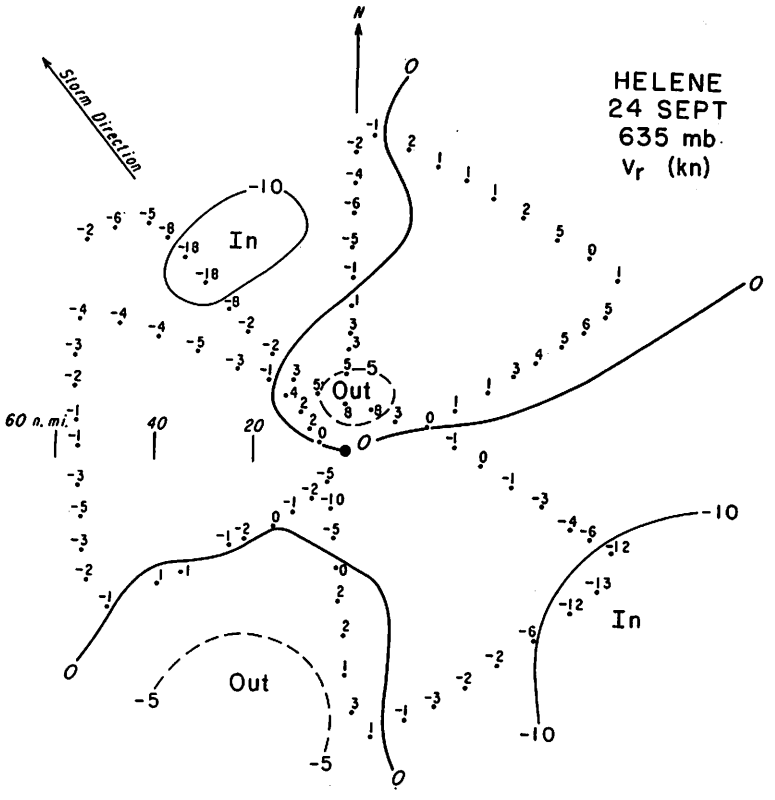

Figure 50. - Radial wind component.

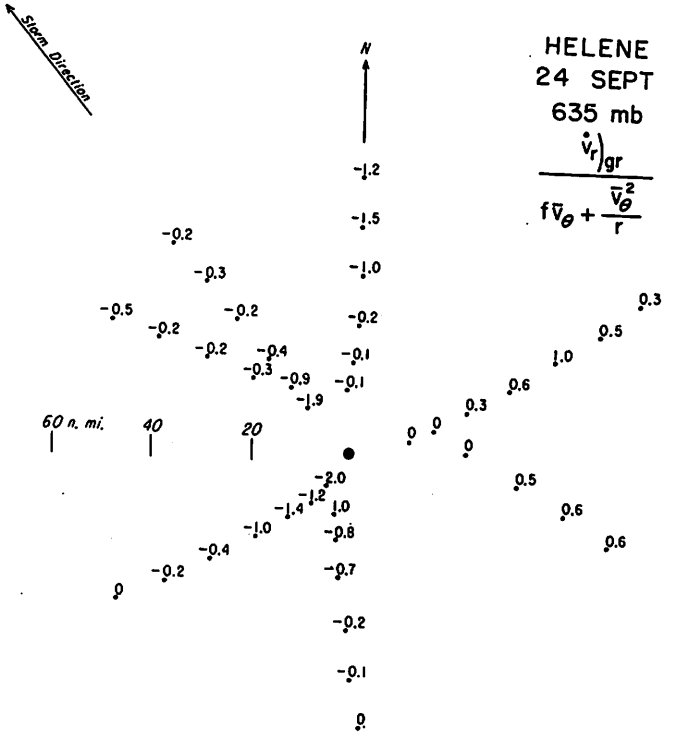

Figure 51.

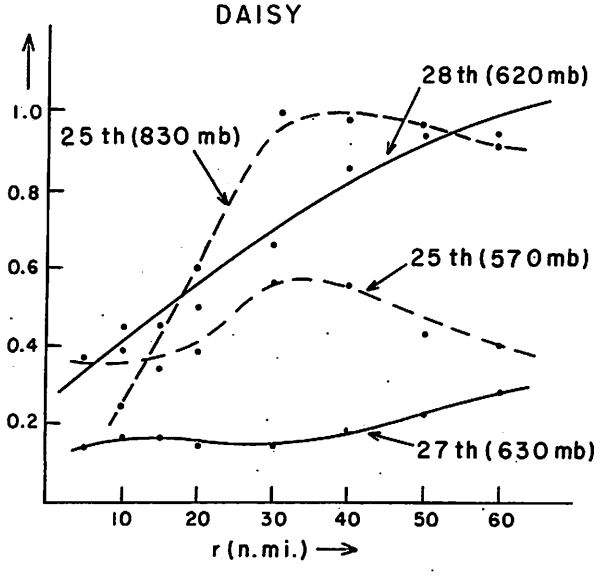

Figure 52.

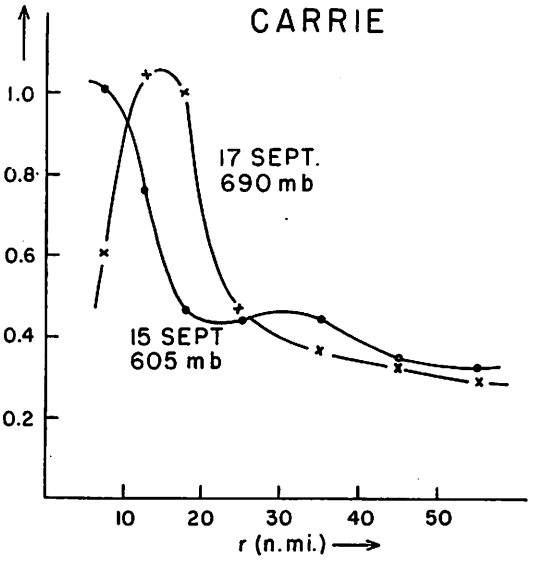

Figure 53.

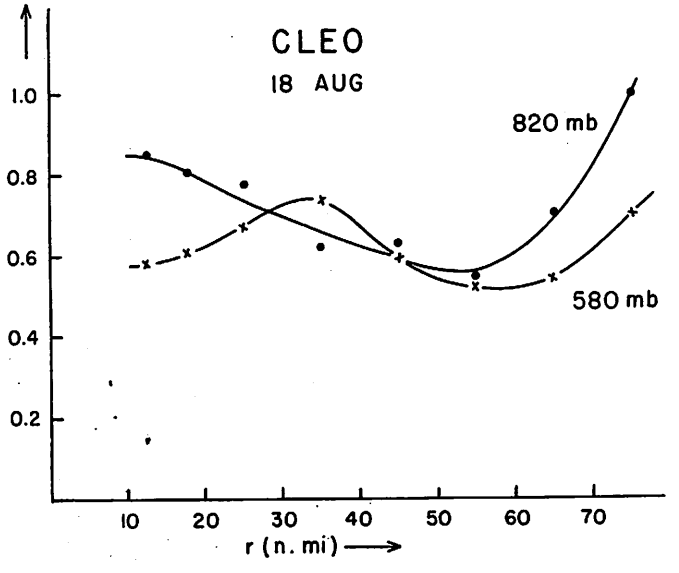

Figure 54.

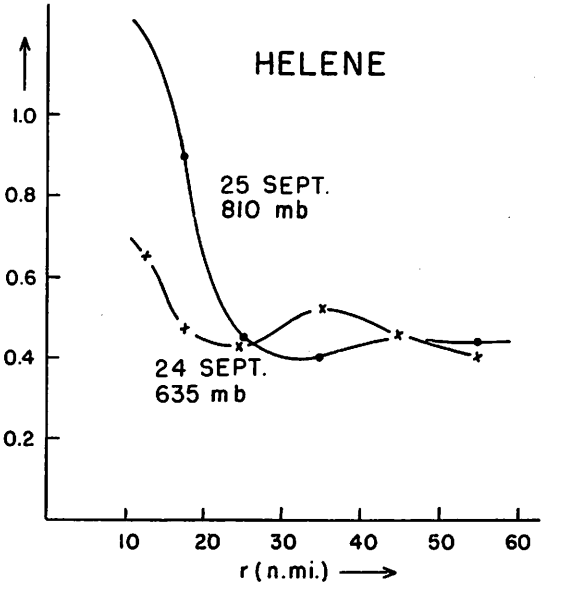

Figure 55.

Figures 52-55: $\dfrac{\overline{\dot{v}_r)_{gr}}}{f\bar{v}_\theta + \dfrac{\overline{v_\theta^2}}{4}}$ plotted against radius. Values have been averaged around the storm <u>without</u> respect of the sign of $\overline{\dot{v}_r)_{gr}}$.

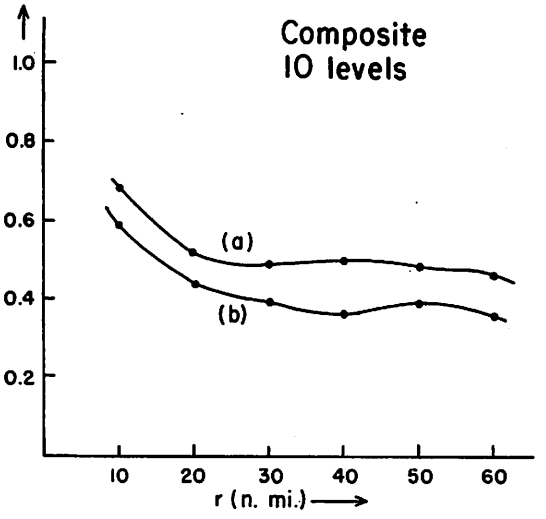

Figure 56.

(a) $$\frac{\overline{\dot{v}_r)_{gr}}}{f\,\overline{v}_\theta + \frac{\overline{v_\theta^2}}{r}}$$

(b) $$\frac{\overline{\dot{v}_r)_{gr}}}{g\,\overline{\frac{\partial D}{\partial r}}}$$

Values are plotted against radius after averaging around the storm without respect to the sign of $\dot{v}_r)_{gr}$.

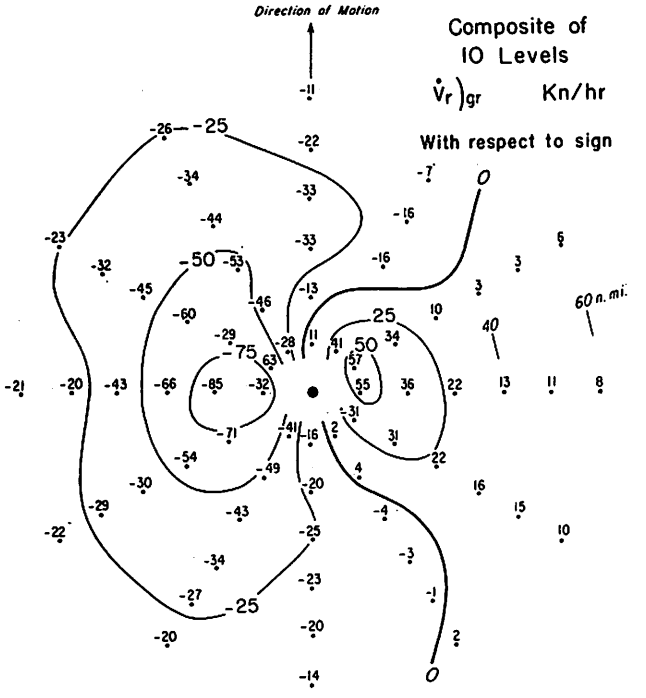

Figure 57.

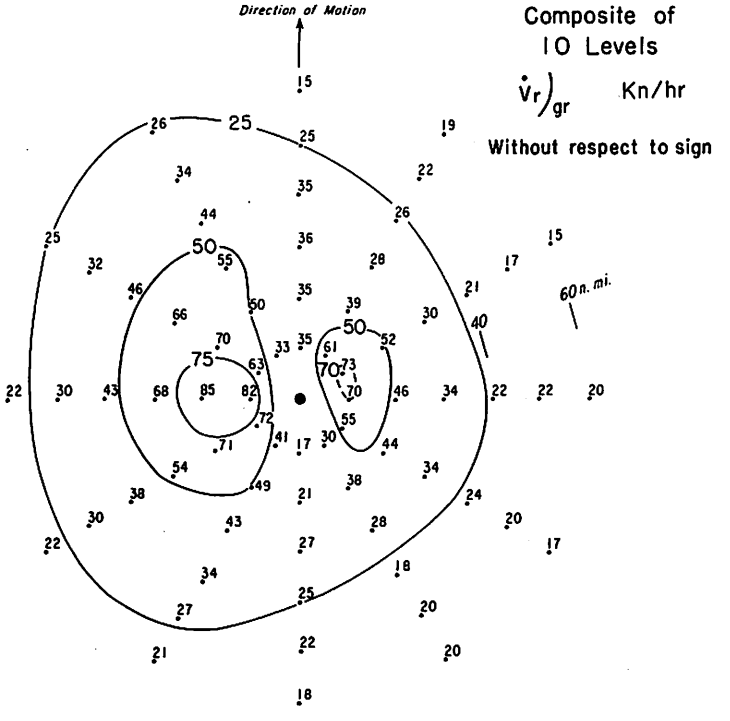

Figure 58.

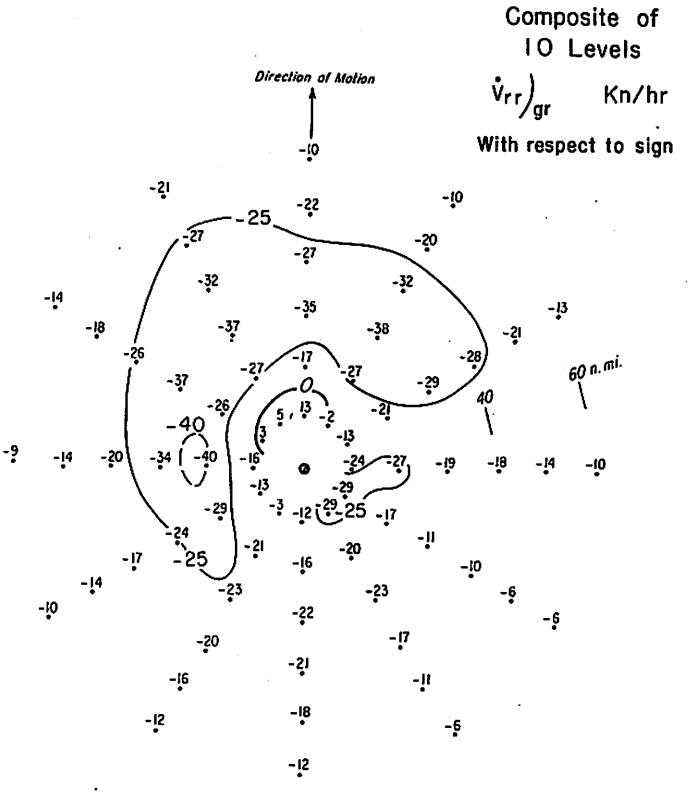

Figure 59.

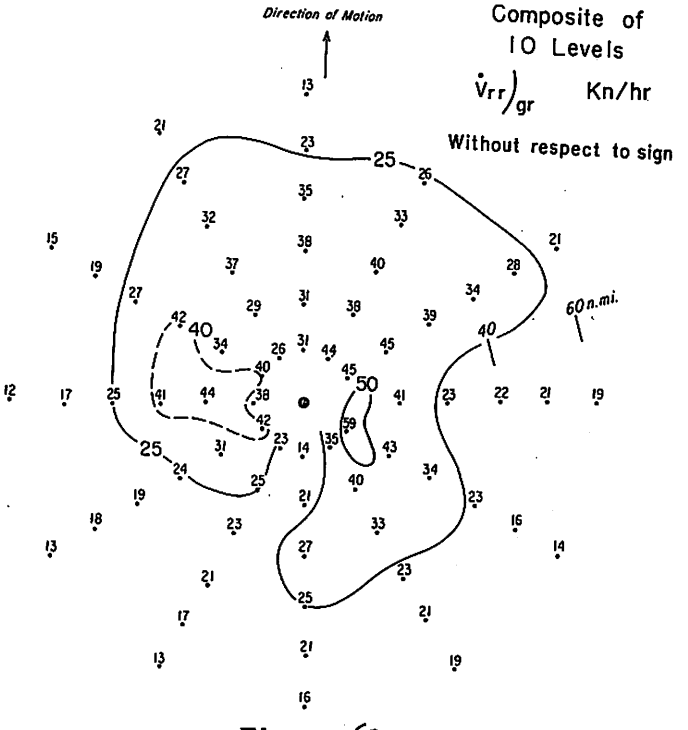

Figure 60.

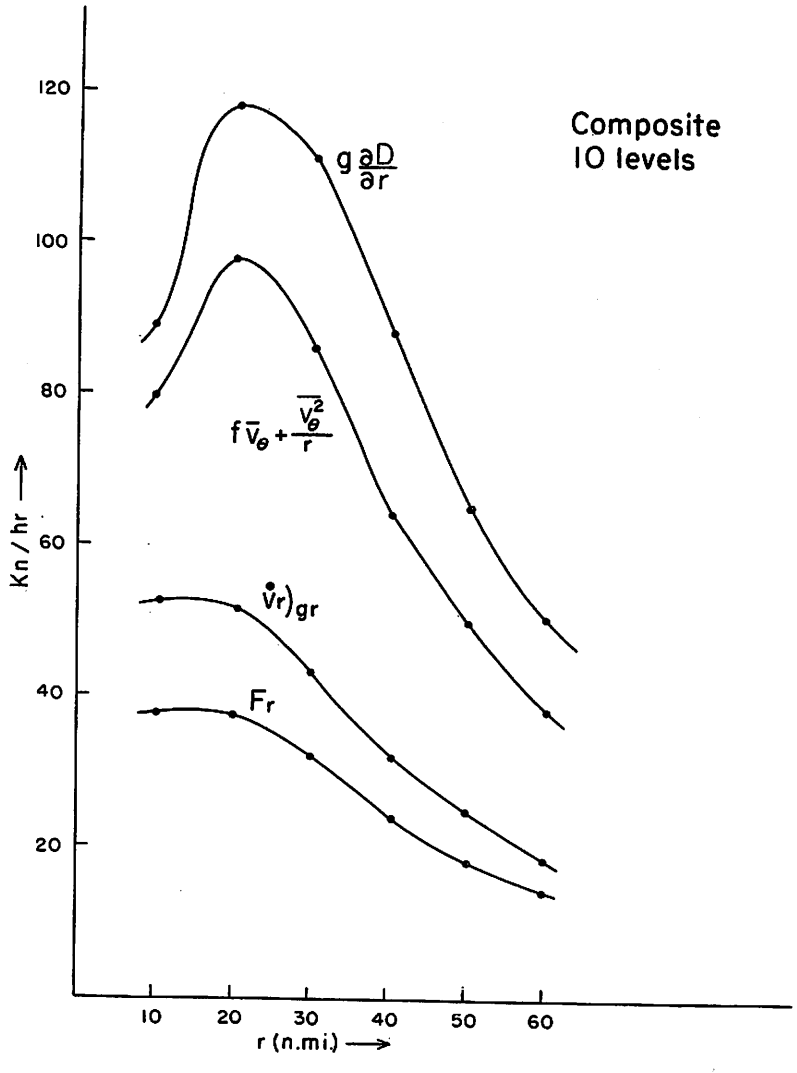

Figure 61.

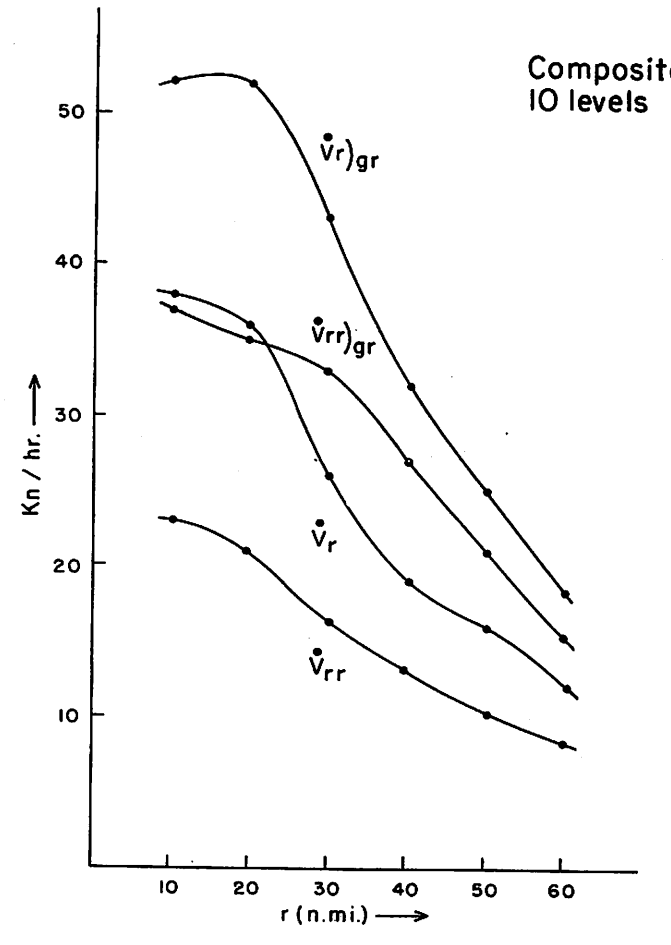

Figure 62.

Radial profiles of various accelerations at selected radii.
Values have been averaged around storm without respect to sign.

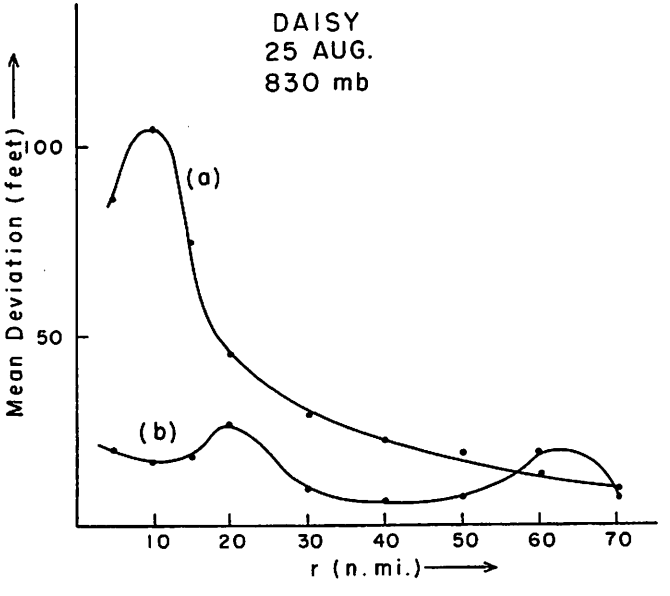

Figure 63. - 830 mb., August 25.

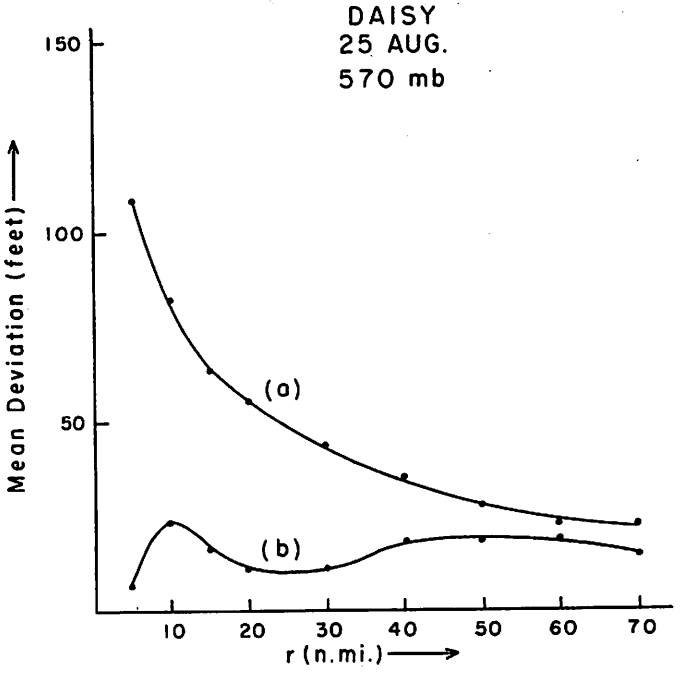

Figure 64. - 570 mb., August 25.

Figures 63-73. - Curve (a), mean deviation of the D_{gr} profiles of the individual radial flight legs at selected radii from their mean value (ft.). Curve (b), mean deviation of the D_{act} profiles of the individual radial flight legs at selected radii from their mean value (ft.).

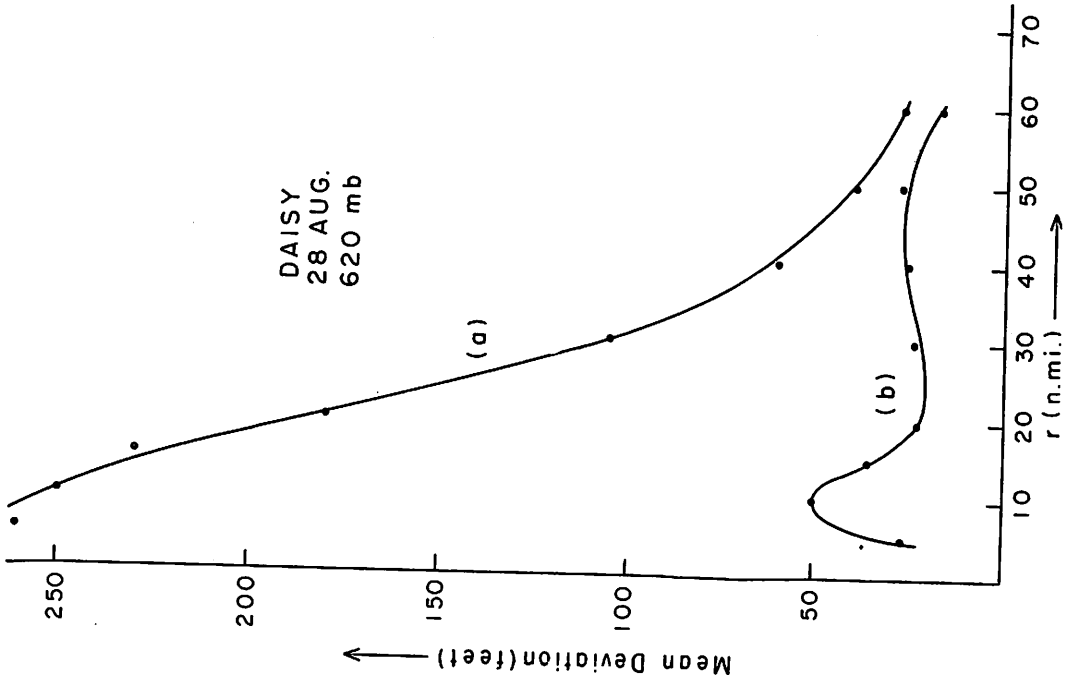

Figure 66.

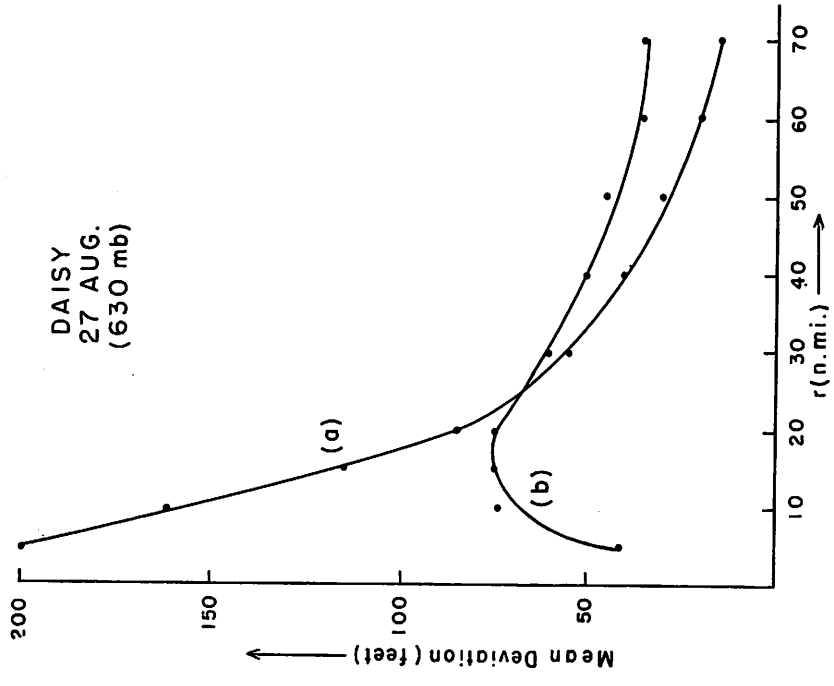

Figure 65.

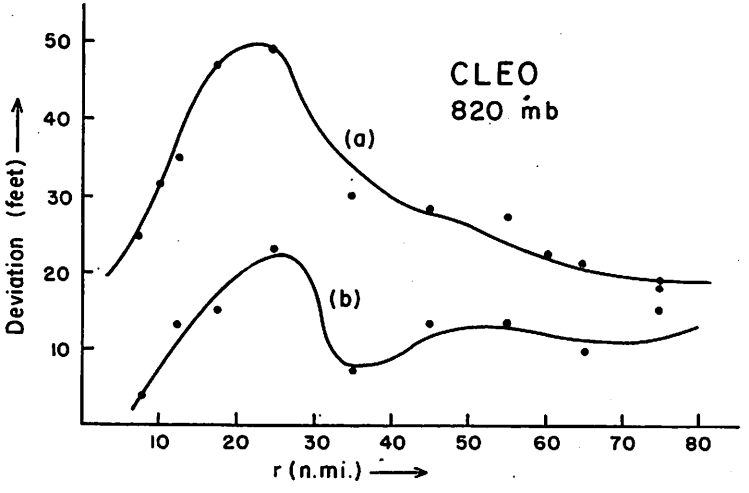

Figure 67.

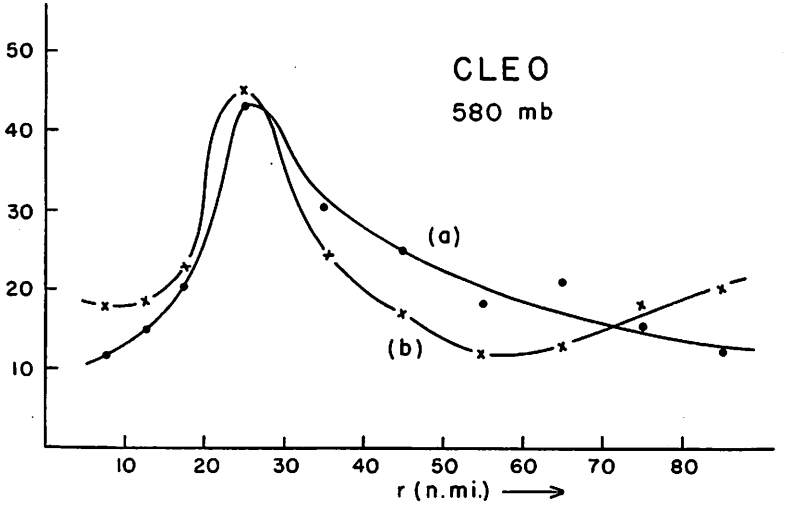

Figure 68.

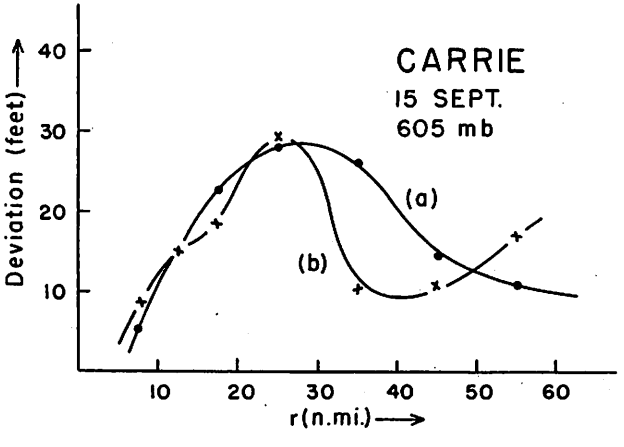

Figure 69.

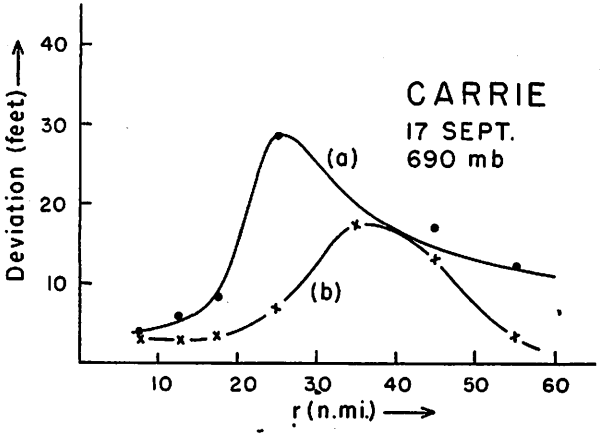

Figure 70.

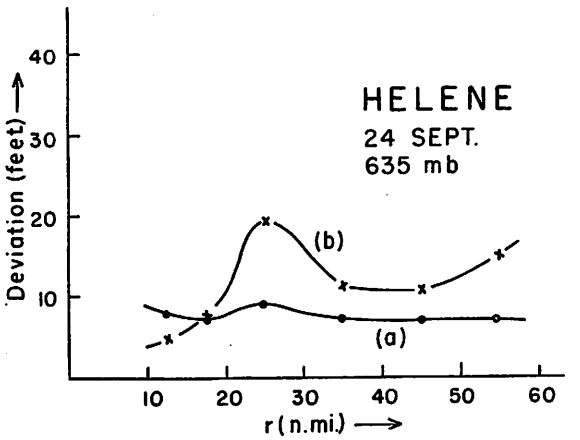

Figure 71.

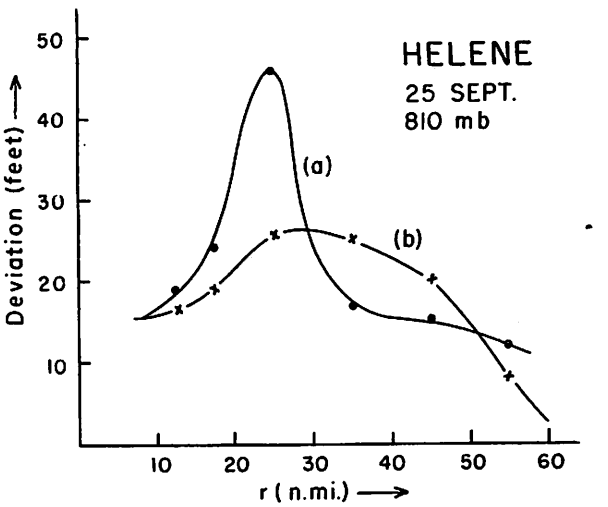

Figure 72.

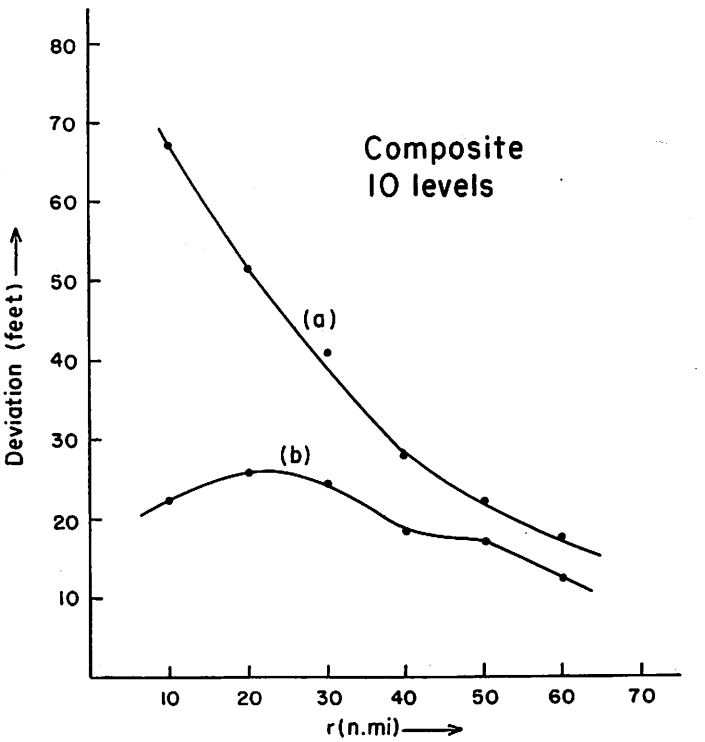

Figure 73.

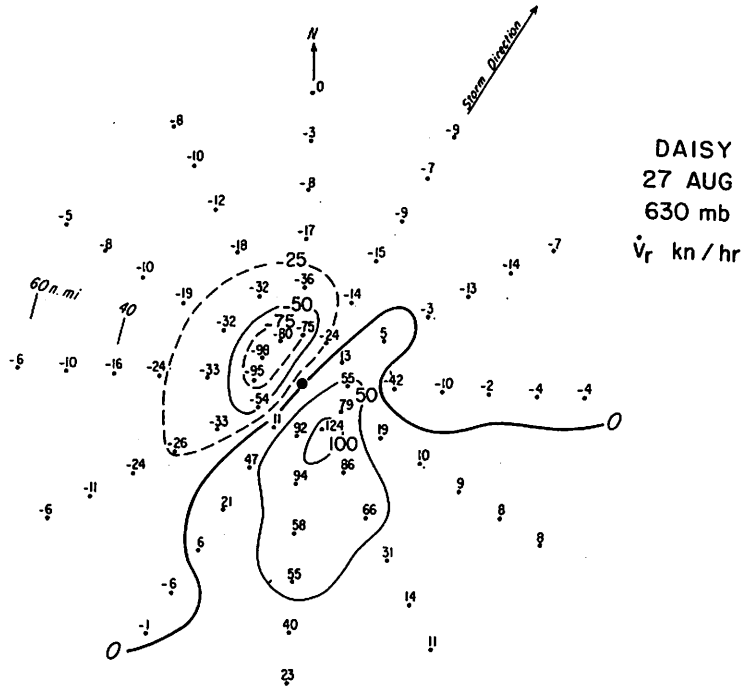

Figure 74. - Field of $\dot{v}_r$ (kt./hr.).

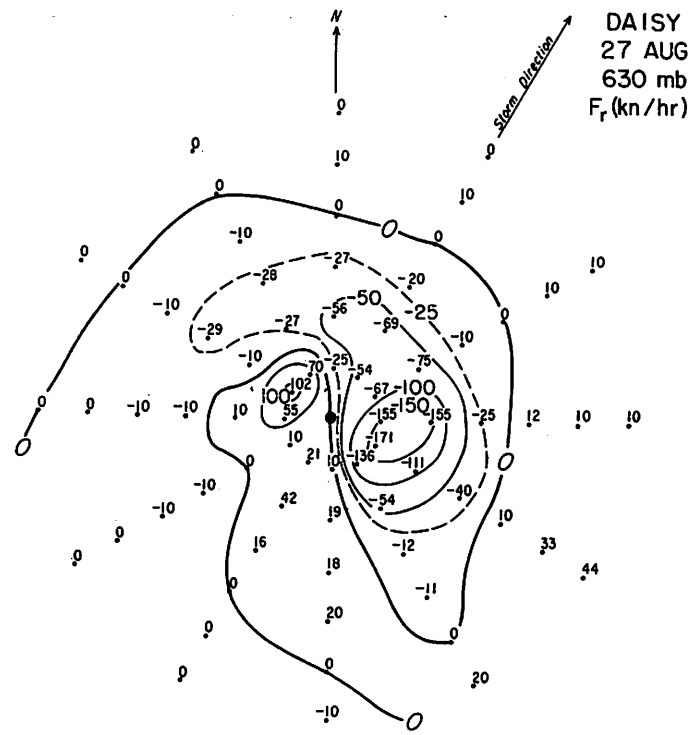

Figure 75. - Computed frictional force (kt./hr.).

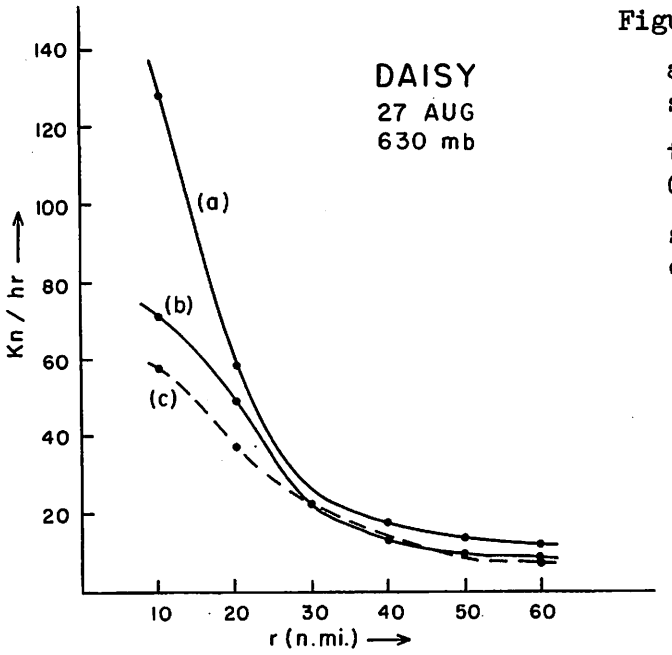

Figure 76. - Curve (a), $\dot{v}_r)_{gr}$ averaged around the storm without respect to sign. Curve (b), F_r averaged around the storm without respect to sign. Curve (c), $\dot{v}_r$ averaged around the storm without respect to sign. All curves: units kt./hr.

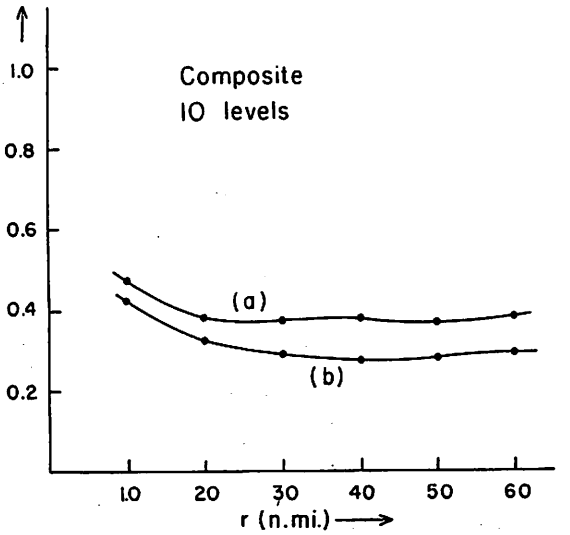

Figure 77. - Curve (a), $\dfrac{\overline{F_r}}{f\,\overline{v_\theta} + \overline{\dfrac{v_\theta^2}{r}}}$ averaged around storm without respect to sign. Curve (b), $\dfrac{\overline{F_r}}{g\,\overline{\dfrac{\partial D}{\partial r}}}$ averaged around storm without respect to sign.

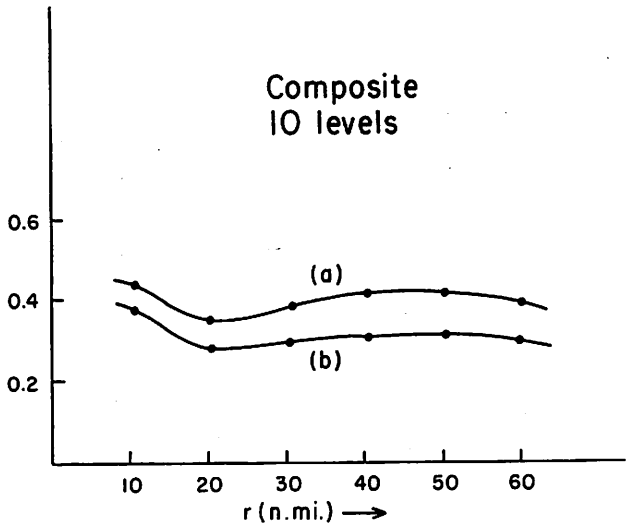

Figure 78. - Curve(a) $\dfrac{\overline{\dot{v}_r}}{f\,v_\theta + \overline{\dfrac{v_\theta^2}{r}}}$ averaged around storm without respect to sign. Curve (b), $\dfrac{\overline{\dot{v}_r}}{g\,\overline{\dfrac{\partial D}{\partial r}}}$ averaged around storm without respect to sign.

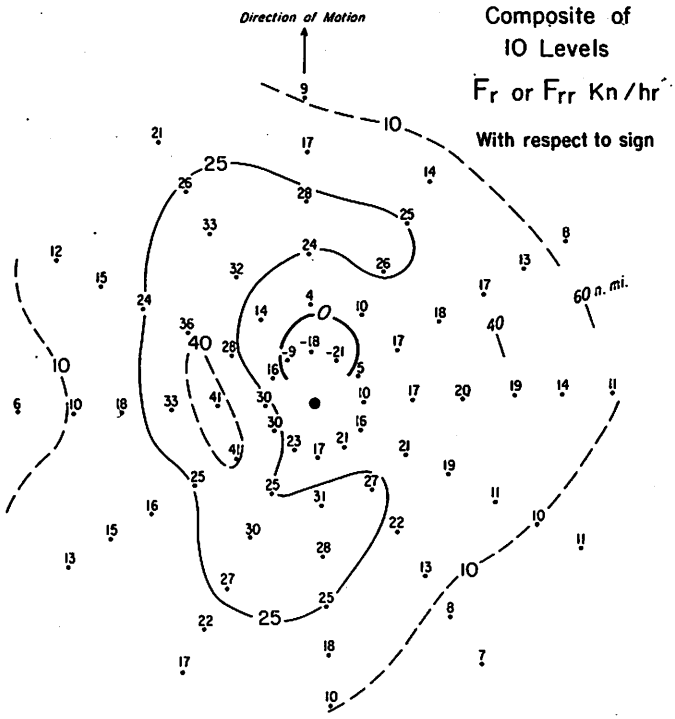

Figure 79.

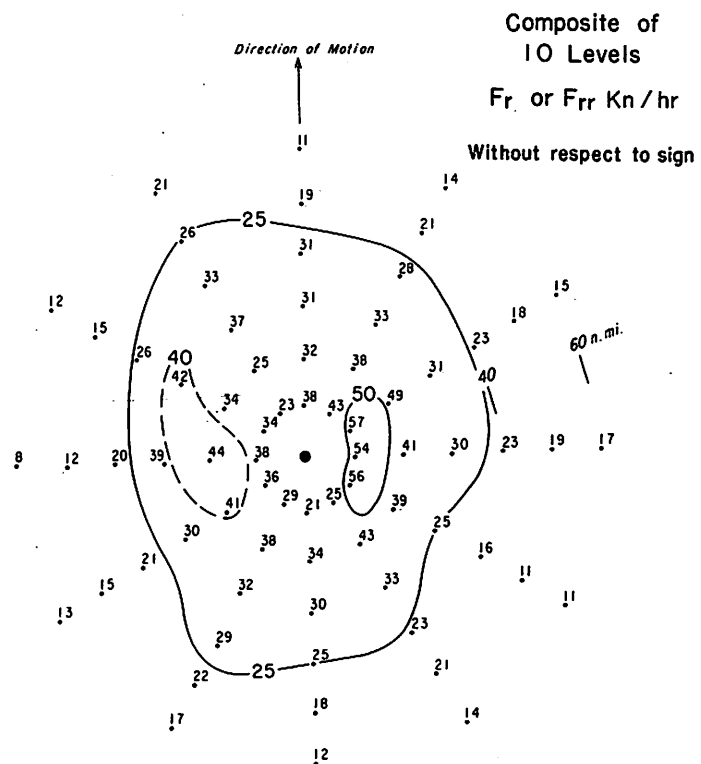

Figure 80.

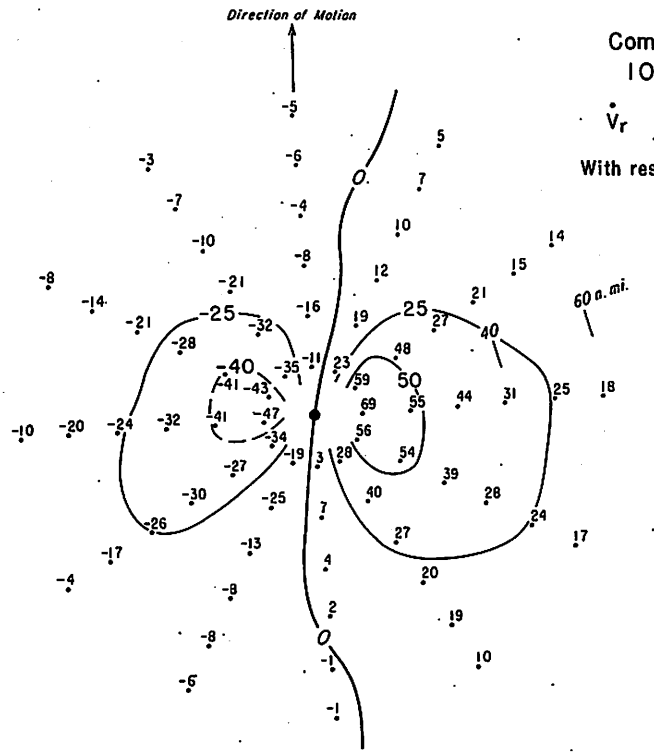

Figure 81.

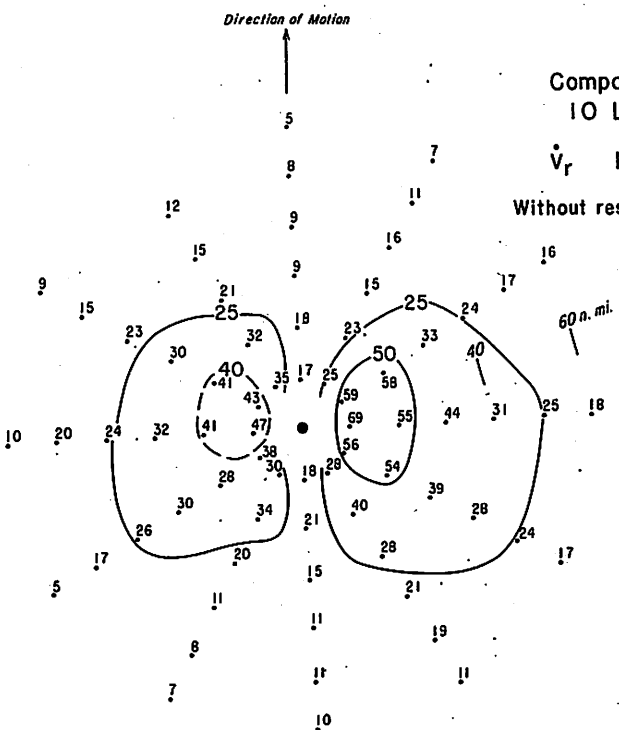

Figure 82.

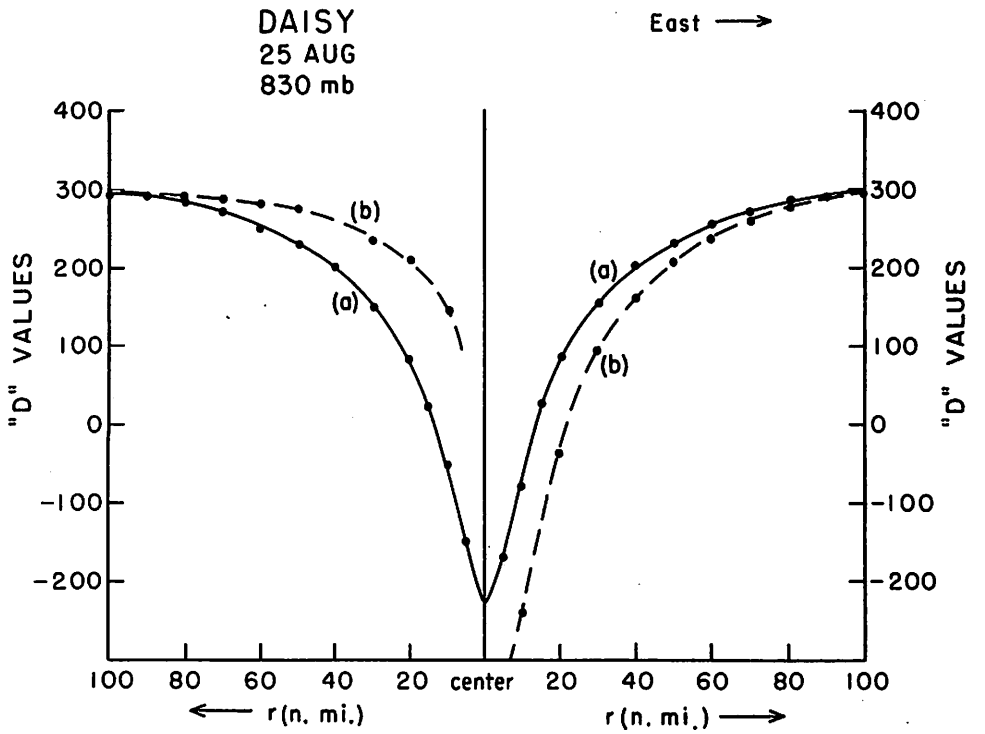

Figure 83. - Curve (a), observed D-profile (D_{act}). Curve (b), computed D-profile necessary to balance observed wind pattern (D_{gr}).

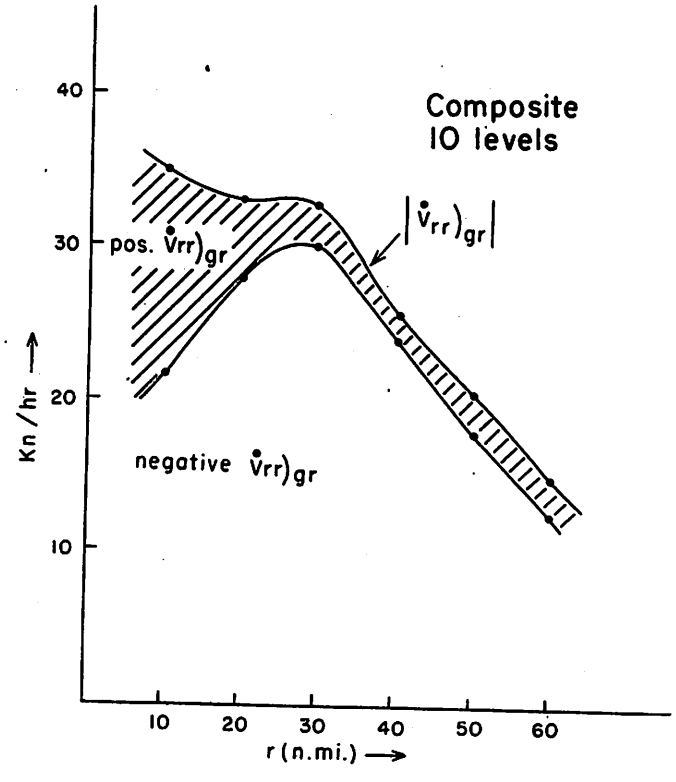

Figure 84.

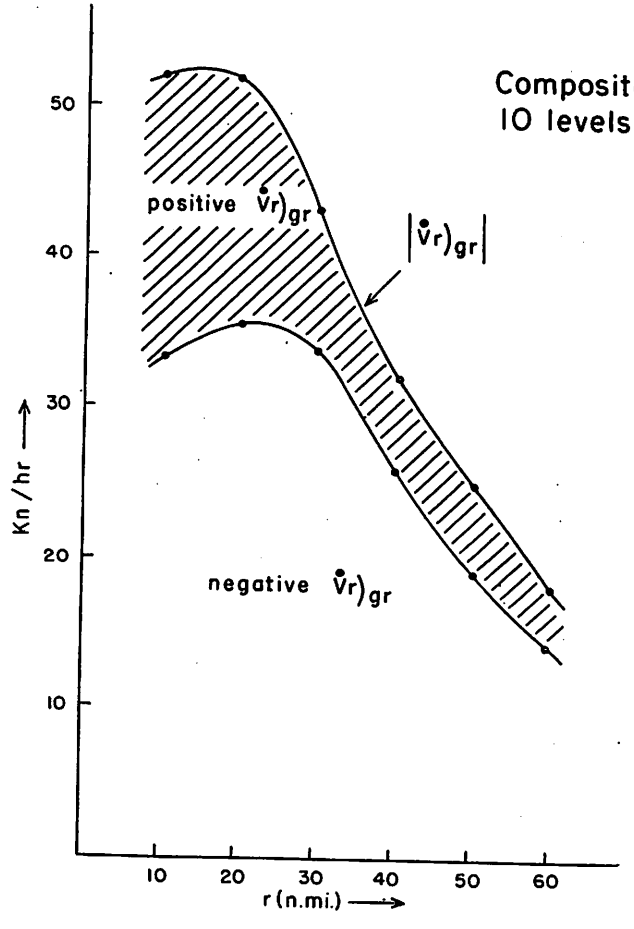

Figure 85.

$|\dot{V}_r)_{gr}|$ and $|\dot{V}_{rr})_{gr}|$ divided into their positive and negative parts after averaging around the storms at selected radii. Illustrates the predominance of positive ($D_{gr} - D_{act}$) i.e., dominance of pressure gradient over centrifugal and Coriolis accelerations, or excess warming.

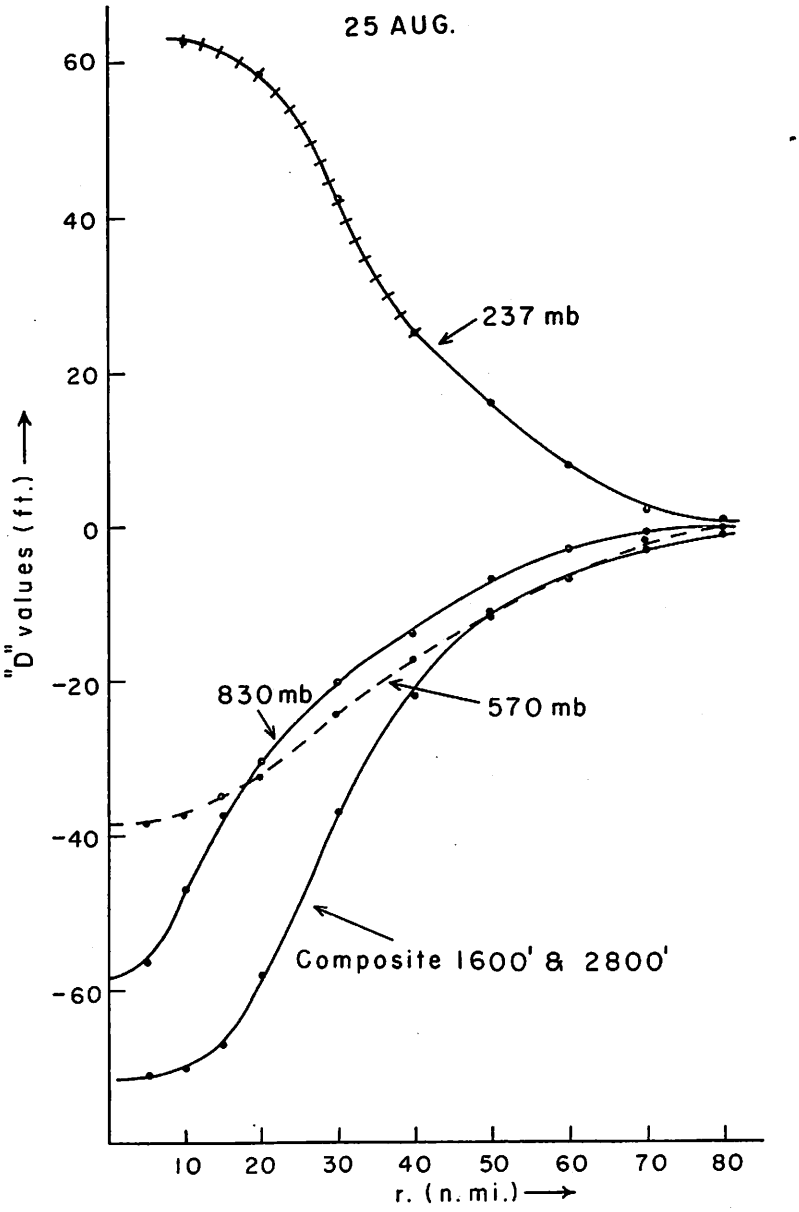

Figure 86. - Daisy accumulated plot of (D_{act} - D_{gr}) from outside reference of 100 n. mi. to inside of the storm. Values averaged around storm at selected radii. Negative values of (D_{act} - D_{gr}) indicate stronger pressure gradient than corresponding wind field.

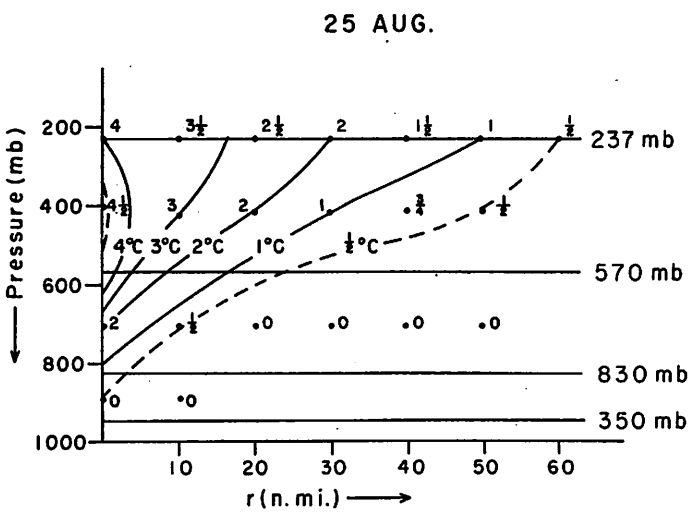

Figure 87. - Vertical cross-section of the computed temperature increase from the temperature values outside the storm area. Values in °C.

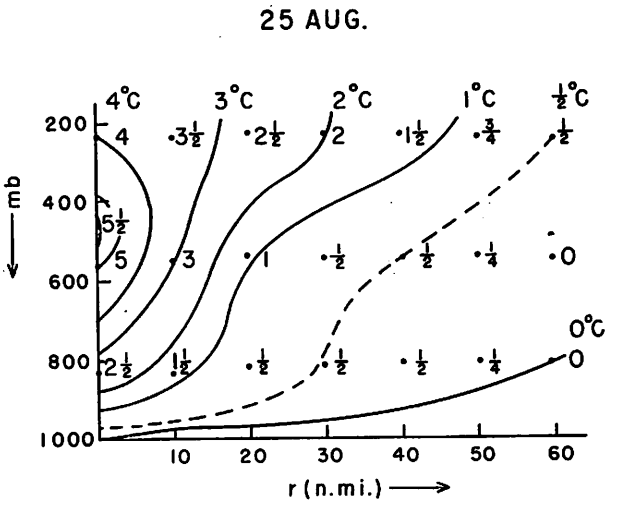

Figure 88. - Vertical cross-section of the observed (aircraft) temperature increase (°C.) from the temperature values outside of the storm.

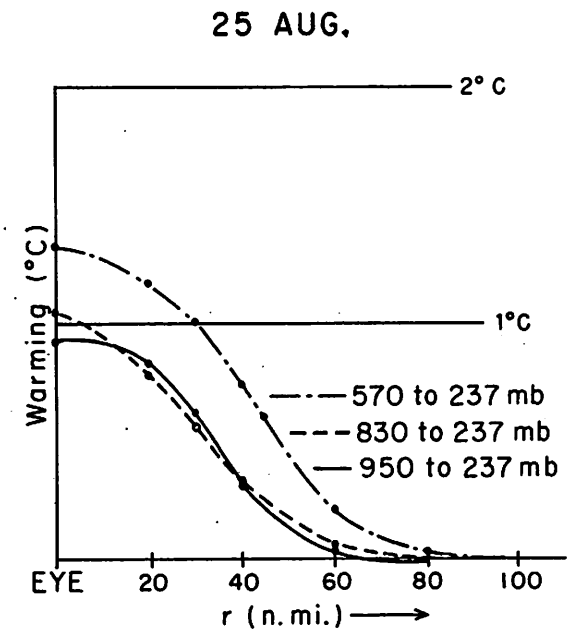

Figure 89. - Excess warming (°C.) between particular pressure layers corresponding to the imbalance of the pressure over the

$$(f\,\overline{v_\theta} + \frac{\overline{v_\theta^2}}{r})$$ acceleration.

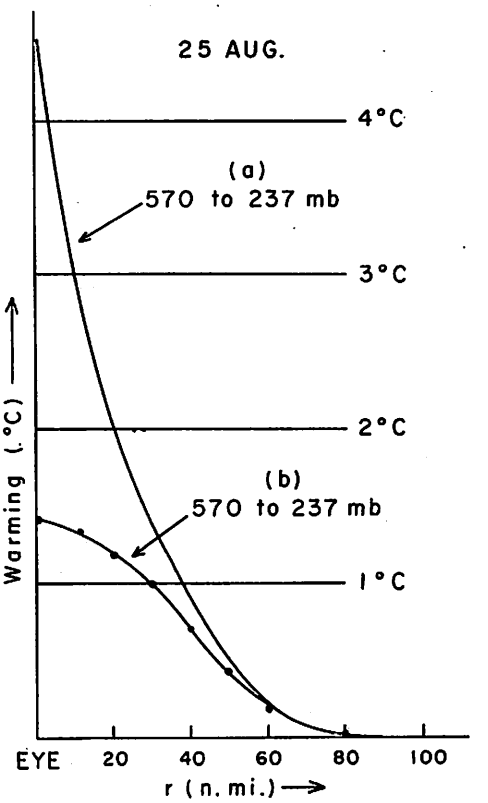

Figure 90. - Comparision of actual warming (curve a) with the acceleration warming (curve b) between 570 and 237 mb. Values in °C.

4. SUMMARY OF PRINCIPAL RESULTS

The principal results from all of the levels within the four storms studied are:

1. The gradient wind equation along the radial direction, as defined in this paper for hurricanes, does not express the radial balance of forces to a satisfactory degree of approximation in nearly all portions of the storm. The quantity $\dot{v}_r)_{gr}$ is nearly always a large fraction of the Coriolis and centrifugal acceleration. In some places $\dot{v}_r)_{gr}$ is even larger than these accelerations.

2. Internal radial friction plays an important role in balancing the cyclindrical radial equation of motion. The frictional acceleration is directed toward the storm center when $\dot{v}_r)_{gr}$ is positive and outward from the storm center when $\dot{v}_r)_{gr}$ is negative. The average magnitude of the radial frictional acceleration for the 10 levels for which area integration could be performed is 25 to 30 percent of the pressure gradient force and 35 to 40 percent of the Coriolis and centrifugal acceleration. These internal radial frictional accelerations may possibly be accounted for by a vertical Reynolds stress term.

3. All deepening or steady state hurricanes must have stronger pressure gradients than centrifugal and Coriolis accelerations in order to account for frictional dissipations.

5. CONCLUSION

In this study the balance of forces in hurricanes has been examined along the radial direction in stationary and moving coordinates; further, the radius of trajectory curvature has been computed in selected portions of ten flight missions. The Coriolis acceleration proved negligible compared to the centrifugal acceleration as expected. But gradient or cyclostrophic balance in general is not achieved by a wide margin, both along the radial axis and in natural coordinates. The pressure gradient far exceeds that required to balance the centrifugal acceleration to the left, and falls somewhat short of the requirement to the right of the direction of motion. In moving coordinates this asymmetry is reduced but by no means eliminated. Hence the maximum wind may be interpreted as produced by "overshooting" toward low pressure far beyond the point of equilibrium. A similar situation appears to exist with respect to many extratropical wind maxima, especially high-speed centers along jet streams.

The field of radial motion shows general outflow ahead of and inflow behind the hurricane. The zero line is to right and left of the direction of motion, approximately where the maximum difference between pressure gradient force and centrifugal acceleration is found. This geometric relation is considered more than a coincidence and supports the preceding deductions about the origin of the maximum wind.

The air is accelerated radially in the sense prescribed by the difference between pressure gradient force and centrifugal acceleration. But the magnitude of the actual acceleration generally falls short of the computed acceleration by a wide margin. Hence it becomes necessary to postulate the existence of large lateral frictional forces which act opposite to the $\dot{v}_r)_{gr}$ accelerations. The magnitude is 10^{-1} to 10^{0} dynes per unit mass which corresponds to a pressure gradient force of 1 mb./5 m. Such large frictional forces previously have not been suspected to exist. Nevertheless, there appears to be no valid reason a priori why the friction should not rise to become a substantially larger fraction of the pressure gradient force in hurricane-type systems than under normal atmospheric circumstances. If so, an important break on hurricane development has been uncovered, and it remains for the future to give a quantitative expression to enter as a constraint in hurricane models.

A few initial steps were taken to relate dynamics and energetics. From the difference between pressure gradient force and centrifugal acceleration, the departure of central pressure from that required to balance the wind field can be computed, also the temperature field which must be assumed with the pressure departure, assuming hydrostatic conditions with the top of the disturbance at 100 mb. Only one case had sufficient flight levels to perform all of these calculations.

In this instance there was a "forced" surface pressure drop of 4 - 5 mb. and an "excess" temperature warming of about 1°C., usually in the high tropospheric layer above 500 mb. From this it appears that hurricane development is related to the capacity of the atmosphere to effect a large heat transport into the upper atmosphere which, from heat balance considerations, must be effected by ascent in narrow channels as demonstrated by Riehl and Malkus [17] for the equatorial trough zone. The relation between dynamics and energetics has merely been touched on in this paper, but one definite suggestion from this aspect of the work is that one should search for conditions in tropical depressions which favor banding the mass ascent into narrow walls or lines.

ACKNOWLEDGMENTS

The author wishes to express his sincere gratitude to Professor Herbert Riehl under whose direction this paper was written. Professor Riehl proposed this topic, encouraged and supervised all phases of its carrying out. The author also wishes to thank the National Hurricane Research Project and its past and present directors Messrs. Robert Simpson, Cecil Gentry, and Harry Hawkins for generously furnishing the valuable data needed to make this study possible. The author expresses his appreciation to the U. S. Weather Bureau for providing financial assistance and to Mrs. Della Friedlander for drafting the illustrations. Thanks are also due to Dr. T. N. Krishnamurti of the University of Chicago and the above mentioned Mr. Robert Simpson for helpful discussions on this subject matter.

REFERENCES

1. M. Ausman, "Some Computations of the Inflow Angle in Hurricanes Near the Ocean Surface," University of Chicago Project Report, 1959, 22 pp. (Unpublished.)

2. D. Brunt, Physical and Dynamical Meteorology, The University Press, Cambridge, 1939, 428 pp.

3. B. Haurwitz, Dynamic Meteorology, McGraw-Hill Book Company, Inc. New York, 1941. (See pp. 192-195.)

4. D. T. Hilleary, and F. E. Christensen, "Instrumentation of National Hurricane Research Project Aircraft," National Hurricane Research Project Report No. 11, U. S. Weather Bureau, 1957, 71 pp.

5. L. F. Hubert, "Distribution of Surface Friction in Hurricanes," Journal of Meteorology, vol. 16, No. 4, Aug. 1959, pp. 393-404.

6. L. A. Hughes, "On the Low-Level Wind Structure of Tropical Storms," Journal of Meteorology, vol. 9, No. 6, Dec. 1952, pp 422-428.

7. C. L. Jordan, D. A. Hurt, Jr., and C. A. Lowrey, "The Structure of Hurricane Daisy on 27 August 1958," Journal of Meteorology, vol. 17, No. 3, June 1960, pp. 337-348.

8. N. E. LaSeur, "An Analysis of Some Detailed Data Obtained by Aircraft Reconnaissance of a Hurricane," Scientific Report No. 5, Contract AF-19 (604) -753, Florida State University, 1957.

9. J. S. Malkus, "On the Thermal Structure of the Hurricane Core," Proceedings, Technical Conference on Hurricanes, American Meteorological Society 1958, Sec. D. 3, pp. 1-2.

10. J. S. Malkus, "Recent Developments in Studies of Penetrative Convection and an Application to Hurricane Cumulonimbus Towers," Technical Report No. 6, Woods Hole Oceanographic Institution, 34 pp. (Unpublished manuscript.)

11. J. S. Malkus, "Cloud Patterns in Hurricane Daisy, 1958," Technical Report No. 8, Woods Hole Oceanographic Institution, 63 pp. (Unpublished manuscript.)

12. J. S. Malkus and H. Riehl, "On the Dynamics and Energy Transformations in Steady-State Hurricanes," Tellus, vol. 12, No. 1, Feb. 1960, pp. 1-20.

13. O. Reynolds, "On the Dynamical Theory of Incompressible Viscous Fluids and the Determination of Criterion," Philosophical Transactions of the Royal Society of London, Ser. (A), vol. 186, 1958 pp. 123-164.

14. H. Riehl, Tropical Meteorology, McGraw-Hill Book Co., Inc., New York, 392 pp.

15. H. Riehl, "On Production of Kinetic Energy from Condensation Heating," pp. 381-399 of The Atmosphere and the Sea in Motion, The Rossby Memorial Volume, Rockefeller Institute Press in association with Oxford University Press, New York, 1959.

16. H. Riehl and R. C. Gentry, "Analysis of Tropical Storm Frieda," National Hurricane Research Project Report No. 17, U. S. Weather Bureau 1958, 16 pp.

17. H. Riehl and J. S. Malkus, "On the Heat Balance in the Equatorial Trough Zone," Geophysica, vol. 6, No. 3/4, 1958, pp. 503-538.

18. Staff Members, National Hurricane Research Project, "Details of Circulation in the High Energy Core of Hurricane Carrie," National Hurricane Research Project Report No. 24, U. S. Weather Bureau,1958, 15 pp.

19. L. Sherman, "On the Wind Asymmetry of Hurricanes," Journal of Meteorology, vol. 13, No. 5, Oct. 1956, pp. 500-503.

APPENDIX

1. RELIABILITY OF THE COMPUTATIONS

The reader's first reaction to this study may be tinged with some skepticism as to the accuracy of the data and the reliability of some of the computations made from the qualitative analysis. This may be particularly true of computations that made use of the radial wind component.

It must be emphasized that the Doppler navigation system, from which all the winds were obtained, is an extremely accurate nagivation instrument. Winds above 10 to 15 kt. are accurate to within 2 to 3 percent in both direction and speed - except at isolated points in turn and in a few heavy rain areas. These areas were not used in the computations. The tangential wind components are just as accurate as the total wind.

All computations where "D" values were used were dependent only on the gradient of the "D" values and not on the absolute values themselves.

It should be remembered that the radial winds used in this study were those of the actual radial wind components and not the relative radial wind components. The magnitudes of the actual radial winds are much greater than the relative radial winds and lend themselves far better to evaluation.

Computations using the actual radial winds were made only from careful field analysis where isolated non-representative values could be disregarded and a relatively smooth well defined pattern could be obtained. Evaluation of $\dot{v}_r)_{gr}$ and $\dot{v}_{rr})_{gr}$ was in no way dependent upon the radial wind.

That there may be a few inherent data and computational shortcomings in certain of the individual levels is not denied. The area integrations did require qualitative analysis. It is felt, however, that in the 10-level composites these possible individual level shortcomings could not and did not disguise the broadscale features displayed.

2. EQUALITY OF FRICTIONAL ACCELERATION IN FIXED AND MOVING STORM CENTER (F_{rr})

The substantial derivative relative to the moving storm center $\dot{v}_{rr}$ is, with the previous stated assumption of constant storm translation,

$$v_{\theta r} \frac{\partial v_{rr}}{r\partial\theta} + v_{rr} \frac{\partial v_{rr}}{\partial r} + w \frac{\partial v_{rr}}{\partial z}$$

where $v_{\theta r}$ and v_{rr} are the relative tangential and radial wind components. The local derivative $\partial v_{rr}/\partial t$ drops because of the steady state assumption. The relation between the substantial derivative with respect to the moving center and that with respect to the fixed center is then with the statement and footnote of page 17

$$\dot{v}_{rr} - \left(- \frac{2v_\theta c_\theta}{r} + \frac{c_\theta^2}{r} - f c_\theta \right) = \dot{v}_r . \qquad (19)$$

Now

$$\dot{v}_r)_{gr} = \dot{v}_r - F_r, \text{ or } F_r = - [\dot{v}_r)_{gr} - \dot{v}_r] \qquad (a)$$

$$\dot{v}_{rr})_{gr} = \dot{v}_{rr} - F_{rr}, \text{ or } F_{rr} = - [\dot{v}_{rr})_{gr} - \dot{v}] \qquad (b)$$

and

$$\dot{v}_{rr})_{gr} = \dot{v}_r)_{gr} + \left(- \frac{2v_\theta c_\theta}{r} + \frac{c_\theta^2}{r} - f\, c_\theta \right) \qquad (c)$$

$$\dot{v}_{rr} = \dot{v}_r + \left(- \frac{2v_\theta c_\theta}{r} + \frac{c_\theta^2}{r} - f c_\theta \right) \qquad (d)$$

from previous stated principles and assumptions. Substituting equations (c) and (d) into equation (6)

$$F_{rr} = - (\dot{v}_r)_{gr} - \dot{v}_r) = F_r \qquad (20)$$

The frictional acceleration with respect to the moving storm center is thus shown to be identical with that with respect to the fixed instantaneous center.